

**Experimental Fire Testing of Damaged Glulam Beam Connections
Retrofitted Using Self-Tapping Screws**

by

Mohamed Hegazi

A thesis

submitted to the Faculty of Graduate Studies
in partial fulfillment of the requirements for the
Degree of Master of Science

in

Civil Engineering

Supervisor

Osama (Sam) Salem, Ph.D., P. Eng.

Associate Professor and Chair – Dept. of Civil Engineering

Lakehead University

Thunder Bay, Ontario

September 2022

© Mohamed Hegazi 2022

Author's Declaration

I hereby declare that I am the sole author of this thesis. This is a true copy of the thesis, including any required final revisions, as accepted by my examiners. I understand that my thesis may be made electronically available to the public.

Abstract

During the lifespan of timber buildings, structural members may exhibit different defects and/or failures. This may include splits that develop due to shrinkage because of changes in the moisture content of wood and/or due to excessive flexure bending, tensile, or shear stresses. To rehabilitate timber structures, there are various retrofitting techniques used to strengthen damaged wood members. Some of the available methods include the utilization of fiber-reinforced polymer wrapping sheets, mechanical fasteners such as self-tapping screws (STS), and glued-in rods. The utilization of STS was proven to be the most economical and easiest retrofitting technique. In ambient conditions, this technique has been shown to greatly increase the strength of wood-steel-wood (WSW) connections when subjected to flexure bending. STS have also been shown to significantly increase the ductility of timber beams utilizing such reinforced connections. Although STS have proved to be very effective in enhancing the strength of glued-laminated timber (glulam) beams with WSW connections in ambient conditions, there has been very minimal research on the effect of STS on retrofitting glulam beams with such connections in fire conditions.

The main objective of this research is to investigate the effects of using STS to retrofit damaged glulam beams in fire conditions. In this study, eight different full-size WSW bolted connection configurations have been retrofitted using STS after being deliberately damaged through physical testing until failure. In a subsequent stage, the retrofitted glulam beam end connections were experimentally tested at elevated temperatures that followed the CAN/ULC-S101 standard fire time-temperature curve while being loaded to 100% of the ultimate design moment capacity of the weakest unreinforced connection configuration. Study parameters included bolt pattern, number of bolts, and the usage of wood insulation to fully conceal the steel connecting components (i.e., bolt heads and nuts, and steel plate edges). The STS effects in terms of confining the glulam beam

sections that exhibited splitting failures, enhancing fire resistance, and ductility of the retrofitted beam end connections were experimentally investigated. The experimental results of the behaviour of the retrofitted glulam beam end connections were compared to those of identical but undamaged, unreinforced connections experimentally tested in a related prior study to better understand the strengthening effects of STS in fire conditions.

Experimental results show that usage of STS prevented failure due to delamination at the glue lines of the glulam beam sections, which commonly develops in unreinforced, undamaged (original) connections. This in turn resulted in greater fire resistance times. Obtained results also show that STS resulted in a significant increase in the strength of the damaged connections; however, the fire resistance times of the unreinforced, undamaged connections were not completely recovered. On average, 85% of the original strength was restored. This is consistent with the results of other published studies that utilized STS in WSW glulam connections but in ambient conditions. It was also observed that the splits of the damaged beams played a significant role in the reduction of their fire resistance times. For STS-reinforced connections with larger initial split widths, the fire resistance time was considerably less mainly due to more penetration of the heat through the wide splits. Finally, when analyzing the time-rotation curves, it was noticed that the failure of the STS-retrofitted connections was more gradual, and the connections experienced a more ductile behaviour compared to that of the unreinforced (original) connections.

Acknowledgements

I would like to extend my sincere gratitude to my supervisor, Dr. Sam Salem, for his exceptional mentorship, support, and guidance throughout my study. I am very grateful for all the time he spent assisting me on this unique research project and for all the knowledge he shared with me since the beginning of my research. I would not have completed this project without his great support.

I would also like to thank Morgan Ellis and Cory Hubbard from the Civil Engineering's Structures Laboratory at Lakehead University for all their assistance during the experimental program of my research project.

Lastly, I would like to thank my family for being by my side throughout my studies. Their wise words, encouragement, and guidance gave me the strength to complete my Masters. This would not have been possible without their great support.

Table of Contents

Abstract.....	ii
Acknowledgements	iv
Table of Contents	v
List of Tables	ix
List of Figures.....	x
List of Equations	xvii
Nomenclature	xviii
Chapter 1: Introduction	1
1.1 Background	1
1.2 Problem Statement	2
1.3 Objectives.....	3
1.4 Thesis Structure.....	3
Chapter 2: Literature Review.....	4
2.1 Structure of Wood	4
2.2 Wood Use as a Building Material	7
2.3 Connections Utilized in Wood Structures.....	8
2.4 Hybrid Wood Connection Failure Modes	13
2.4.1 Row shear-out resistance	15
2.4.2 Splitting resistance	16

2.4.3	Yielding resistance	16
2.5	Performance of Bolted Wood-Steel-Wood (WSW) Connections with No Reinforcement	20
2.6	Reinforcement and Retrofitting Techniques of Wood Connections	23
2.6.1	FRP reinforcement	24
2.6.2	Glued-in rods.....	28
2.6.3	Self-tapping screws	33
2.7	Wood Properties at Elevated Temperatures	48
2.7.1	Wood design for fire safety.....	48
2.7.2	Behaviour of timber at elevated temperatures	50
2.7.3	Effects of fire on the mechanical properties of wood	56
2.8	Behavior of Wood-Steel-Wood-Connections in Fire.....	58
2.8.1	Heat transfer in hybrid wood-steel-wood connections in fire	58
2.8.2	Fire resistance of hybrid wood-steel-wood connections at elevated temperatures	63
2.9	Wood Reinforcement Behaviour When Exposed to Fire.....	65
Chapter 3: Methodology and Test Assemblies Details		67
3.1	Introduction	67
3.2	Ambient Temperature Testing	67
3.3	Fire Resistance Testing	73
3.4	Materials.....	76

3.4.1	Glulam beam sections	76
3.4.2	T-stub steel connectors.....	76
3.4.3	Self-tapping screws	82
3.5	STS and Bolts Spacing.....	83
3.6	Loading.....	84
3.7	Thermocouples	85
3.8	Test Matrix	88
Chapter 4: Experimental Tests Results and Discussion		89
4.1	Introduction	89
4.2	Ambient Temperature Tests Results	89
4.3	Fire Resistance Test Results.....	90
4.3.1	Effects of using self-tapping screws in the unprotected connections	93
4.3.2	Effects of using self-tapping screws in the protected connections	99
4.3.3	Effects of the number of bolts on the fire resistance of the unprotected connections	108
4.3.4	Effects of the number of bolts on the fire resistance of the protected connections	108
4.3.5	Effects of the bolt pattern on the fire resistance of the unprotected connections	109
4.3.6	Effects of the bolt pattern on the fire resistance of the protected connections	113
4.4	Time-Temperature Curves	117
4.4.1	Time-temperature curves of the unprotected connections	117
4.4.2	Time-temperature curves of the protected connections	122

4.4.3	Charring rates	125
Chapter 5: Conclusions and Recommendations		129
5.1	Conclusions	129
5.2	Recommendations for Future Work.....	130
References		132

List of Tables

Table 2.1 Strength properties of glulam beams	6
Table 2.2 - Shear testing results summary	12
Table 2.3 WSW connections results summary	22
Table 2.4 Strength properties of various fibres and polymers	25
Table 2.5 Effective number of bolts for reinforced vs unreinforced connections	34
Table 2.6 Results summary for reinforced vs. unreinforced connections	43
Table 2.7 Charring rates of different wood species	51
Table 2.8 Eurocode model on the effect of density on the charring rate of wood	52
Table 2.9 Temperature vs. thermal conductivity of wood	54
Table 2.10 Fire testing results	65
Table 3.1 24f-EX glulam beam mechanical properties	76
Table 3.2 Test matrix	88
Table 4.1 Ambient temperature results.	90
Table 4.2 Summary of all fire resistance tests.	91
Table 4.3 Calculated charring rates.....	127

List of Figures

Figure 2.1 Inner structure of a tree trunk	5
Figure 2.2 Wood orthogonal axes based on grain direction.	6
Figure 2.3 Double shear hybrid connection in timber structures.....	9
Figure 2.4 Shear testing set-up	10
Figure 2.5 Shear testing nail arrangements	10
Figure 2.6 Failure modes for bolted wood connections	14
Figure 2.7 Ductile failure modes for wood connections	18
Figure 2.8 Ambient temperature test setup	20
Figure 2.9 Details of bolts arrangement: (a) bolts arrangements in Pattern 1; (b) bolt arrangements in Pattern 2	21
Figure 2.10 FRP-reinforced specimens' detail: (a) FRP placed perpendicular to grain; (b) FRP placed at 45° angle to grain.....	27
Figure 2.11 FRP-reinforced specimens detail: (a) FRP placed at angle 45° to grain; (b) FRP placed at angle 90° to grain	28
Figure 2.12 Variation of placing GiR into wood: (a) a hole is drilled vertically and glue is injected; (b) Glue is injected into a hole perpendicular to where the rod is to be placed	29
Figure 2.13 Anchorage length vs Pull-out strength for GiR connection from different studies	30
Figure 2.14 Rod diameter vs Pull-out strength for GiR connection for different studies	31
Figure 2.15 Density vs Pull-out strength for GiR connection for different studies.....	31
Figure 2.16 Fully threaded ASSY® VG STS	33
Figure 2.17 Geometry of specimens tested (M1 to M10), including the number of reinforcing STS.....	35

Figure 2.18	Load-displacement curve for a beam subjected to parallel to grain tensile load (M1-M4) non-reinforced beam; (M5 to M6) reinforced beam with no contact between dowels and STS; (M6 to M7) reinforced beam with contact between dowels and STS	36
Figure 2.19	Bolted connection test set up	37
Figure 2.20	Test configurations: (a) Unreinforced beam; (b) Reinforced beam; (C) Retrofitted beam	38
Figure 2.21	Test setup	39
Figure 2.22	The different STS-bolt arrangements studied: (a) A-CR; (b) B-CR; (c) C-CR	40
Figure 2.23	Resulted moment-rotation curves	41
Figure 2.24	Utilized connection configuration	42
Figure 2.25	Resulted load-displacement curve	44
Figure 2.26	General test setup	45
Figure 2.27	Dimensions and placement of the STS	46
Figure 2.28	Moment-deformation graph for unreinforced connection	46
Figure 2.29	Moment-deformation graph for reinforced connection	47
Figure 2.30	Failure modes of STS-reinforced connection: (a) 4d; (b) 5d	48
Figure 2.31	Wood section charring	51
Figure 2.32	Temperature vs. thermal conductivity of wood	54
Figure 2.33	Temperature vs. specific heat of wood	55
Figure 2.34	Temperature vs. density of wood	56
Figure 2.35	Effect of temperature on the strength of softwood	57
Figure 2.36	Effect of temperature on the modulus of elasticity of softwood	58
Figure 2.37	Thermal analysis finite element model	59

Figure 2.38 Schematic for test specimens	60
Figure 2.39 Temperature vs. time for FE model and experiments	61
Figure 2.40 Bolt cross-section temperatures.....	62
Figure 2.41 Dowel cross-section temperatures.....	62
Figure 2.42 CAN/ULC-S101 and ISO 834 standard fire curves	63
Figure 3.1 Ambient temperature test setup for the connection configuration with four bolts in Pattern 2 without fire protection (4BP2NP).....	69
Figure 3.2 Details of the connection configuration with four bolts in Pattern 1 without fire protection (4BP1NP).....	69
Figure 3.3 Details of the connection configuration with four bolts in Pattern 2 without fire protection (4BP2NP).....	70
Figure 3.4 Details of the connection configuration with six bolts in Pattern 1 without fire protection (6BP1NP).....	70
Figure 3.5 Details of the connection configuration with six bolts in Pattern 2 without fire protection (6BP2NP).....	71
Figure 3.6 Depiction of the damage to the 4-bolt protected connections utilizing the second bolt pattern (P2) when the ambient test was terminated.	72
Figure 3.7 Failure modes exhibited by the 4-bolt unprotected connections utilizing the first and second bolt patterns (P1 and P2) when the tests were terminated	72
Figure 3.8 Lakehead University Fire Testing and Research Laboratory (LUFTRL)	74
Figure 3.9 Fire testing furnace	74
Figure 3.10 Typical fire test setup.	75

Figure 3.11 Steel T-stub connector details for the 4-bolt connection configuration with bolt pattern one (P1): (a) isometric view; (b) front view; (c) back view; (d) top view.....	78
Figure 3.12 Steel T-stub connector details for the 4-bolt connection configuration with bolt pattern two (P2): (a) isometric view; (b) front view; (c) back view; (d) top view.	79
Figure 3.13 Steel T-stub connector details for the 6-bolt connection configuration with bolt pattern one (P1): (a) isometric view; (b) front view; (c) back view; (d) top view.....	80
Figure 3.14 Steel T-stub connector details for the 6-bolt connection configuration with bolt pattern two (P2): (a) isometric view; (b) front view; (c) back view; (d) top view.	81
Figure 3.15 SWG ASSY VG plus CSK self-tapping screw (STS)	82
Figure 3.16 Top view of the glulam beam showing six STS installed.	83
Figure 3.17 Spacing of installed STS.....	84
Figure 3.18 Thermocouples arrangement in the connection configurations with bolt pattern (P1)	86
Figure 3.19 Thermocouples arrangement in the connection configurations with bolt pattern (P2)	87
Figure 4.1 Initial state of the STS-retrofitted, unprotected connection configuration that utilized four bolts in the first bolt pattern (4BP1NP).....	94
Figure 4.2 Fire testing timeline for the STS-retrofitted, unprotected connection configuration that utilized four bolts in the first bolt pattern (4BP1NP).....	94
Figure 4.3 Initial state of the STS-retrofitted, unprotected connection configuration that utilized six bolts in the first bolt pattern (6BP1NP).....	95
Figure 4.4 Fire testing timeline for the STS-retrofitted, unprotected connection configuration that utilized six bolts in the first bolt pattern (6BP1NP).....	96

Figure 4.5 Initial state of the STS-retrofitted, unprotected connection configuration that utilized four bolts in the second bolt pattern (4BP2NP).....	97
Figure 4.6 Fire testing timeline for the STS-retrofitted, unprotected connection configuration that utilized four bolts in the second bolt pattern (4BP2NP).....	97
Figure 4.7 Initial state of the STS-retrofitted, unprotected connection configuration that utilized six bolts in the second bolt pattern (6BP2NP).....	98
Figure 4.8 Fire testing timeline for the STS-retrofitted, unprotected connection configuration that utilized six bolts in the second bolt pattern (6BP2NP).....	99
Figure 4.9 Initial state of the STS-retrofitted, protected connection configuration that utilized four bolts in the first bolt pattern (4BP1P).....	100
Figure 4.10 Fire testing timeline for the STS-retrofitted, protected connection configuration that utilized four bolts in the first bolt pattern (4BP1P).....	101
Figure 4.11 Initial state of the STS-retrofitted, protected connection configuration that utilized six bolts in the first bolt pattern (6BP1P).....	102
Figure 4.12. Fire testing timeline for the STS-retrofitted, protected connection configuration that utilized six bolts in the first bolt pattern (6BP1P).....	103
Figure 4.13 Initial state of the STS-retrofitted, protected connection configuration that utilized four bolts in the second bolt pattern (4BP2P).....	104
Figure 4.14 Fire testing timeline for the STS-retrofitted, protected connection configuration that utilized four bolts in the second bolt pattern (4BP2P).....	105
Figure 4.15 Initial state of the STS-retrofitted, protected connection configuration that utilized six bolts in the second bolt pattern (6BP2P).....	106

Figure 4.16 Fire testing timeline for the STS-retrofitted, protected connection configuration that utilized six bolts in the second bolt pattern (6BP2P). 107

Figure 4.17 Time-rotation relationships of the STS-retrofitted, unprotected connection configurations that utilized four bolts in the first (4BP1NP) and second bolt patterns (4BP2NP). 110

Figure 4.18. Time-rotation relationships of the undamaged, unreinforced and unprotected connection configurations that utilized four bolts in the first (4BP1NF1) and second bolt patterns (4BP2NF1) 110

Figure 4.19 Time-rotation relationships of the STS-retrofitted, unprotected connection configurations that utilized six bolts in the first (6BP1NP) and second bolt patterns (6BP2NP). 112

Figure 4.20 Time-rotation relationships of the undamaged, unreinforced, and unprotected connection configurations that utilized six bolts in the first (6BP1NF1) and second bolt patterns (6BP2NF1) 112

Figure 4.21 Time-rotation relationships of the STS-retrofitted, unprotected connection configurations that utilized six bolts in the first (6BP1NP) and second bolt patterns (6BP2NP). 113

Figure 4.22 Time-rotation relationships of the undamaged, unreinforced, and protected connection configurations that utilized four bolts in the first (4BP1PF1) and second bolt patterns (4BP2PF1) 114

Figure 4.23 Time-rotation relationships of the STS-retrofitted, protected connection configurations that utilized six bolts in the first (6BP1P) and second bolt patterns (6BP2P). ... 116

Figure 4.24 Time-rotation relationships of the undamaged, unreinforced, and protected connection configurations that utilized six bolts in the first (6BP1PF1) and second bolt patterns (6BP2PF1)	117
Figure 4.25. Time-temperature relationships of the STS-retrofitted, unprotected connection configurations that utilized four bolts in the first bolt pattern (4BP1NP).....	118
Figure 4.26 Time-temperatures relationships of the STS-retrofitted, unprotected connection configurations that utilized four bolts in the second bolt pattern (4BP2NP).....	119
Figure 4.27 Time-temperatures relationships of the STS-retrofitted, unprotected connection configurations that utilized six bolts in the first bolt pattern (6BP1NP).....	120
Figure 4.28 Time-temperatures relationships of the STS-retrofitted, unprotected connection configurations that utilized six bolts in the second bolt pattern (6BP2NP).....	121
Figure 4.29 Time-temperatures relationships of the STS-retrofitted, protected connection configurations that utilized four bolts in the first bolt pattern (4BP1P)	122
Figure 4.30 Time-temperatures relationships of the STS-retrofitted, protected connection configurations that utilized four bolts in the second bolt pattern (4BP2P).....	123
Figure 4.31 Time-temperatures relationships of the STS-retrofitted, protected connection configurations that utilized six bolts in the first bolt pattern (6BP1P)	124
Figure 4.32 Time-temperatures relationships of the STS-retrofitted, protected connection configurations that utilized six bolts in the second bolt pattern (6BP2P).....	125
Figure 4.33 Relationship between the calculated charring rate and fire resistance time of the eight STS-retrofitted connection configurations tested	128

List of Equations

Equation 2.1 Total factored row shear-out resistance	15
Equation 2.2 Factored resistance of perpendicular to grain of wood members	16
Equation 2.3 Yielding resistance of wood members	17
Equation 2.4 Embedment strength of fastener embedded parallel to wood grain.....	19
Equation 2.5 Embedment strength of fastener embedded perpendicular to wood grain	19
Equation 2.6 Bolts yield strength of bolts other than CSA or ASTM bolts	19
Equation 2.7 Charring rate equation to account for wood density	52
Equation 4.1 Charring rate.....	126

Nomenclature

WSW: Wood-Steel-Wood Connection

SWS: Steel-Wood-Steel Connection

WWW: Wood-Wood-Wood Connection

FRP: Fibre Reinforced Polymer

STS: Self-tapping Screws

FRR: Fire Resistance Rating

WDM: Wood Design Manual

NBCC: National Building Code of Canada

4BP1NP: Four Bolts Arranged in Pattern 1 Without Fire Protection

4BP2NP: Four Bolts Arranged in Pattern 2 Without Fire Protection

6BP1NP: Six Bolts Arranged in Pattern 1 Without Fire Protection

6BP2NP: Six Bolts Arranged in Pattern 2 Without Fire Protection

4BP1P: Four Bolts Arranged in Pattern 1 With Fire Protection

4BP2P: Four Bolts Arranged in Pattern 2 With Fire Protection

6BP1P: Six Bolts Arranged in Pattern 1 With Fire Protection

6BP2P: Six Bolts Arranged in Pattern 2 With Fire Protection

TC: Thermocouple

Chapter 1: Introduction

1.1 Background

In timber design, hybrid connections such as wood-steel-wood (WSW) are commonly used to connect wood members and transfer loads. A WSW connection consists of metal (steel) fasteners which can be made up of bolts, screws, nails, or dowels. The overall strength and stiffness of the connection depend on the fasteners (i.e., bolts/dowels arrangements and numbers of bolts/dowels) and the properties of the wood section. In fire conditions, since metal is much more conductive than wood, the heat conducted from the metal fasteners into the wood members results in a higher charring rate at the connection, which rapidly affects the strength of the residual section. This makes the connections the weakest components of wood structures in fire conditions. Considering that the resistance of connection will most likely govern the fire resistance of wood assemblage (Maraveas et al., 2015), studying the behaviour of hybrid connections such as WSW in fire conditions is of critical importance to researchers. Experimental research conducted by Owusu (2019) on glulam beam WSW connections exposed to fire has shown that concealing the steel components (i.e., bolts and plates) using wood plugs and strips significantly increases the fire resistance of the connection. However, it was also observed that other modes of failure can occur in WSW connections whether the steel components are concealed or exposed. In the Owusu (2019) study, wood splitting failure along the glue planes was unexpected and it resulted in immediate failure of the connections. In another recent study conducted by Okunroumu et al. (2020) the effects of concealing and reinforcing WSW connections in fire were investigated. From the said study, it was concluded that when the connection was reinforced with self-tapping screws and the steel components were concealed, the beam-end connections achieved fire resistance times

surpassing 45 minutes which exceeded the fire resistance rating required by the National Building Code of Canada (NBCC, 2020).

1.2 Problem Statement

During the lifespan of timber structures, structural members may exhibit a variety of failure modes. This may include splits that develop due to shrinkage as a result of changes in the moisture content of wood and/or due to excessive flexural bending, tensile, or shear stresses. To rehabilitate timber structures, there are various retrofitting techniques to follow. Some of the available methods include the utilization of fibre-reinforced polymer (FRP) wrapping sheets, self-tapping screws (STS), and glued-in rods. STS have been proven to be the most economical and easiest retrofitting technique. For flexural bending reinforcement, STS are inserted perpendicular to the wood grain of the wood member to resist and transfer perpendicular-to-wood grain tensile and shear stresses that can not be resisted in large concentrations by wood members. In ambient conditions, STS have been shown to greatly increase the strength of concealed wood-steel-wood (WSW) connections when subjected to flexural bending. They also have been shown to significantly increase the ductility of timber beams with end connections reinforced with STS. Although STS have proved to be very effective in enhancing the strength of glued-laminated timber (glulam) beams with WSW connections in ambient conditions, there has been very minimal research on the effect of STS on retrofitting glulam beams with such connections in fire conditions. Furthermore, it was seen from past experimental research, that when unreinforced WSW glulam beam connections are exposed to fire, they commonly experience splits at the glue planes. This leads to premature failure of the connection. As such, it was proposed to utilize STS to address this shortcoming of glulam beams with WSW connections in fire.

1.3 Objectives

The following are the main objectives of this research:

- To experimentally investigate the effects of using STS reinforcement on the fire resistance of damaged glulam beam WSW connections. The beams tested were subjected to flexural loading and shear force until splits were present along the top and bottom rows of bolts.
- To determine how much of the original strength and fire resistance of the beams is restored when the damaged beams are reinforced with STS and re-tested in fire.
- To investigate whether the usage of STS can prevent glue line failure, which was very common in the unreinforced WSW connections and often led to premature failure in fire conditions.
- To investigate the effect of the damage within the glulam beam connections (i.e., the width of the splits) on the fire resistance of the beam connections when STS are used.

1.4 Thesis Structure

This thesis is divided into five chapters. Chapter one provides a brief introduction to the research work, including background information, problem statement, and main objectives of this research. Chapter two presents a summary and review of the most relevant research studies in the available literature. Chapter three outlines and describes the methodology, test setup, and procedure followed in the experimental program of this research. Chapter four represents in detail the results of the experimental research program as well as provides a comprehensive discussion on the influence of utilizing STS to reinforce damaged glulam beam-end WSW connections and how it restores considerable amounts of the strength and fire resistance of such connections. Finally, Chapter five provides a list of the conclusions that have been drawn from this new experimental study and highlights the most important recommendations for future work.

Chapter 2: Literature Review

2.1 Structure of Wood

Wood is one of the oldest and most used construction material worldwide. It is a natural fibre-composite material, made up of cellulose fibres arranged in a lignin matrix. Further, wood is an anisotropic material, and hence, its strength properties such as tensile strength, bending strength, and compressive strength, vary based on the type of wood, loading orientation, and moisture content. This anisotropy can be observed in the arrangement of cells in a tree where 90-95% of cells are aligned parallel to the tree trunk, 5-10% of cells are located in the radial direction, and no cells are present in the tangent direction. A cross-section of a tree trunk is shown in Figure 2.1 which illustrates the inner structure of the tree. The three main sections in the trunk are the heartwood, the sapwood, and the bark. The heartwood has no role and hence is physiologically inactive, the sapwood is where all storage occurs, and the bark protects the interior of the tree trunk. Trees can be categorized into two categories: softwoods, such as Douglas Fir, Hem-Fir, SPF, and hardwoods, like hickory, and Maple (Department of Materials Science and Metallurgy, University of Cambridge, 2014).

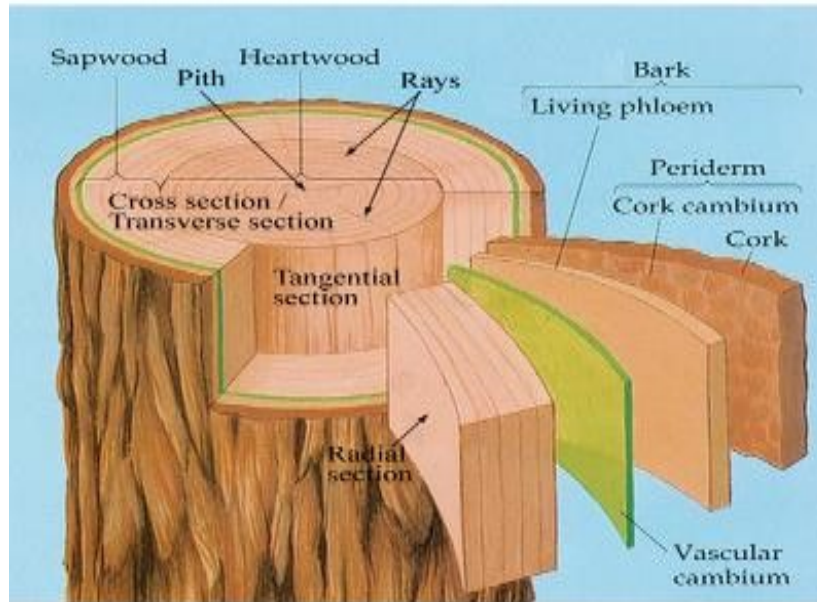


Figure 2.1 Inner structure of a tree trunk (Adapted from the Department of Materials Science and Metallurgy, University of Cambridge, 2014).

Wood is an anisotropic material, and hence its strength properties vary with respect to three orthogonal directions, Figure 2.2. The three orthogonal directions are Longitudinal (L), Radial (R), and Tangential (T). The longitudinal direction lies parallel to the fiber direction, whereas the radial and tangential directions are located perpendicular to the fiber direction, with the radial direction perpendicular to the growth rings, and the tangential direction parallel to the growth rings (Winandy, 1996). The strength of wood is greatest when loaded parallel to the grain. When loaded perpendicularly, wood products have very low strength and tend to split easily. Table 2.1 illustrates the strength properties of glulam wood obtained from Nordic Structures (2015) and evaluated by the Canadian Construction Materials Centre (CCMC).

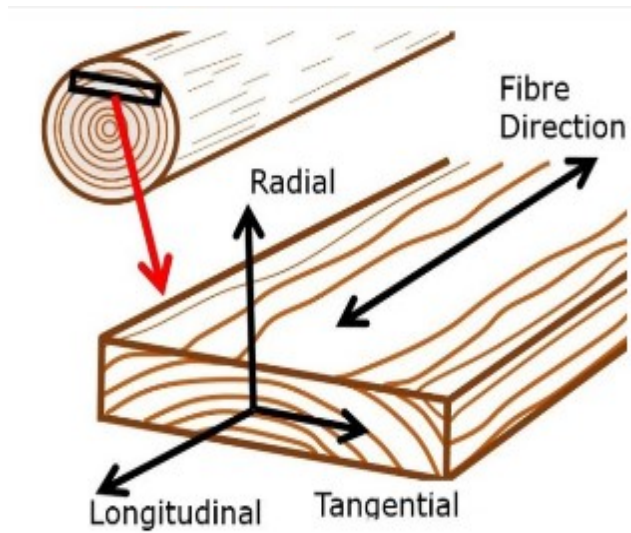


Figure 2.2 Wood orthogonal axes based on grain direction (Adapted from Fragkia and Foged, 2020).

Table 2.1 Strength properties of glulam beams (Adapted from Nordic Structures, 2015).

Property	Units (MPa)
Compression parallel to the grain	33.0
Compression perpendicular to the grain	7.5
Tension parallel to the grain	20.4
Modulus of elasticity	13,100
Flexural bending	30.7
Longitudinal shear	2.2

2.2 Wood Use as a Building Material

As building codes in North America and around the world are acting to combat climate change, many are starting to consider the impact of construction on the environment. As such, many are encouraging the use of sustainable building materials, such as wood. The use of wood as a building material offers an environmental advantage other materials lack. One of the greatest advantages of using wood is its sustainability. Wood is the only major renewable construction material (Wood Design Manual, 2020), and that can be recycled and reused at the end of its life span. Further, wood products require the least amount of energy to manufacture, transport, and use as compared to steel, concrete, and aluminum (Falk, 2009). Other environmental advantages of wood include reduced greenhouse gas emissions, which mitigate climate change by absorbing carbon dioxide instead of releasing it. Roughly 10 billion tonnes of wood are used globally each year. The popular use of wood is also attributed to its low cost, which is 60 times lower compared to steel/ton, as well as high specific strength. In terms of strength, many wood products especially engineered wood products such as glulam, and CLT offer strength properties that are comparable to materials such as concrete and steel.

While wood products offer a sustainable, energy-efficient, and low-cost choice as a building material, one of the main shortcomings of wood products is their combustible behaviour. Although wood products have adequate strength properties, fire resistance is usually the limiting design parameter. Many codes around the world, including the National Building Code of Canada (NBCC, 2020) restrict the use of wood products in high-occupancy, high-rise structures. As such, subsection 3.2.2 of division B of the previous version of the National Building Code of Canada (NBCC 2015) specifies the maximum number of stories for wood construction as six (6), with a maximum floor area of 1500 m². This limited number of storeys can be partially attributed to the

relatively limited research on the behaviour of wood design when exposed to fire. NBCC requires all wood structures to have a fire-resistance rating (FRR), which is defined as the time a component can resist fire before failure. FRR varies depending on the occupancy, the size of the structure, and accessibility to firefighters. FRR ranges from 0 to 120 minutes, with most buildings commonly having an FRR between 45-60 minutes (NBCC, 2015).

In the current version of the National Building Code of Canada (NBCC, 2020), the maximum number of stories for buildings primarily made of wood is 12 storeys. This increase in the number of storeys is attributed to the introduction of the encapsulated mass timber construction (EMTC) method. The EMTC is a construction method that consists of engineered wood materials such as glulam, cross-laminated timber (CLT), and nail-laminated timber (NLT) that is encapsulated by other materials, such as concrete. This encapsulation enhances the fire resistance times of timber members by resisting the spread of the fire which in turn increases the fire resistance times of timber structures. The minimum FRR for encapsulated mass timber is 50 minutes (NBCC, 2020). However, for floors, the minimum FRR for EMTC buildings is two hours (NBCC, 2020).

2.3 Connections Utilized in Wood Structures

Wood structures may be divided into two types: Heavy timber structures and light framing structures. Heavy timber structures consist of larger section sizes of sawn or glue-laminated timber. In light framing structures, simple connectors such as nails and screws are typically utilized. On the other hand, in heavy timber structures, connections such as bolts, dowels, and steel plates are used as these structures generally carry higher loading (Peng et al., 2011). The connectors in heavy timber structures can be divided into three cartridges: wood-wood-wood (WWW), wood-steel-wood (WSW), and steel-wood-steel (SWS) connections. For a WWW connection, the central member is a wood member, whereas, in a hybrid WSW connection, the central member is a steel

plate. Hybrid SWS members have steel plates on each side of the middle wood member. Figure 2.3 illustrates a schematic of the three different connection types. Bolts or dowels are utilized as connectors. WSW connections will be utilized in this research and hence the performance of these connections will be discussed throughout this chapter. Additionally, the failure modes of these connections will be provided in the sections below.

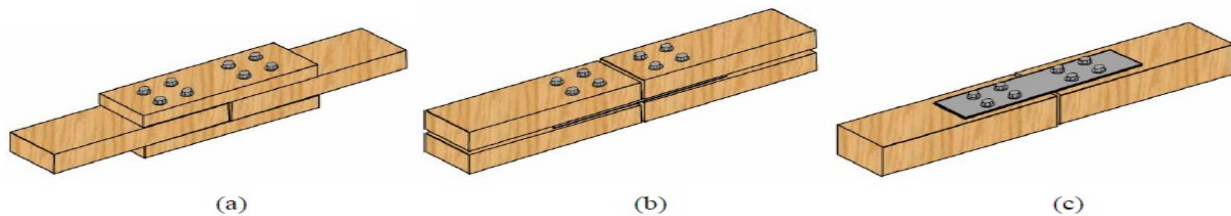


Figure 2.3 Double shear hybrid connection in timber structures, (a) WWW, (b) WSW, (c) SWS
(Adapted from Peng et al., 2011).

For light frame structures, nails are the most commonly used fasteners. Nails are available in many lengths and cross-sectional areas. Nails may be installed in timber members by hand or by machines. If nails are to be driven into dense timber, there is a risk of excessive splitting of the timber occurring. In order to avoid splitting, a predrilled hole which is typically 80% less in diameter than the nail diameter is drilled into the wood (Livingstone, 2015). Ruan et al. (2021) investigated the effect of the arrangement of wooden nails on the shear strength of timber-to-timber connection. In this study, a total of 90 shear tests were conducted using different types and arrangements of nails. The nails were used to connect three timber boards. The load was applied perpendicular to the boards and the specimens were loaded until failure. Figure 2.4 illustrates a schematic of the testing set up.

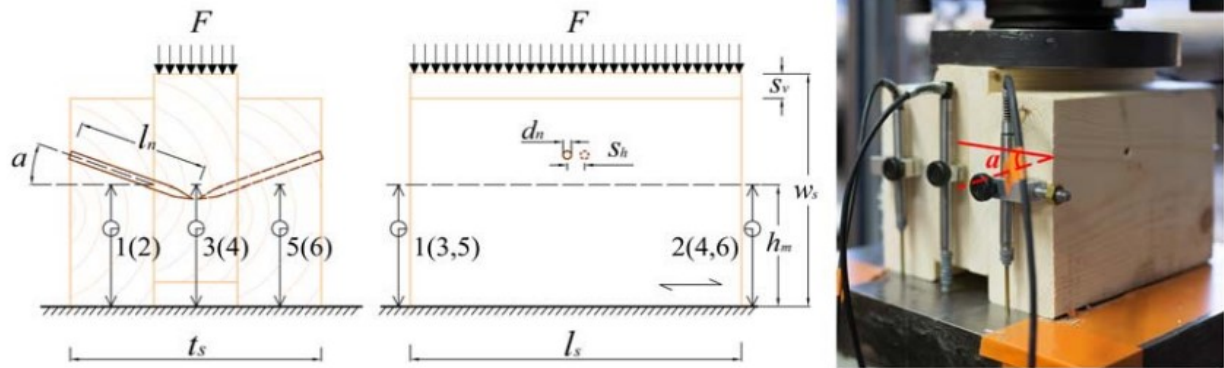


Figure 2.4 Shear testing set-up (Adapted from Ruan et al., 2021).

As part of the experimental study, four nail arrangements were studied. The arrangement of the nails is shown in Figure 2.5. In the first arrangement (S), one nail per shear plane was inserted at angle $\alpha = 0^\circ$. In the second arrangement (C), the nails were instead in a shear-compression arrangement at angles $\alpha = 15^\circ$ and 30° . In the third arrangement (T), the nails were instead in a shear-tension arrangement at angles $\alpha = 15^\circ$ and 30° . In the last arrangement (X), two nails per shear plane were inserted using a cross-arrangement.

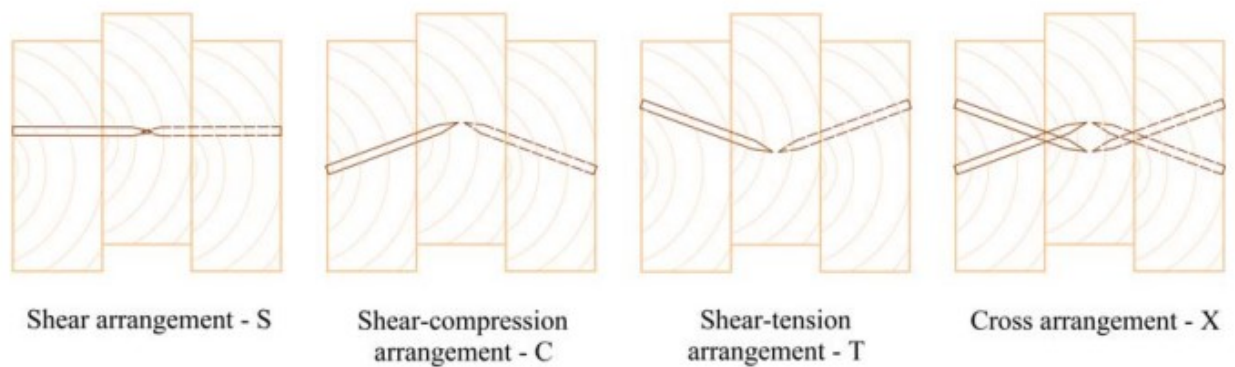


Figure 2.5 Shear testing nail arrangements (Adapted from Ruan et al., 2021).

When considering the single shear plane arrangements (S-T), results have shown that bolts loaded in the shear-tension arrangement achieved 43% higher strength compared to the S arrangement and

82% higher strength compared to the C arrangement. This could be attributed to the fact that in the T arrangement, the stresses were mainly tensile, with no compressive stresses that result in embedment failure. Conversely, in the Shear-Compression (C) arrangement, it was observed that embedment failures between the nails and the boards had taken place due to the compression stresses. This in turn resulted in lower shear strength for the S and C arrangements. Unsurprisingly, the shear strength for X arrangement nails was higher as compared to the first three single-plane arrangements.

When considering the angle of inclination of the nails for the single shear planes (Arrangements S-T), placing the nails at 30° resulted in higher shear resistance for all connections as compared to 15° arrangements. However, the difference was very small (10% or less); therefore, the author could not conclude for certainty that placing the nails at higher inclinations provides more efficiency as compared to lower inclinations without conducting more testing at a variety of inclinations angles. Conversely, for the double plane X arrangement, placing the nails at 15° resulted in higher shear resistance for all connections as compared to 30° . This was due to the significantly higher slip modules (deformation of nails with respect to loading) of the Compression nails as compared to the tension nails at higher angles, which in turn did not result in the full utilization of the compression nails. The results of the testing experiment are summarized in Table 2.2.

Table 2.2 - Shear testing results summary (Adapted from Ruan et al., 2021).

Nail Arrangement and Inclination	Shear Resistance (kN)
Arrangement S ($\alpha = 0^0$)	2.12
Arrangement C ($\alpha = 15^0$)	1.67
Arrangement T ($\alpha = 15^0$)	3.04
Arrangement X ($\alpha = 15^0$)	5.11
Arrangement C ($\alpha = 30^0$)	1.71
Arrangement T ($\alpha = 30^0$)	3.34
Arrangement X ($\alpha = 30^0$)	4.55

Another type of connection used in timber structures is the dowel-type fasteners. Dowels are circular rods made of timber or metal that are driven into wood members to connect them. According to Eurocode 5, the dowels must have a minimum diameter of 6 mm (Eurocode 5, 2004). The load-carrying capacity of dowel-type fasteners is calculated using Johansen's (1949) Yield Theory. Three parameters that affect the load carrying of dowel-type fasteners include the yield strength of the dowels, embedment strength of the timber, and the withdrawal strength of the dowel (Eurocode 5, 2004). The embedment strength of wood is dependent on the wood density, fastener diameter, angle between the load and grain direction of the wood, moisture content, and friction between the wood and the connection (Livingstone, 2015). Eurocode 5 (2004) outlines a variety of failure modes and associated equations for calculating the embedment strength and withdrawal strength of timber-to-timber and timber-to-steel connections. Section 2.4 of this chapter outlines the variety of failure modes and equations of wood connections.

Screws are another type of fastener used in timber structures. Screws can be driven into the wood members manually or using power equipment such as drilling. The main distinction between screws and nails is that screws have higher withdrawal strength as compared to nails (Livingstone, 2015). Glued joints are another type of connection used to connect timber structures. Advantages of glued joints over fasteners include stiffer connection and better appearance. Glued-in joints also offer more resistance to corrosive atmospheres as compared to metal fasteners. During fire, glued joints made of thermosetting resins are safer than metal fasteners due to their lower heat conductivity which in turn leads to lower charring (Livingstone, 2015).

2.4 Hybrid Wood Connection Failure Modes

Wood connection should be designed so that the factored resistance of the connection is greater than the applied load. A wood connection may fail by yielding, row shear out, group shear out, net tension, or splitting (Wood Design Manual, 2020). Yielding can occur either as a brittle or ductile failure, whereas splitting, row and group shear out, and net tension are brittle failures (Wood Design Manual, 2020). Yielding of the bolts can take place when the force is applied in any direction with respect to the grain (Wood Design Manual, 2020). Row shear-out failure occurs when a specimen is loaded parallel to the grain and along each fastener row, whereas group shear-out failure occurs when a connection is loaded parallel to the grain along multiple rows (Wood Design Manual, 2020). Splitting failure occurs when members are loaded perpendicular to the grain. The different failure modes of wood connection are illustrated in Figure 2.6. For an unreinforced bolted connection, it was observed in experiments, including by Owusu (2019), and Petrycki and Salem (2019), that the most common failure is row shear out, splitting, and yielding (crushing). Hence, the design requirements for these failure modes will be discussed in accordance with CSA-O86-19.

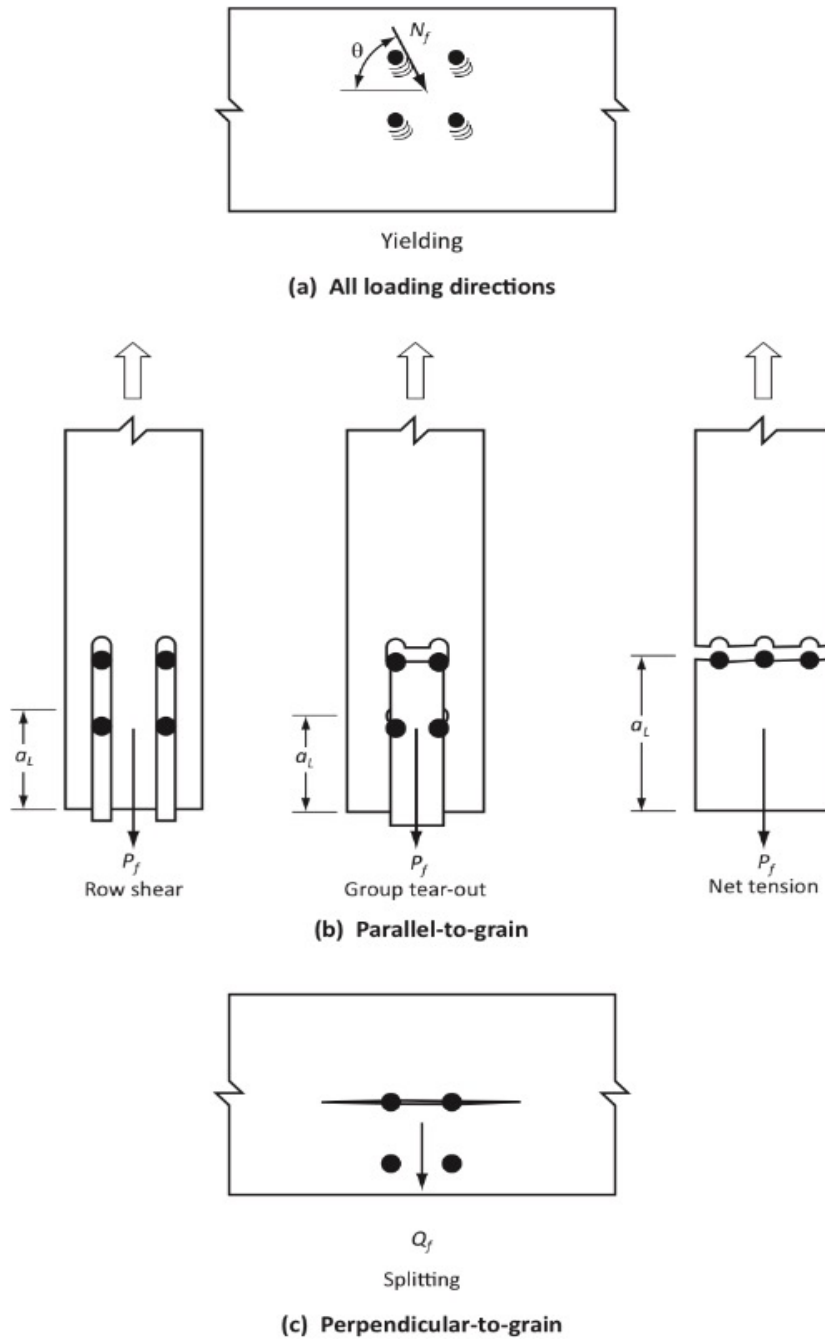


Figure 2.6 Failure modes for bolted wood connections (Adapted from the Canadian Wood Council, Wood Design Manual, 2020)

2.4.1 Row shear-out resistance

According to CSA O86-19, the total factored row shear resistance of a connection in a wood member is calculated using the following equation:

Equation 2.1 Total factored row shear-out resistance (Adapted from Wood Design Manual, 2020)

$$SPR_{r i} = \phi_w PR_{r j \min} n_R \quad \text{Eqn. (2.1)}$$

Where:

$\phi_w =$ Brittle failure resistance factor = 0.7

$PR_{r j \min} =$ The lowest row shear resistance in any row in the connection

$$= 1.2 f_v (K_D K_{sv} K_T) K_{IS} t n_c a_{cr i}$$

$f_v =$ Specified longitudinal shear values

$K_{IS} =$ 0.65 for side members; 1 for internal members

$t =$ Member thickness

$n_c =$ number of fastener/row

$a_{cr i} =$ minimum of spacing of fastener in a row (S_r), or loaded edge distance (a_L)

$K_D =$ load duration factor, $K_T =$ treatment factor, K_{ST}

$=$ service condition factor for longitudinal shear (i.e wet or dry)

2.4.2 Splitting resistance

Splitting failure in wood connection occurs when the wood is loaded perpendicular to the grain.

The factored resistance of perpendicular to the grain of wood members is:

Equation 2.2 Factored resistance of perpendicular to grain for wood members (Adapted from Wood Design Manual, 2020)

$$QS_{r_i} = \phi_w QS_i (K_D K_{SF} K_T) \quad \text{Eqn. (2.2)}$$

Where,

$$\phi_w = \text{Brittle failure resistance factor} = 0.7$$

$$QS_i = 14 t \sqrt{\frac{d}{1 - \frac{d_e}{d}}}$$

Where,

$$t = \text{Member thickness, mm}$$

$$d_e = \text{Effective depth of member, mm} = d - e_p$$

$$e_p = \text{unloaded edge distance, mm}$$

If more than one member is present, the splitting resistance of the connection is calculated by summing the resistance of each member (i.e. $QS_{r_T} = \sum QS_{r_i}$)

2.4.3 Yielding resistance

The yielding failure in wood members is dependent on the number of shear planes in a connection.

To prevent yielding, the yielding resistance N_r should be greater than the factored yield force N_f

Equation 2.3 Yielding resistance for wood members (Adapted from Wood Design Manual, 2020)

$$N_r = \phi_y n_u n_s n_f \quad \text{Eqn. (2.3)}$$

Where,

$\phi_y =$ yielding failure resistance factor = 0.8

$n_u =$ unit lateral yielding resistance

$n_s =$ number of shear planes

$n_f =$ number of fastener in connection

The unit lateral yielding resistance is dependent on the number of members in the connections, and the different modes a connection can fail in yielding. Figure 2.7 shows the variety of ways yielding can occur in timbers connections and the governing unit yielding resistance. The unit lateral yielding resistance, n_u , is taken as the least value from (a) to (g)

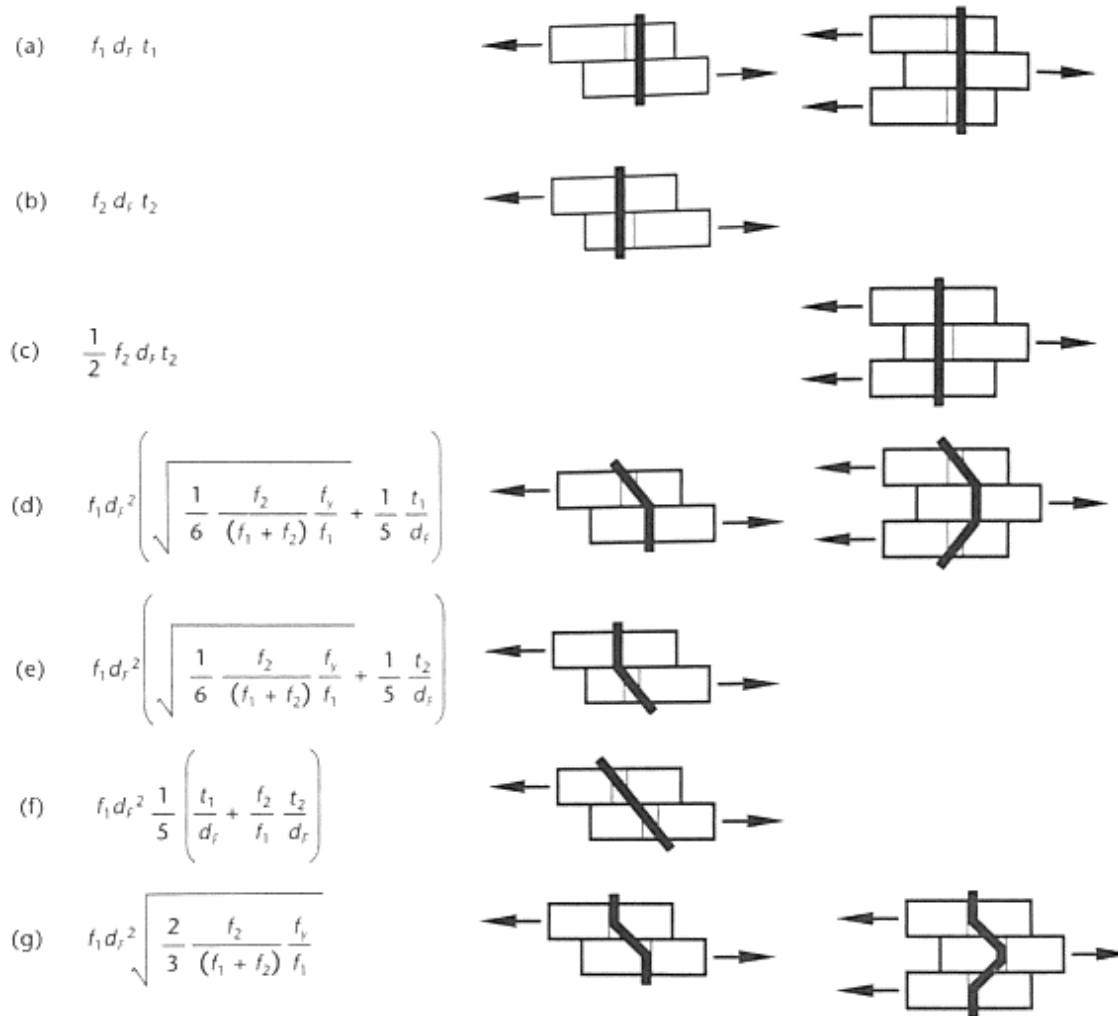


Figure 2.7 Ductile failure modes for wood connections (Adapted from the Canadian Wood Council, Wood Design Manual, 2020)

Where:

f_1, f_2 are the embedment strengths for the side member and main member respectively, MPa

d_f = diameter of the fastener, mm

t_1, t_2 = thickness of the member or the bearing length of the dowel, whichever is lower

f_y = Bending yield strength for the bolt:

For a fastener embedded parallel to the grain, the embedment strength is given by the following equation:

Equation 2.4 Embedment strength for fastener embedded parallel to wood grain (Adapted from Wood Design Manual, 2020)

$$50 G (1 - 0.01d_f) J_x, \quad \text{Eqn. (2.4)}$$

Where, G is the mean relative density as given in table A.12.1 in WDM, and $J_x = 1.0$

For a fastener embedded perpendicular to the grain, the embedment strength is given by the following equation:

Equation 2.5 Embedment strength for fastener embedded perpendicular to wood grain (Adapted from Wood Design Manual, 2020)

$$22 G (1 - 0.01d_f) J_x \quad \text{Eqn. (2.5)}$$

The yield strength for bending of the fastener for ASTM A307 bolts is 310 MPa

For other CSA or ASTM bolts the yield strength is:

Equation 2.6 Bolts yield strength for bolts other than CSA or ASTM bolts (Adapted from Wood Design Manual, 2020)

$$\frac{f_{ym} + f_{um}}{2}, \quad \text{Eqn. (2.6)}$$

Where, f_{ym} and f_{um} are the yield and ultimate bolts strengths, respectively

2.5 Performance of Bolted Wood-Steel-Wood (WSW) Connections with No Reinforcement

Connections are used to transfer load between members. They are also the weakest link in any wood assembly, and therefore it is critical to understand the behaviour of those connections when loaded. In a bolted connection subjected to a load perpendicular to the grain, the strength of the connection is governed by the type of wood, member thickness, number of bolts, and bolts arrangement (WDM, 2020). To study the performance of a bolted WSW connection under bending, Owusu (2019) investigated the effect of bolts arrangement and the number of bolts on the carrying capacity of a connection on a 184 x 362 x 1600 mm black spruce–pine, grade 24f-EX glulam beam. The beam was free on one end and fixed to a column on the other end. The load was applied at the free end until failure of the connection at a rate of 2.0 kN/minute. The beam was connected to the column using a concealed T-stub with a thickness of 12.7 mm and A325M, high strength bolts were used. The test set up is shown in Figure 2.8.



Figure 2.8 Ambient temperature test setup (Adapted from Owusu, 2019)

The study was conducted on two different bolt patterns. In the first pattern, bolt rows were placed symmetrically close to the top and bottom of the beam. In the second pattern, the bottom row bolts

were raised to mid-height to better resist the tensile stresses developed at the top of the beam. Both patterns are depicted in Figure 2.9. In addition, the effect of increasing the number of bolts from 4 to 6 on moment capacity was also investigated.

Upon test completion, it was observed that the 4-bolt connections failed by splitting along the top row of the connection; however, bolts arranged in the second pattern experienced some row shear-out failure. The row-shear out failure of pattern two was due to the yielding of the bottom bolts, which also resulted in the considerable increase in the moment resistance in pattern two, as the connection experienced more ductility. In terms of moment capacity, the placement of the bolts in the tensile zone (pattern two) resulted in a 92% increase in the moment resistance as compared to pattern one.

When 6 bolts were used in the first pattern, the moment capacity was 44 kN.m. Therefore, this is a 66% increase compared to the 4 bolts configuration. It is worth noting that for the 6 bolts arrangement in position 2, the test was not completed due to the failure of the supporting column. The results of this test are summarized in Table 2.3.

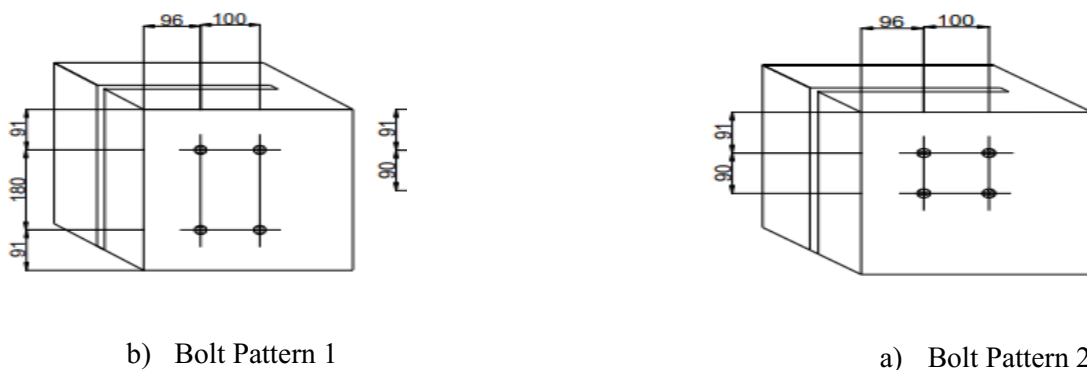


Figure 2.9 Details of bolts arrangement: (a) Bolts arrangements in Pattern 1; (b) Bolt arrangements in Pattern 2 (Adapted from Owusu, 2019)

Table 2.3 WSW connections results summary (Adapted from Owusu, 2019).

Connection Bolt Pattern	Failure Load (kN)	Maximum Moment (kN.m)	Maximum Rotation (kN.m)	Failure Mode
4BP1NA	18.9	26.5	0.012	Splitting
4BP2NA	36.3	50.9	0.042	Splitting/Eventual row shear out
6BP1NA	31.4	44	0.015	Splitting
6BP2NA (test was not completed due to failure of steel column)	38.2	53.5	0.023	-

In another study conducted by Petrycki and Salem (2019), a semi-rigid WSW connection subjected to monotonic load was tested. The study was conducted to determine the strength of the wood connection in the case of a column removal scenario. The test consisted of two symmetrical beams attached to a column placed in between them. The beam-to-column connection was assumed to be perfectly rigid, and each beam was pinned on the other end. The loading was applied monotonically on the column at a displacement rate of 2 mm/min. This rate was to account for the load carried by the lower floor column that is presumed to have been removed. The connection of this test consisted of concealed T-stub connector plate, identical to the one used in the Owusu (2019), and either four or six (2 bolts/row) A325M high-strength structural steel bolts. The parameters studied in this test included the effect of end distance, number of bolts, and use of reinforcing of STS on the moment capacity, and failure mode of the connection. The effect of STS will be discussed in the next section. The end distance of one configuration was four times the diameter of the bolt

(4d), and in the other configuration was five times the diameter of the bolt (5d). The results showed that increasing the end distance from 4d to 5d, while keeping the number of bolts at four increased moment resistance by a factor of 1.9, whereas increasing the end distance to 5d and using six bolts increased the moment resistance by a factor of 1.3. The increase in end distance resulted in higher rotation for both 4 and 6 bolts and hence more ductile behaviour. Moreover, increasing the number of bolts from 4 to 6, while keeping the end distance at 4d increased the moment resistance by a factor of 2.22, whereas increasing the bolts from 4 to 6 while keeping the end distance at 5d increased the moment by a factor of 1.53. Therefore, for this type of bolted connection, the effect of increasing the number of bolts had a greater effect in increasing the moment capacity than increasing the end distance. Further, in all scenarios, the beam failed by splitting. The splitting occurred either between the end of the beam and the first bolts or between the bolts in a row. As will be explained in the next section, the use of STS in bolted connections prevents early splitting failure and considerably increases the moment resistance and the ductility of this type of connection.

2.6 Reinforcement and Retrofitting Techniques of Wood Connections

When timber members are loaded, they are susceptible to many modes of failure in different directions. Although wood has high strength when loaded parallel to grain in both tension and compression, it has very low shear, tensile, and compression resistance when loaded perpendicular to the grain. Bending loading induces perpendicular-to-grain stresses in wood beams and is considered critical and may result in a single failure or the complete failure of the structure. As was shown in the previous section, for a bolted connection, early splitting failure occurred in beams when subjected to bending loading because of low perpendicular-to-grain resistance (Petrycki and Salem, 2019). To strengthen the beams against this failure, reinforcement of the beams may be

necessary. Some of the available reinforcement methods include the use of fiber-reinforced polymer (FRP), Glued-in rods, and self-tapping screws (STS). In this section, past studies on the effect of these reinforcing techniques on increasing the strength of wood beams, particularly when subjected to bending and shear stresses will be presented.

2.6.1 FRP reinforcement

Fiber-reinforced polymers (FRP) are composite materials consisting of fibers that are embedded in a polymeric resin. The fiber provides load-carrying capacity and stiffness, while the polymeric resin protects and transfers the load among the fibers (Hollaway and Teng, 2008). Compared to other materials such as steel, FRP offers the advantage of a high strength-to-weight ratio and the ease of handling (Harte and Dietsch, 2015). Table 2.4 illustrates the different types of fiber materials and their mechanical properties (Hollaway and Teng, 2008). In the past, FRP were used mainly to reinforce concrete structures, but recently have been used to reinforce timber structures. FRP can be utilized as pultruded rods inserted at critical locations or as plates between damaged wood members to increase the load capacity. For internal reinforcement, groves can be made whereby rods and plates are inserted and bonded using adhesive to the wood members. When pultruded plates and rods are used, adhesive bonding is used to embed the FRP with the wood. The adhesive is first applied to the wood and then FRP is placed on the wood under pressure. It is worth noting that the adhesive plays a critical role as it must bond with both the wood and the FRP. There are four types of adhesives used. These include epoxies, polyurethanes, polyesters, phenolics, and amino plastics (Broughton and Hutchinson, 2003). Due to their good gap-filling properties, thixotropy, and minimal curing shrinkage, two-part cold-cure epoxy adhesives have typically been found to be the most effective for on-site bonding (Pizzo and Smedley, 2015). If they are to be

used as external reinforcement, FRP plates are bonded to the wood at critical locations (Harte and Dietsch, 2015).

Table 2.4 Strength properties for various fibres and polymers (Adapted from Hollaway and Teng, 2008).

Material	Modulus of Elasticity (GPa)	Tensile Strength (MPa)	Failure Strain (%)	CTE ($10^{-6} \text{ }^{\circ}\text{C}^{-1}$)	Density (g/cm^3)
E-glass	70-80	2000-4800	3.4-4.5	5.0-5.4	2.5-2.6
Carbon (HM)	390-760	2400-3400	0.5-0.8	-1.45	1.85-1.9
Carbon (HS)	240-280	4100-5100	1.60-1.73	-0.6 - -0.9	1.75
Aramid	62-180	3600-3800	1.9-5.5	-2.0	1.44-1.47
Basalt	82-110	860-3450	5.5	3.15	1.52-2.7
Polymer	2.7-3.6	40-82	1.4-5.2	30-54	1.10-1.25

Notes: CTE: Coefficient of thermal expansion; HM: High modulus; HS: High strength.

FRP reinforcement in bending

The use of FRP to reinforce beams under bending loads has been widely investigated (Harte and Dietsch, 2015). The reinforcement can be in the form of pultruded rods, or plates. Rods are inserted and bonded internally at locations with high tensile or compressive stresses, whereas plates can be placed externally at the tension side of members (Harte and Dietsch, 2015). It is worth noting that when FRP are used externally, they are only placed at the tension side of the member, and not on the compression side to avoid buckling failure of the plates. Nowak et al. (2013) have conducted a study to investigate the effect of Carbon Fiber Reinforced Polymer (CFRP) on the strengthening of sawn timber and glulam beams. It was shown that the use of only 1.5%-2% of CFRP reinforcement increased the bending strength by 90 and 100% respectively. Further, it was shown

that the ductility of the beam increased as the load was increased, due to the yielding of the reinforcement at high stresses. Also, the use of CFRP resulted in less variation of wood properties during loading as compared to unreinforced beams. Similarly, Johns and Lacroix (2000) and Rafter and Harte (2011) have studied the use of Glass Fiber Reinforced Polymer (GFRP) reinforcement on the bending behaviour of beams. Like CFRP, a small percentage of reinforcing resulted in a significant increase in bending strength, and less variation of properties. That being said, the stiffness of the beam was less than that of CFRP reinforcement due to the lower stiffness of GFRP compared to CFRP. With GFRP, the beams showed little ductility with respect to load; however, ductility increased as more reinforcement was added (Rafter and Harte, 2011).

FRP reinforcement for perpendicular to grain tensile loading

In addition to bending, Coureau et al. (2001) investigated the effect of FRP reinforcement on the perpendicular-to-grain tensile strength of wood beams. Beams experience high perpendicular-to-grain tensile stress at notches, holes, and curve-shaped beams. GFRP plates were used to reinforce notched glulam beams. Beams reinforced with a 43 mm GFRP plate achieved a 103% increase in strength as compared to unreinforced beams. Increasing the width of the GFRP plate to 85 mm resulted in a 187% increase in strength as compared to the unreinforced beams (Coureau et al., 2001). Upon failure of the notches with increased loads, delamination failure mode was observed at the FRP plates. Further, Jockwer (2015) investigated the debonding behaviour of GFRP rods when placed in two configurations: In the first configuration, reinforcements were placed perpendicular to the grain and in the second, reinforcements were placed at 45 ° to the grain. Figure 2.10 shows both configurations. In the first configuration, it was observed that the debonding took place at the lower portion of the beam due to the lower laminate area as compared to the top of the beam. When CFRP were placed at a 45° angle, debonding occurred at the top of the beam near the

support, as a result of bearing stresses between the wood, which has a low perpendicular compression resistance, and the CFRP reinforcement which has a high parallel to grain tensile resistance. Although the load-carrying capacity of the beams was increased, both configurations did not prevent cracking at the notched location.

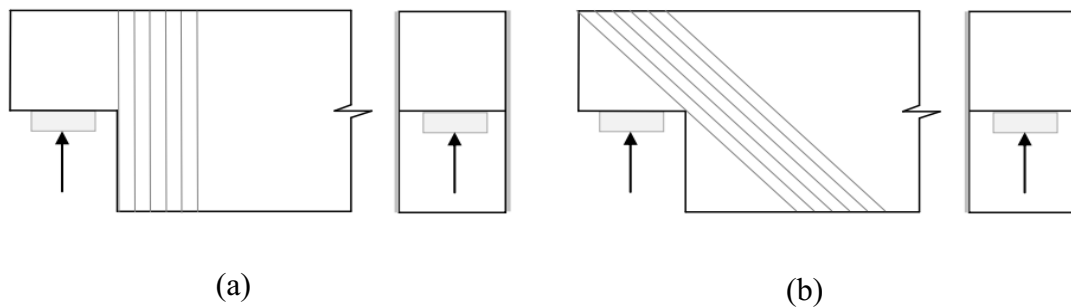


Figure 2.10 FRP-reinforced specimens' detail: (a) FRP Placed Perpendicular to grain; (b) FRP placed at 45° angle to grain (Adapted from Jockwer, 2015).

FRP use for shear reinforcement

Moreover, FRP reinforcement can be used as shear reinforcement at regions of high shear stress. The reinforcement can be internal FRP rods or external plates. For internal FRP rods, the shear reinforcement is placed at different angles, β , perpendicular to the grain as shown in Figure 2.11. Studies have shown that for high shear stresses, placing the rods at 45° to the grain is more effective than placing them perpendicular to the grain (Blass and Bejtka, 2014). Triantafillou (1997) studied the reinforcement effect of GFRP on medium and small-scale glulam beams. In this study, the FRP rods were placed internally at an angle, $\beta = 90^\circ$ to the grain. For this configuration, the load-carrying capacity of the beams was increased by 50%. On the other hand, Widmann et al. (2012) conducted a series of tests on full timber beams with existing cracks reinforced internally with CFRP rods at an angle $\beta = 45^\circ$. The results of the tests indicated that the reinforcement increased

the shear strength and stiffness of the damaged beam significantly, however, the original strength and stiffness of the beam were not restored.

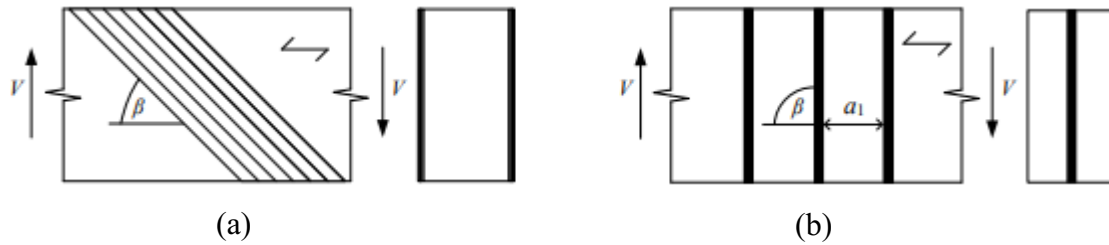


Figure 2.11 FRP-reinforced specimens' detail: (a) FRP placed at angle 45° to grain; (b) FRP placed at angle 90° to grain (Adapted from Widmann et al., 2012).

2.6.2 Glued-in rods

Glued-in rods (GiR) are another effective way to reinforce or retrofit timber members. Like FRP, GiR are used to reinforce timber members in weak zones, such as at locations of high tensile stresses perpendicular to the grain, bending, and shear stresses. Although GiR have been used to strengthen timber structures since the 1980s, there exist no design criteria or design approach in many design codes (Steiger et al., 2004). GiR reinforcement is usually used with softwood glulam with metric threaded rods. The most common way of gluing the rod into the wood is by drilling a hole that is 1 to 4 mm larger than the rod into the wood. The adhesive is then injected into the hole and the rods are then set into the holes (Harte and Dietsch, 2015). Another method is to drill another hole perpendicular to the hole where the rod is to be placed and adhesive is injected until glue pours out of the hole that contains the rod (Harte and Dietsch, 2015). Figure 2.12 shows the various methods involved in placing GiR in wood members. The most used adhesive is Phenol-Resorcinol-formaldehyde (PRF), epoxies, and polyurethanes (PUR). It's worth noting that epoxy bonds very

well with steel and wood, thereby making wood the weakest link in the GiR connection (Harte and Dietsch, 2015).

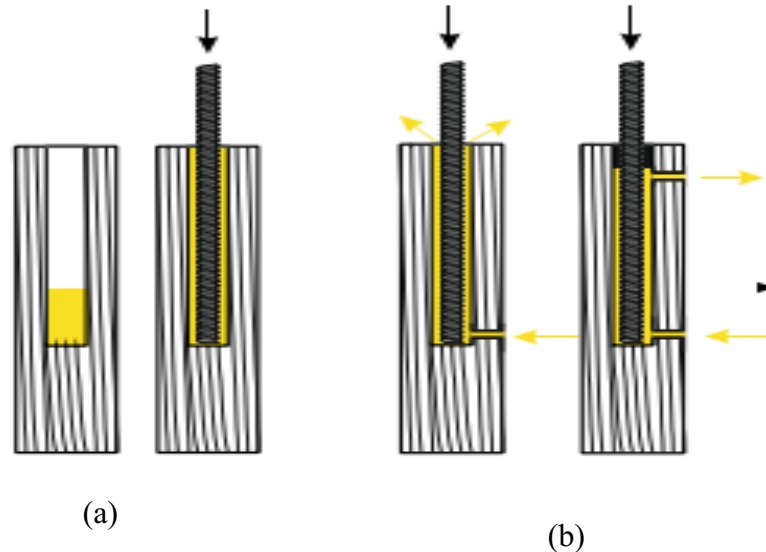


Figure 2.12 Variation of Placing GiR into Wood: (a) a hole is drilled vertically and glue is injected; (b) Glue is injected into a hole perpendicular to where the rod is to be placed (Adapted from Steiger et al., 2015).

Failure in GiR connection can occur in different modes, including material failure of the rod, buckling of the rod, splitting failure of the wood, and pull-out failure of the rods, as a result of a failure of adhesive at either steel-adhesive interface, wood-adhesive interface or cohesive failure of the adhesive (Harte and Dietsch, 2015). Most of the literature available focuses on the pull-out resistance of rods when loaded axially parallel to the grain (Harte and Dietsch, 2015). The pull-out strength in relation to the diameter of the rod and the anchorage length was studied experimentally by Riberholt (1988), EN 1995-2 (2003), GIROD project (2002), DIN1052:2008-12 (2008), Feligioni, et al., (2003), Steiger et al. (2007), and NZ Timber Design Guide (2007). Figures 2.13 and 2.14 illustrate the pull-out strength of a single axially loaded GiR with varying anchorage length and rod diameter, respectively. Epoxy adhesive was used in all the experiments

shown in Figures 2.13 and 2.14. As evident from Figures 2.13 and 2.14, pull-out strength increases linearly as the anchorage length, and the diameter of the rod is increased. Further, the effect of wood density on pull strength was investigated in studies by Riberholt (1988), EN 1995-2 (2003), GIROD project (2002), DIN1052:2008-12 (2008), and Feligioni et al., (2003). The conclusion of whether the density had any effect on the pull-out strength varied between studies. For instance, most studies including one by EN 1995-2 (2003) showed that density has no effect on the pull-out strength. Other studies conducted by Riberholt (1988), and Feligioni et al., (2003) showed that the pull-out strength increases linearly as density is increased. A summary of the findings of the different studies is shown in Figure 2.15.

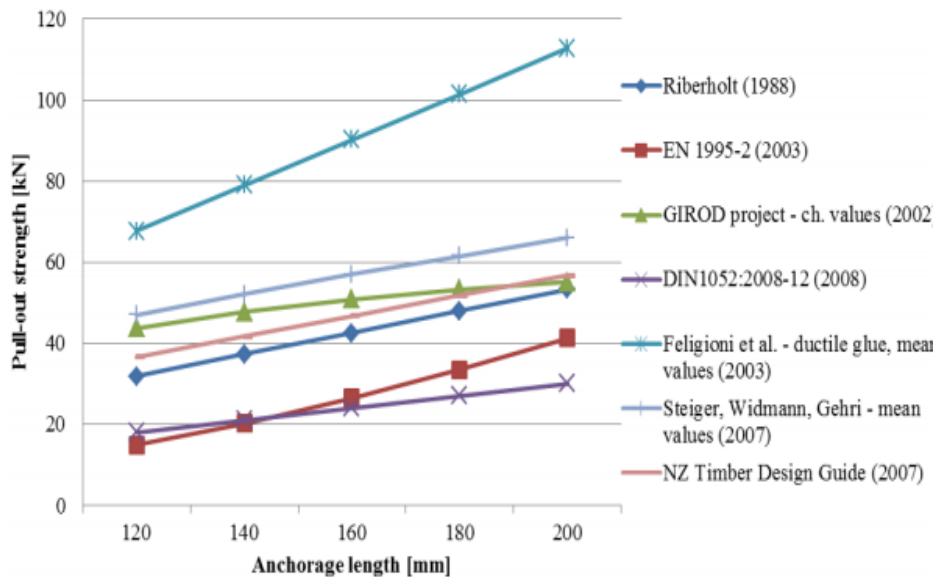


Figure 2.13 Anchorage length vs Pull-out strength for GiR connection from different studies

(Adapted from Harte and Dietsch, 2015).

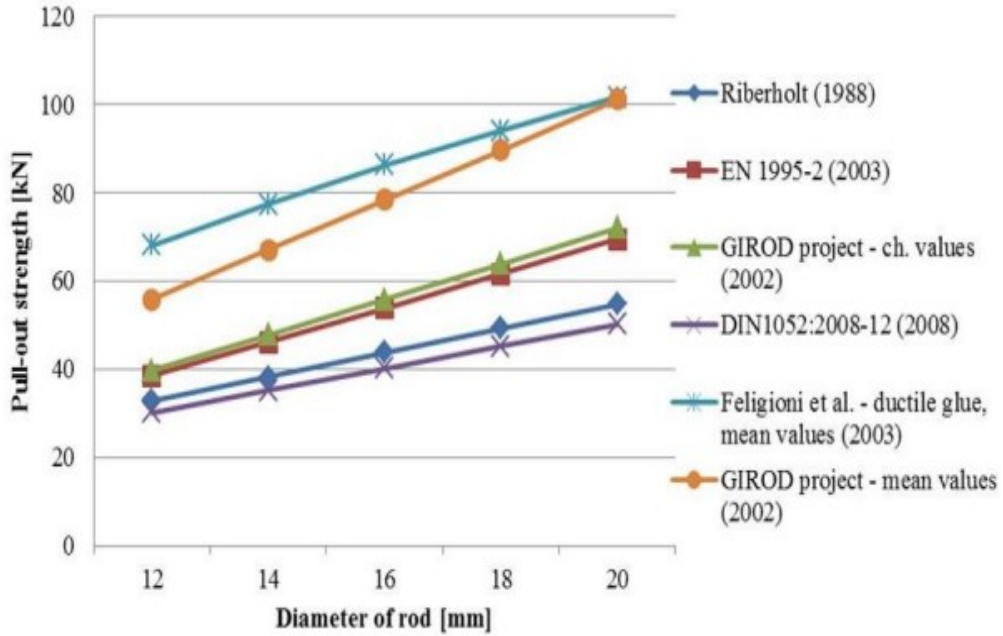


Figure 2.14 Rod diameter vs Pull-out strength for GiR connection for different studies (Adapted from Harte and Dietsch, 2015).

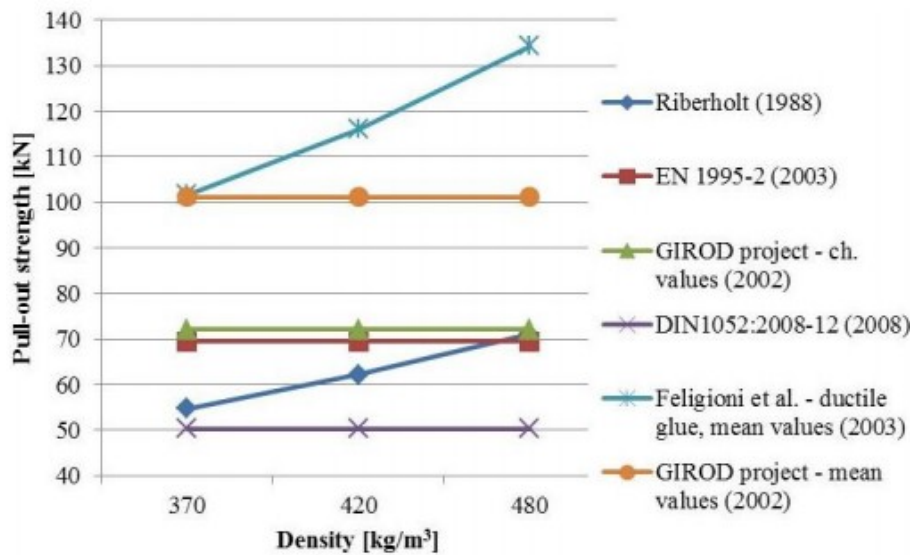


Figure 2.15 Density vs Pull-out strength for GiR connection for different studies (Adapted from Harte and Dietsch, 2015).

GiR use for tension perpendicular to grain reinforcement

As mentioned earlier, timber performs poorly when loaded in tension perpendicular to the grain. This type of loading arises in beams that are notched, curved, or have holes. Similar to the use of rebars in concrete, GiR may be utilized in those high-stressed regions to overcome this deficiency. In a study conducted by Steiger et al. (2004), GiR was observed to limit initial cracking, or if the members are already cracked it stops the crack propagation. It was also observed that GiR restored the original load-bearing capacity in damaged beams due to cracks. Chapter 6.8 of EN 1995-1-1 outlines the design rules for GiR for perpendicular- to-grain tensile stresses. The code assumes that wood has no tensile resistance perpendicular to the grain and cracking already occurred.

GiR use for shear reinforcement

GiR reinforcement can also be used in regions with high shear stresses. Their use can prevent shear cracks or strengthen already cracked beams by restoring some load-bearing capacity. Steiger et al. (2015) investigated the use of STS and GiR to overcome shear deficiency in a series of numerical and experimental trials. It was concluded that placing GiR at a 45 ° angle from the beam axis resulted in the most efficient shear resistance. The use of GiR also provided the wood members with higher stiffness. Although many studies have been conducted on the use of GiR for shear, no design guidelines exist in any code.

GiR use for bending reinforcement

When it comes to bending, the available literature outlines the use of GiR in the form of FRP. The use of FRP reinforcement in bending was discussed in the previous section.

2.6.3 Self-tapping Screws

In this section, the properties and types of fully threaded STS and the effect of using fully threaded STS on the load carrying of the connection will be investigated and compared to connections without reinforcement. Figure 2.16 illustrates a type of STS screw used for reinforcement. This screw is a fully threaded ASSY® VG structural screw provided by MTC Solution and is approved by building codes in Canada.

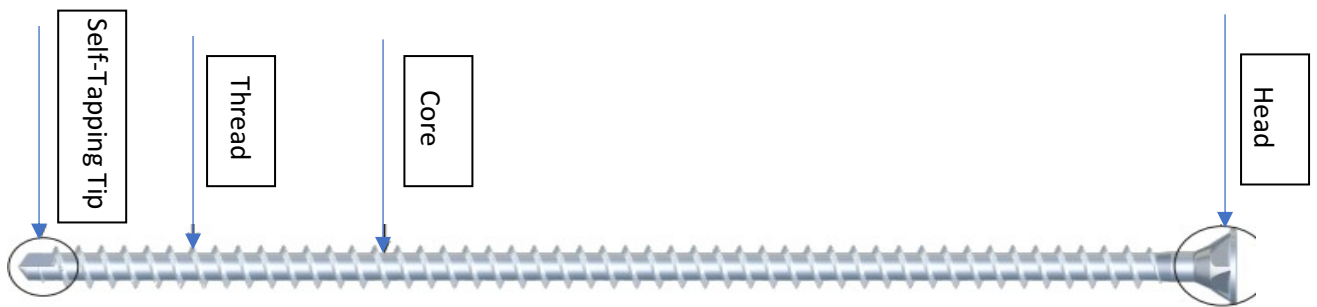


Figure 2.16 Fully threaded ASSY® VG STS (Adapted from MTC Solutions).

As mentioned earlier, wood has a low perpendicular-to-grain tension and shear resistance, which can lead to early brittle failure due to splitting in a bolted connection. The use of fully threaded STS perpendicular to the grain will make up for this shortcoming as the shear and tensile forces will be carried by the STS instead of the wood. Also, the use of fully threaded STS results in a ductile failure, as the STS begins to yield under loading. As was shown in the experimental study conducted by Owusu (2019), bolted connection specimens failed mostly by splitting, and some experienced row-shear out failure. The use of reinforcing STS was recommended by Owusu (2019) to reinforce the connection against these brittle failures.

Further, as a factor of safety to prevent brittle failures, the Eurocode reduces the effective number of bolts present in a connection (Eurocode 5, 2004). For example, if 10 bolts were used in the

connections, the effective number of bolts is reduced to 6.67 to account for the early splitting of the bolted connection, Table 2.5. On the other hand, if reinforcing is provided, it is expected that no early splitting failure will occur and hence all the bolts in the connection are effective, meaning if 10 bolts were used with reinforcing bars, 10 bolts are effective as well.

Table 2.5 Effective number of bolts for reinforced vs. unreinforced connections (Adapted from EN1995-1-1, 2004).

Number of fasteners in connection	1	2	3	4	5	6	7	8	9	10
Net effective fasteners in connection	1	1.56	2.26	2.92	3.57	4.21	4.84	5.46	6.07	6.67

Effect of STS on load carrying capacity and ductility

To understand the effect of STS on load carrying and ductility on wood members, Blaß and Schädle, (2011) conducted an experiment on a glulam beam with dowel-type connections reinforced with STS and subjected to tensile load applied parallel to the grain. Three different geometries of beams, with different numbers of bolts, were tested. In the first geometry, no STS reinforcement was used (M1 to M4); the second geometry (M5 to M6) consisted of ten STS, and the third variation consisted of twenty STS (M7 to M10). Figure 2.17 illustrates the three different variations. The results, including ductility and load-carrying capacity, were compared to that of an unreinforced beam. Figure 2.18 shows the load-displacement curve for the three different variations. From the graph, it is evident that the unreinforced beam (M1 to M4) experienced very little ductility. When ten STS were used (M5 to M6), the ductility of the specimen increased, but

when twenty STS were used (M7 to M10), the beam experienced a significant increase in ductility as well as increased load-carrying capacity.

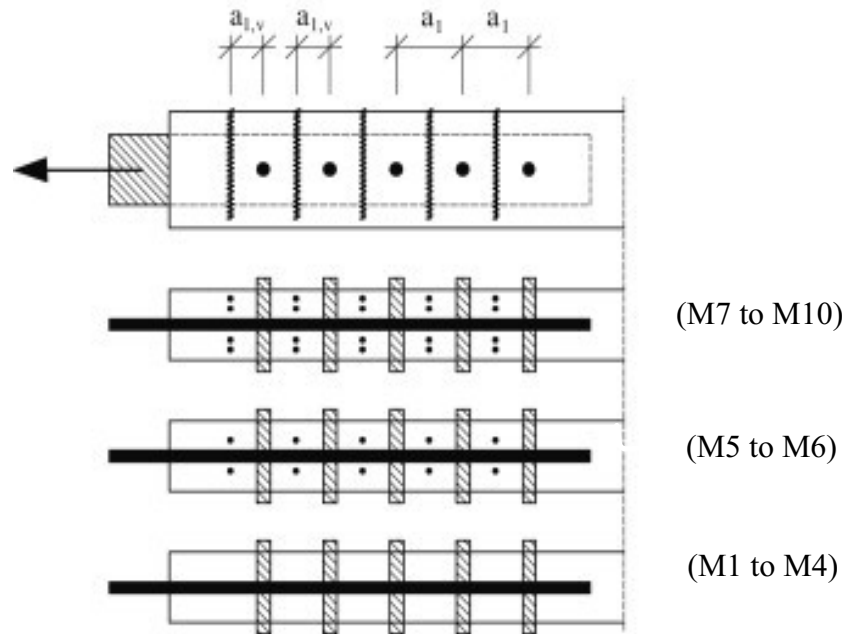


Figure 2.17 Geometry of specimens tested (M1 to M10), including the number of reinforcing STS (Adapted from Blaß and Schädle, 2011).

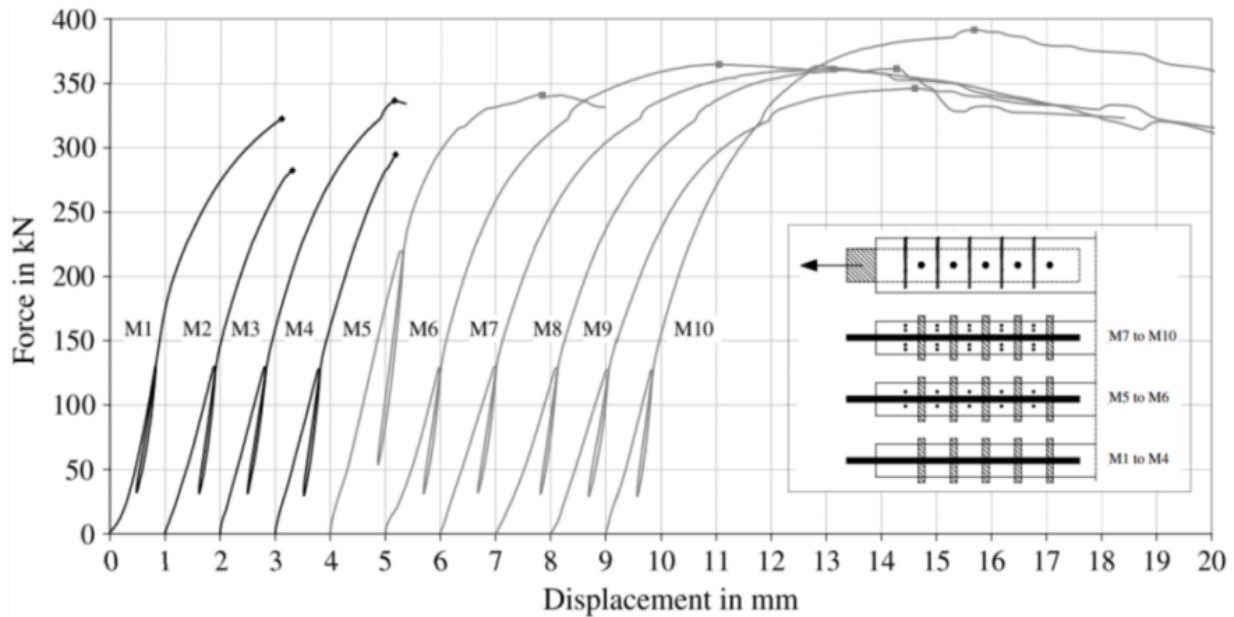


Figure 2.18 Load-Displacement curve for a beam subjected to parallel to grain tensile load (M1-M4) non-reinforced beam; (M5 to M6) reinforced beam with no contact between dowels and STS; (M6 to M7) reinforced beam with contact between dowels and STS (Adapted from Blaß and Schädle, 2011)

The effect of STS on ductility and strength for a bolted glulam connection subjected to bending was also investigated by (Lam et al., 2008). In this study, three (3) beam configurations were tested: unreinforced, reinforced, and retrofitted. The beam and column materials were 24f-E Douglas fir/Larch Glulam with dimensions of 304 x 130 mm. The STS, 300 mm in length and 8 mm in diameter, were placed perpendicular to the grain in the beam. A slotted-in plate was used to connect the beam and column. The beam was subjected to monotonic loading. The test set up of the experiment is shown in Figure 2.19.



Figure 2.19 Bolted connection Test Set Up (Adapted from Lam et al., 2008).

The maximum moment resistance for the unreinforced connection was 31.49 kN.m with a maximum rotation of 2.97 °. It was observed that the beam's moment capacity quickly decreased with the formation of cracks. On the other hand, the reinforced beam had a moment capacity of 65.88 kN.m with 16.59 ° rotation, and the retrofitted beam had a moment capacity of 58.85 kN.m with 13.29 ° rotation. Therefore, the use of STS in the reinforced beam resulted in a moment capacity increase by a factor of 2.1, and the use of STS in the retrofitted beam increased the moment resistance by a factor of 1.87. Also, as evident from the maximum rotation values, the ductility of the beam was greatly improved with the use of STS. The failure mode of the unreinforced, reinforced, and retrofitted beam is illustrated in Figure 2.20.

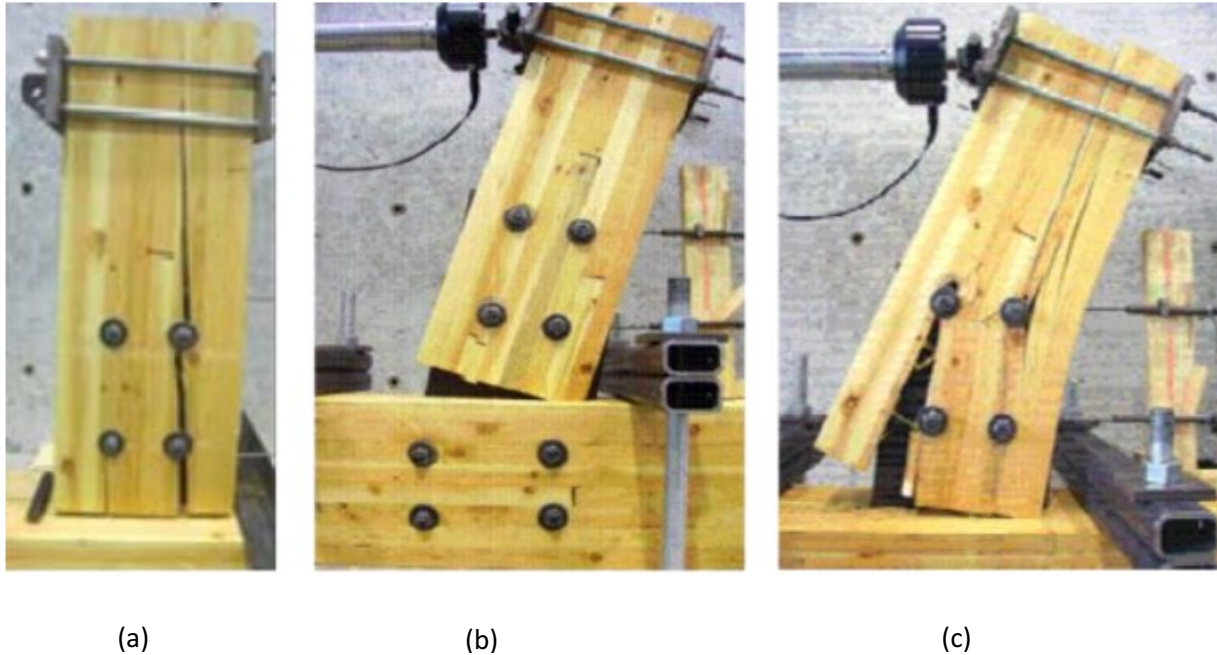


Figure 2.20 Test configurations: (a) Unreinforced beam; (b) Reinforced beam; (C) Retrofitted beam (Adapted from Lam et al., 2008).

Placement configuration of STS with respect to bolts

Many codes, including the Eurocode 5, and the NBCC (2020) specify the edge distance and end distance for the bolts. However, there are no prescribed provisions for the placement of the reinforcing STS. Lam et al. (2010) investigated the effect of bolt edge distance and the placement configuration of STS on the moment carrying capacity of 24f-E Douglas Fir glulam beam to column connection. A 9.5 mm steel plate was slotted into the beam and used to connect the beam to the column. Both the beam and column had a dimension of 130 mm x 304 mm. A load was applied at the free end of the beam. Figure 2.21 shows a general setup of the test. The test was carried out with the column member placed on the ground and the load was applied horizontally.



Figure 2.21 Test setup (Adapted from Lam et al., 2010).

Three different bolts-STs arrangements were studied. In the first arrangement, A-CR, the bolts had an edge distance of 94.5 mm, and three STS were placed with equal spacing of 135 mm. For the B-CR and C-CR configurations, the edge distance was reduced to 49.5 mm, and five STS were placed. In the C-CR tests, the STS were bearing directly on the bolts. The arrangement of STS of each configuration is shown in Figure 2.22.

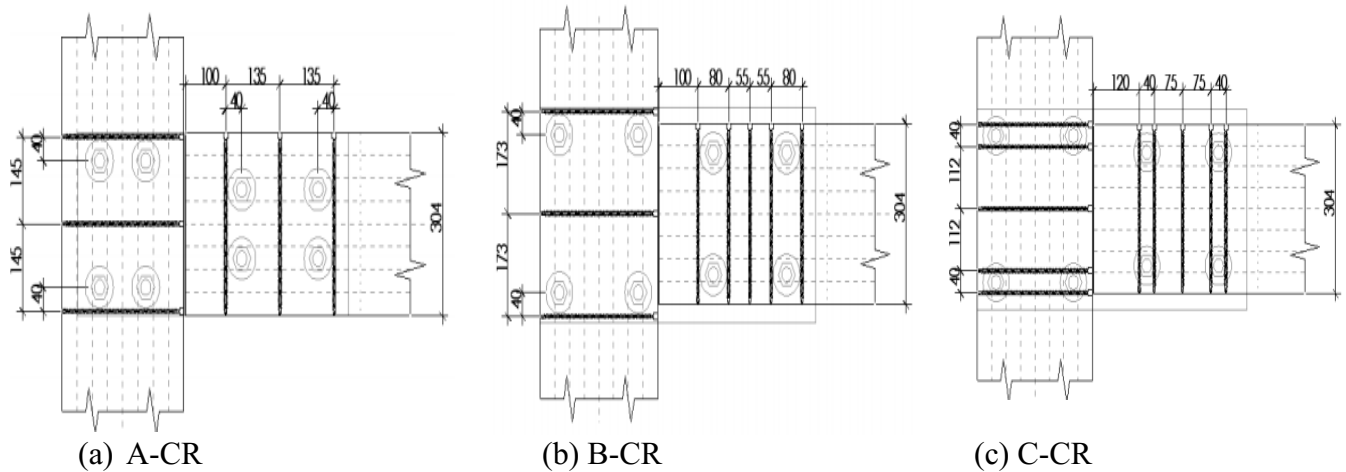


Figure 2.22 The different STS-bolt arrangements studied: (a) A-CR; (b) B-CR; (c) C-CR

(Adapted from Lam et al., 2010).

The results of this study indicated that the reduced edge distance and bearing of the STS on the bolts resulted in an increase in the moment capacity of the connection. When the edge distance was reduced by half, the moment resistance of the connection increased by a factor of 1.3. Also, the placement of the STS screws directly on top of the bolts resulted in slightly higher moment resistance. The max moment for A-CR was 76.64 kN.m, 103.83 kN.m for B-CR, and 105.90 kN.m for C-CR. The slight increases in the moment strength when STS were placed directly on top of the bolts can be attributed to the increases in the embedment strength. The moment-rotation graph for each connection configuration is shown in Figure 2.23. The use of STS was also observed to prevent early splitting.

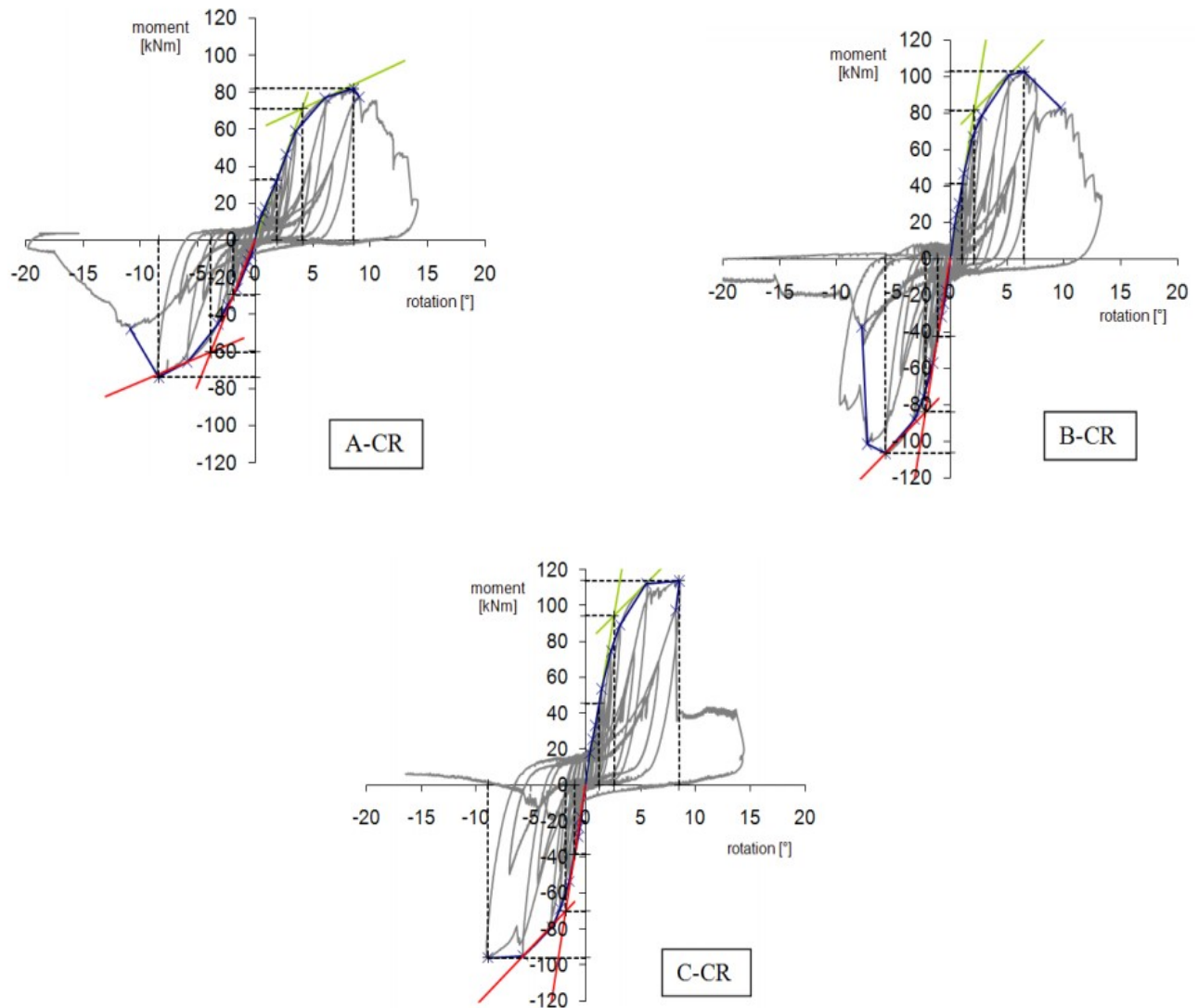


Figure 2.23 Resulted moment-rotation curves (Adapted from Lam et al., 2010).

Echavarria (2007) conducted an experimental investigation on a reinforced, and unreinforced timber beam with a single bolt of 15.9 mm (5/8") subjected to tensile load parallel using a universal testing machine. The specimen had a moisture content of 12%. The reinforcement STS used was a GRK fastener with a length of 90 mm, a diameter of 6 mm, and a threaded length of 70 mm. The

reinforcement screw was placed at a distance equal to the diameter of the bolt. A sketch of the connection configuration is shown in Figure 2.24.

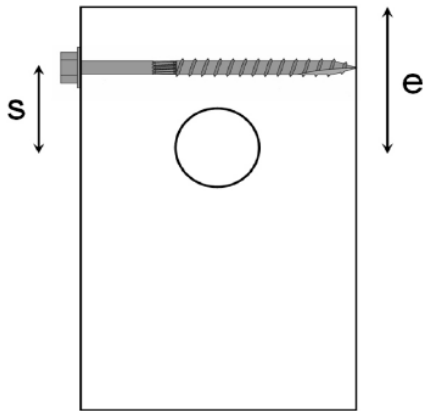


Figure 2.24 Utilized connection configuration (Adapted from Echavarría, 2007).

The effect of the loaded end distance of the bolts, when used with the reinforcement, was also studied. The summary of the load-carrying capacity of the reinforced connection as compared to the unreinforced connection and accounting for the end distance is summarized in Table 2.6.

Table 2.6 Results summary for reinforced vs. unreinforced connections (Adapted from Echavarría, 2007).

Bolt diameter (mm)	e/d	Thickness (mm)	Reinforced load-carrying capacity (kN)	Non-Reinforced load-carrying capacity (kN)	Ratio of Reinforced and Non-Reinforced load-carrying capacity (%)
15.9	2	38	9.8	4.4	120%
15.9	3	38	12.7	12.1	4.7%
15.9	4	38	17.4	17.3	0.8%
15.9	5	38	18.4	18.2	1.0%

As seen from the results, the STS were most effective when the end distance of the bolts is shortest (e/d). This suggests that the use of STS may result in a more compact and efficient connection, without the need to provide large end distances. The load-carrying capacity for the reinforced connection increases by a factor of 2.2 as compared to the un-reinforced connection. Consistent with other studies, the reinforced connection resulted in a more ductile behaviour as compared to un-reinforced, as shown in the load-displacement curve in Figure 2.25. All in all, reinforcement resulted in increased load-bearing capacity, smaller joint configuration, fewer cracks, and higher ductility.

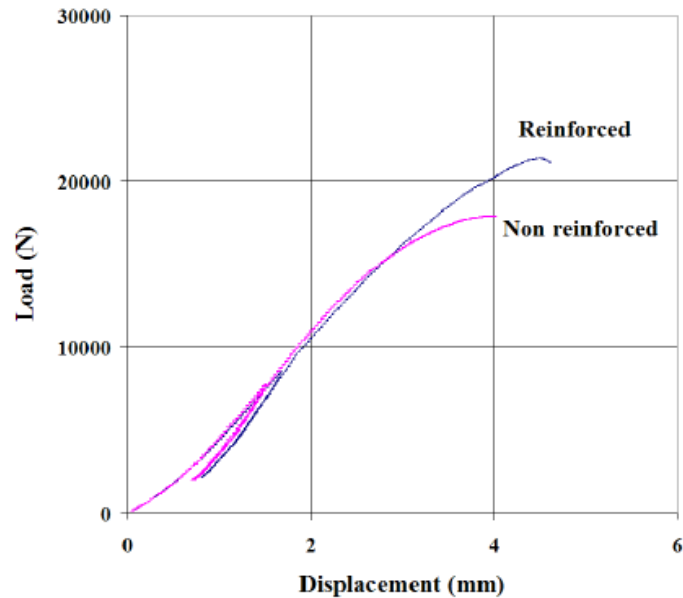


Figure 2.25 Resulted load-displacement curve (Adapted from Echavarría, 2007).

STS effect on moment capacity, and failure behaviour in column removal scenario

In many design guidelines, beam-to-column connections are assumed to be pinned, and hence no moment carrying is assumed. One disadvantage of this assumption is that in case a column is damaged from a lower or above storey as a result of fire, or any other accidental event, the pinned connection will not be able to resist the extra loading as a result of this failure (Petrycki and Salem 2019). One way to mitigate this risk is to use a rigid or semi-rigid beam-column connection. In a study conducted by Petrycki and Salem (2019), the effect of STS on the moment carrying capacity, and failure mode of a glulam beam in a column removal scenario was studied. The general set up of the test consisted of two symmetrical glulam beams connected to a column placed between them. The beam-to-column connection for both beams was assumed to be perfectly rigid, and the ends of each beam were pin supported. A general setup of this experiment is shown in Figure 2.26,

including the dimension of the specimens, and the location of LVDT (to measure rotations and deflection).

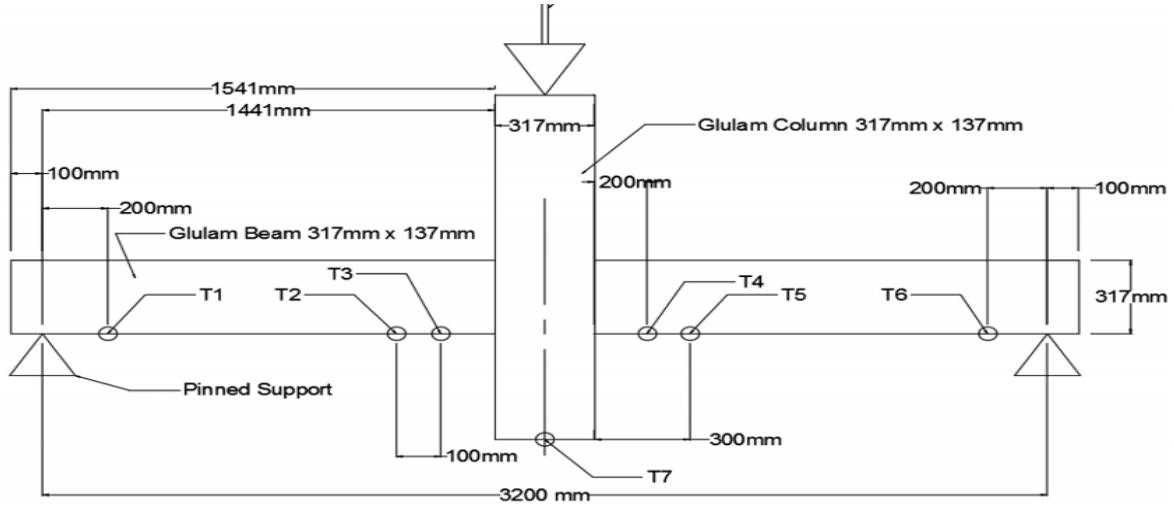


Figure 2.26 General test setup (Adapted from Petrycki and Salem, 2020)

The loading was applied monotonically on the column at a displacement rate of 2 mm/min. This rate was to account for the load carried by the lower floor column that is presumed to have been removed. The connection of this test consisted of a concealed T-stub connector plate identical to the one used in Owusu (2019) research (explained above), and either four or six bolts. A325M high-strength structural steel bolts reinforced with six (6) SWG ASSY VG Plus CSK STS of 300 mm in length and diameter of 8 mm were used. The dimension and placement of the STS with respect to the bolts and the T-plate are shown in Figure 2.27. A similar test was conducted but without the use of reinforcement. Upon the completion of the tests, it was observed that the STS effectively increased the moment carrying capacity, improved ductility, and prevented early cracking from occurring in the beam. The moment – deformation graph for the unreinforced and reinforced beam with 4, and 5 bolts (4b4d, 4b5d), as well as the reinforced beam is shown in

Figures 2.28 and 2.29, respectively. As evident from the graph, STS increased the moment capacity by a factor of 2.4 for the connection configuration with 4 bolts with an end distance of 4d and 1.3 when 6 bolts were used with an end distance of 4d. Further, the moment capacity increased by a factor of 2.0 for the connection configuration with 4 bolts with an end distance of 5d, and by a factor of 1.5 when 6 bolts were used with an end distance of 5d.

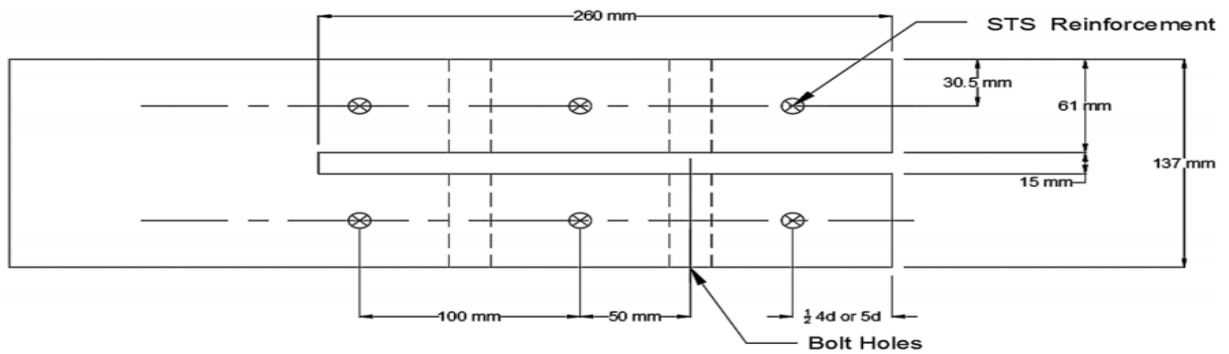


Figure 2.27 Dimensions and placement of the STS (Adapted from Petrycki and Salem, 2020)

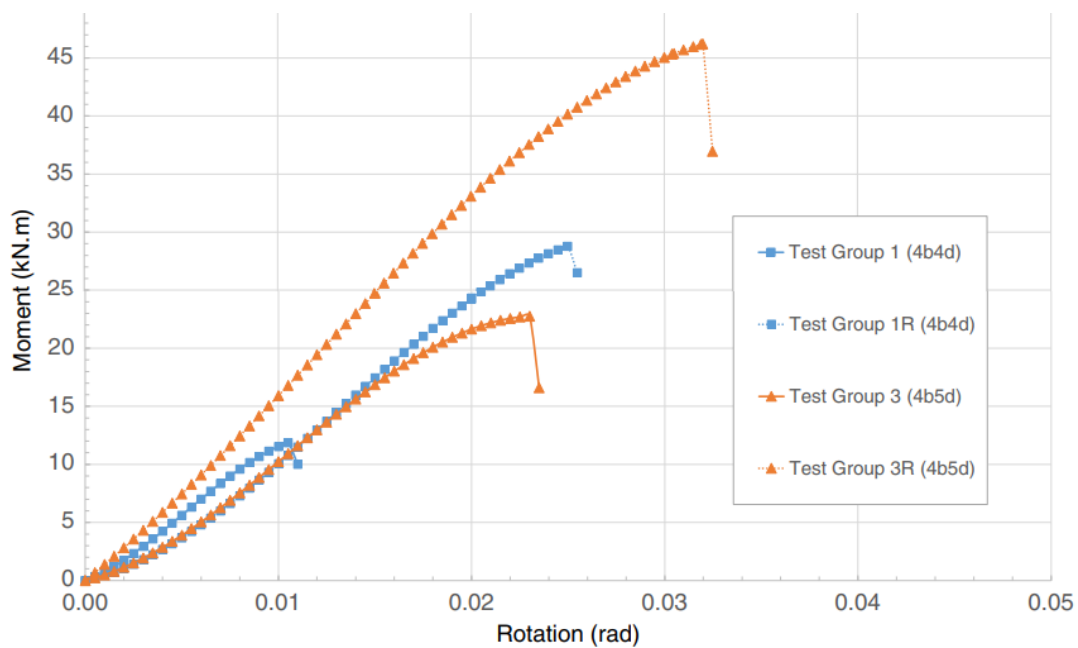


Figure 2.28 Moment-deformation graphs for unreinforced connections (Adapted from Petrycki and Salem, 2020)

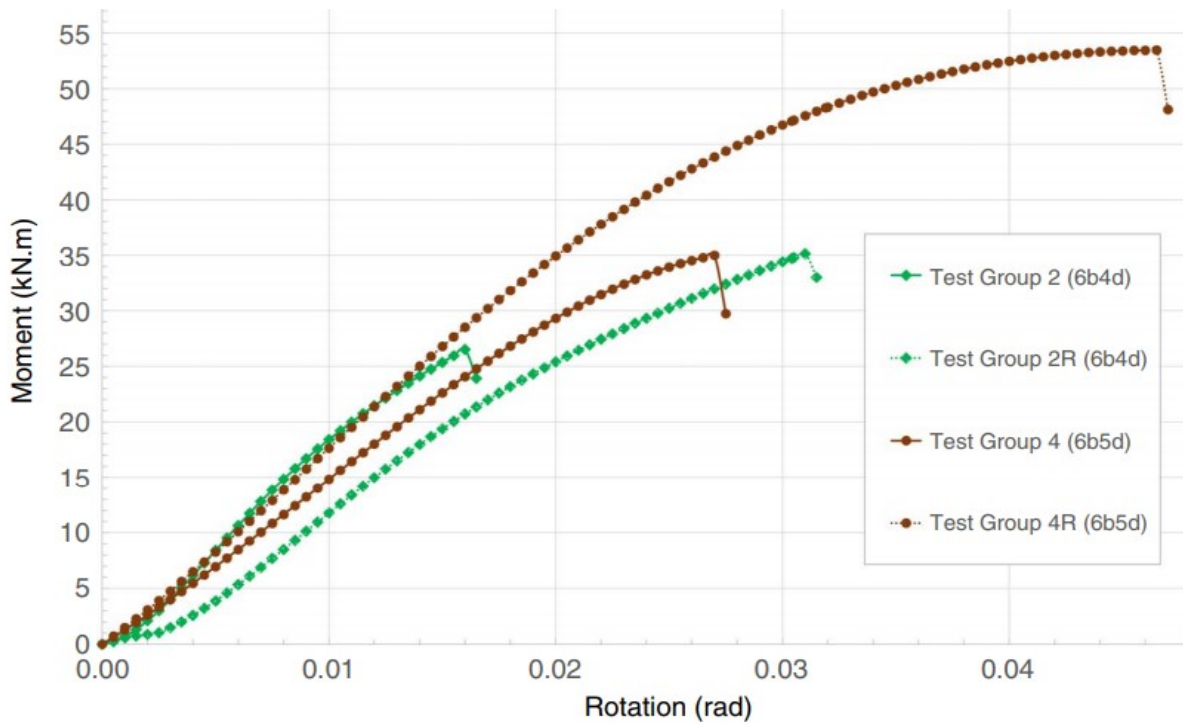


Figure 2.29 Moment-deformation graphs for reinforced connections (Adapted from Petrycki and Salem, 2020)

Also, STS provided much higher ductility as compared to unreinforced beams. The unreinforced beam exhibited cracking and brittle failure when the number of bolts was increased from 4 to 6. On the other hand, when the number of bolts increased from 4 to 6 in the reinforced connection, the beam exhibited more ductile behaviour, indicating that STS dissipated the energy of the connection that caused the brittle failure in the unreinforced beam. The unreinforced beam failed mainly by splitting along the bolt's rows, without any significant row-shear out. On the other hand, the mode of failure of STS in this experiment was primarily row-shear out. When the section was first loaded, STS prevented any premature splitting cracks from occurring. However, as the loading increased, tensile stresses were transferred to the STS, resulting in yielding and ultimate failure of the STS. The yielding of the STS imposed a high additional load on the specimen, which ultimately

led to a brittle failure in a form of row-shear out. This indicates that the STS absorbed all the early splitting stresses until ultimately yielding and resulting in the row-shear out failure. The failure mode of the connection configuration with 4 bolts of 4d and 5d respectively is shown in Figure 2.30. The order of failure that took place is also numbered.

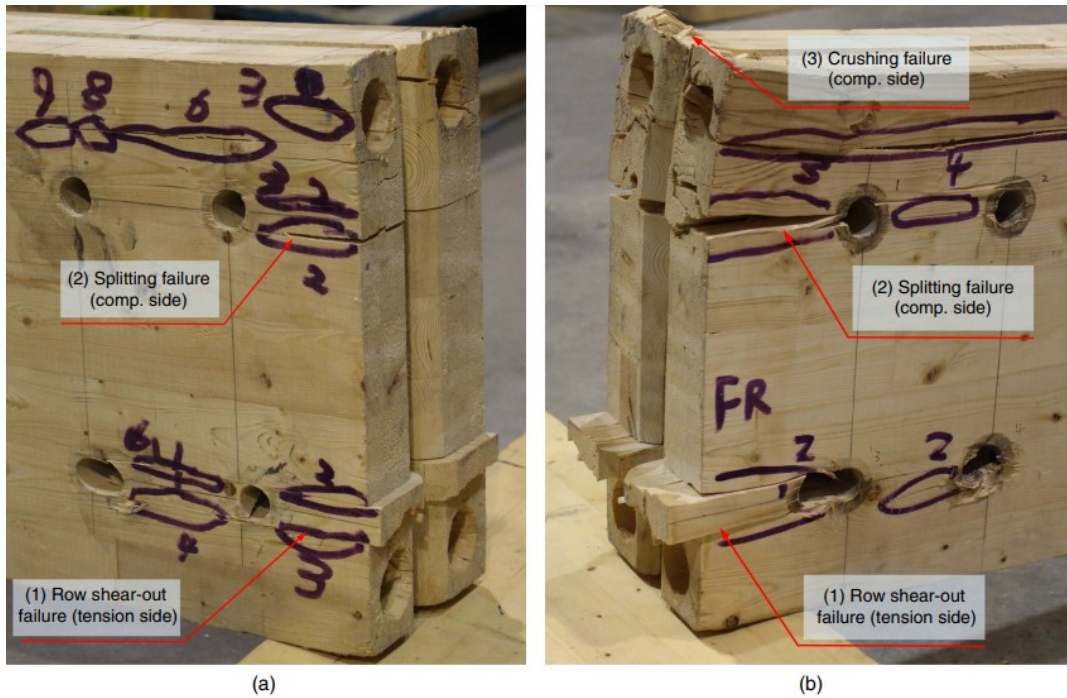


Figure 2.30 Failure modes of STS-reinforced connections: (a) 4d; (b) 5d (Adapted from Petrycki and Salem, 2020).

2.7 Wood Properties at Elevated Temperatures

2.7.1 Wood design for fire safety

Wood products offer a sustainable and energy-efficient choice for building materials. However, one of the main shortcomings of wood products is their combustible behaviour. Ensuring that members can withstand applied loads in both ambient and fire conditions is part of an appropriate design for wood structures. Although wood products have adequate strength properties, fire resistance is usually the limiting design parameter. For example, many codes including the

National Building Code of Canada (NBCC) restrict the use of wood products in high-rise structures. Subsection 3.2.2 of division B of the NBCC (2020) specifies the maximum number of stories for wood construction as 6 (six). This limited number of storeys can be partially attributed to the relatively limited research on the behaviour of wood when exposed to fire. NBCC (2020) requires all wood structures to have a fire-resistance rating (FRR), which is defined as the time a component can resist fire before failure. FRR varies depending on the occupancy, the size of the structure, and accessibility to firefighters. FRR ranges from 0 to 120 minutes, with most buildings commonly having an FRR between 45-60 minutes (NBCC, 2020).

The fire-resistance of wood elements can be calculated in accordance with Annex B of CSA O86-19. This method was published in 2014 and applies to sawn timber, glulam, CLT, and SCL (WDM, 2017). Known as the "reduced (or effective) cross-section", this method calculates the fire resistance by considering the strength of the residual cross-section after charring or burning of the section. As will be discussed further in this literature, charring is the mass loss of wood cross section due to fire. The strength of the residual is calculated in the same way as the ambient strength is calculated. In addition to charring, a portion of the section beyond the char layer is subtracted, which further reduces the size of the section. This portion is considered to have zero-strength and typically has a depth of 7 mm (WDM, 2020).

In timber design, connections such as wood-steel-wood (WSW), are used to connect assemblage and transfer loads. Under fire loading, the connection is the weakest zone of any wood structure, and hence the resistance of the connection will most likely govern the fire resistance of wood assemblage (Maraveas et al., 2015). WSW connections consist of metal (steel) fasteners which can be made up of bolts, screws, nails, plates, and dowels. The strength of the section is dependent on the wood section and the fastener. Since metal is much more conductive than wood, the heat

conducted from the metal fastener into the wood members results in a higher charring rate at the connection, which rapidly affects the strength of the residual section. It should be noted that the charring rate varies depending on the type of fastener. The resistance of the assembly is also affected by the strength loss in the fastener's mechanical properties due to fire. As such, it is important to know the behaviour of both timber and steel under fire to determine their loading capacity and fire resistance.

2.7.2 Behaviour of timber at elevated temperatures

The fire resistance of wood connections is related largely to their thermal properties (Maraveas et al., 2015). As such, it is imperative to know properties such as char rate, conductivity, specific heat, and density of wood products when exposed to elevated temperatures.

Charring rate

When timber is exposed to fire, it undergoes thermal degradation, known as pyrolysis or charring which produces combustible gasses, and leads to reduced cross-section, Figure 2.31, (White and Woeste, 2013). The reduction in cross-section areas leads to decreased load-carrying capacity (Moment). It is worth noting that the char layer serves as insulation for the residual cross-section, thus reducing the char rate further beyond the char layer (Frangi and Fontana, 2003). The charred layer is assumed to have no strength capacity. According to studies by Truax (1959), Browne (1958), and Reszka (2008), timber charring begins at around 280°-300°C.

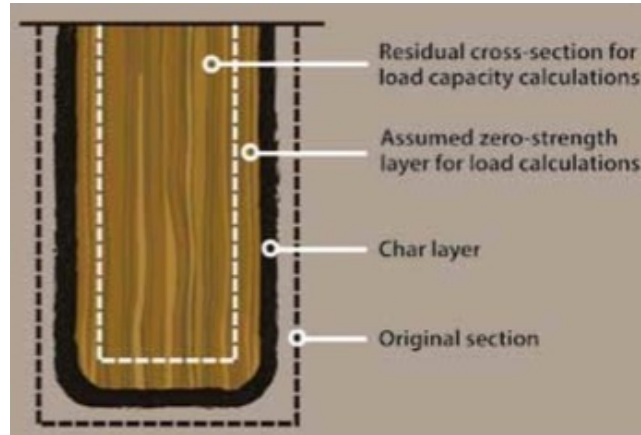


Figure 2.31 Wood Section Charring (Adapted from White and Woeste, 2013).

Charring rate, β , is defined as the ratio between the charring depth and duration of fire (mm/min). The charring rate is dependent on the wood species, moisture content, wood density, and type of fire. For ISO 834 fire, the charring rate is constant. Table 2.7 illustrates the charring rate for different types of wood species as given in Eurocode 5 (2004), without considering the wood density.

Table 2.7 Charring rates of different wood species (Adapted from Cachim and Franssen, 2009).

Wood type		β_0
Softwood and beech	Glued laminated timber with a characteristic density of $\geq 290 \text{ kg/m}^3$	0.65
	Solid timber with a characteristic density of $\geq 290 \text{ kg/m}^3$	0.65
Hardwood	Solid or glued laminated hardwood with a characteristic density of 290 kg/m^3	0.65
	Solid or glued laminated hardwood with a characteristic density of $\geq 450 \text{ kg/m}^3$	0.5

To account for the density, the Australian code standard AS 1720.4 uses the following formula. **Equation 2.7** Charring rate equation to account for wood density (Adapted from the Australian code standard AS 1720.4)

$$\beta = 0.4 + \left(\frac{280}{\rho}\right)^2 \quad \text{Eqn. (2.7)}$$

On the other hand, the Eurocode 5 (2004) developed a conduction model to investigate the charring rate for densities of 200, 290, 450, 600, and 800 kg/m³. It is worth noting that the model does not distinguish between hardwood and softwood. For the model, the coefficient of heat transfer was assumed 9 W/m²K for unexposed surfaces and 25 W/m²K for exposed surfaces. Moisture content was assumed 12%, and surface emissivity was 0.8. The model was subjected to standard fire as per Eurocode 5, part 1-2. The result of this model is shown in Table 2.8.

Table 2.8 Eurocode model on the effect of density on the charring rate of wood (Adapted from Cachim and Franssen, 2009).

Density (kg/m ³)	200	290	450	600	800	1000
Charring rates at 60 min	1.032	0.876	0.682	0.600	0.512	0.461

The results of this model were compared to the Australian code formula. For density greater than 700 kg/m³, the model and the Australian code formula yield similar results. However, for a density lower than 600 kg/m³, the Australian code formula results in a much higher charring rate. This discrepancy between the model and the Australian code formula may be attributed to the model

not accurately predicting the moisture content at this density. For 450 kg/m³ density, the model and Australian code formula results are similar.

Thermal conductivity

Knudson (1975), Fredlund (1993), Mehaffey (1994), Janssens (1994), and Konig (2000) studied the thermal conductivity of wood as temperature increases. Figure 2.32 shows the outcomes of each of those studies. As evident from the graph, the thermal conductivity of wood is reduced at a temperature of 300 °C which is when the char layer is formed. As noted, the charring layer acts as an insulating layer for the residual section. Beyond 500 °C the thermal conductivity drastically increases due to the presence of cracks in the wood as shrinkage occurs, and the char layer is consumed. This in turn increases the radiation and convection heat transfer within the wood. EN1995-1-2 provided tabulated values for the heat conductivity of wood as temperature increases. Table 2.9 illustrates the thermal conductivity values with respect to the temperature of wood as per the Eurocode 5 (2004).

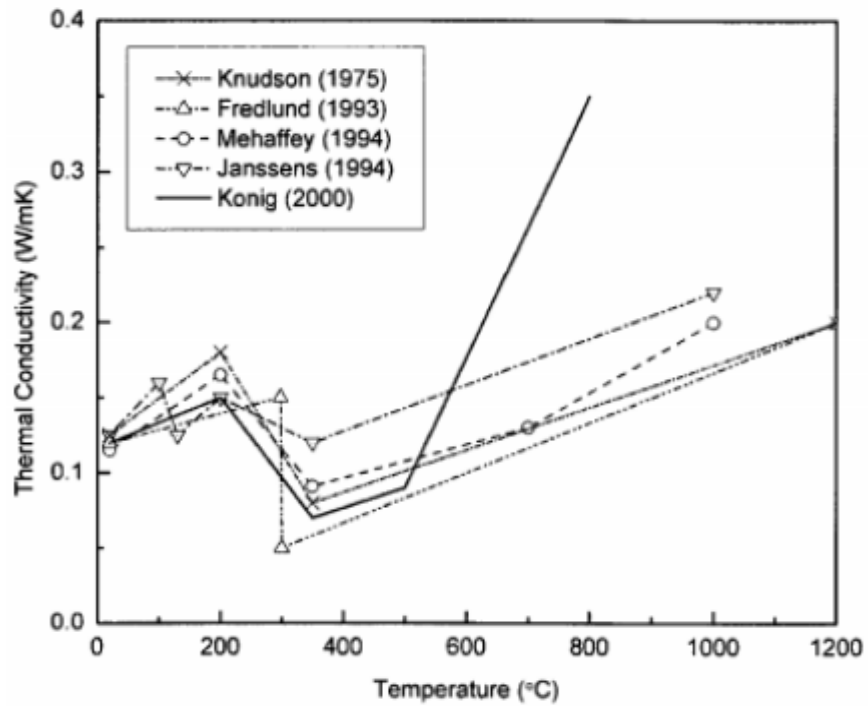


Figure 2.32 Temperature vs. thermal conductivity of wood (Adapted from Peng et al., 2011)

Table 2.9 Temperature vs. thermal conductivity of wood (Adapted from Eurocode 5, 2004).

Temperature (°C)	Thermal Conductivity (Wm ⁻¹ K ⁻¹)
20	0.12
200	0.15
350	0.07
500	0.09
800	0.35
1200	1.50

Specific heat

The specific heat of wood products was studied by different researchers including Gammon (1987), Mehaffey (1994), Janssens (1994), and Konig (2000). The specific heat of wood with respect to temperature is depicted in Figure 2.33. As was shown in Mehaffey (1994) and Konig (2000) findings, the specific heat is at its greatest at roughly 100 °C, which is the evaporation point of moisture within the wood. This can be explained as a high amount of heat (thermal energy) is required for the transition from the liquid to the vapor stage. The slight variation of specific heat values of the different studies can be explained as the properties of wood varies depending on the type of wood used, moisture content, density, etc.

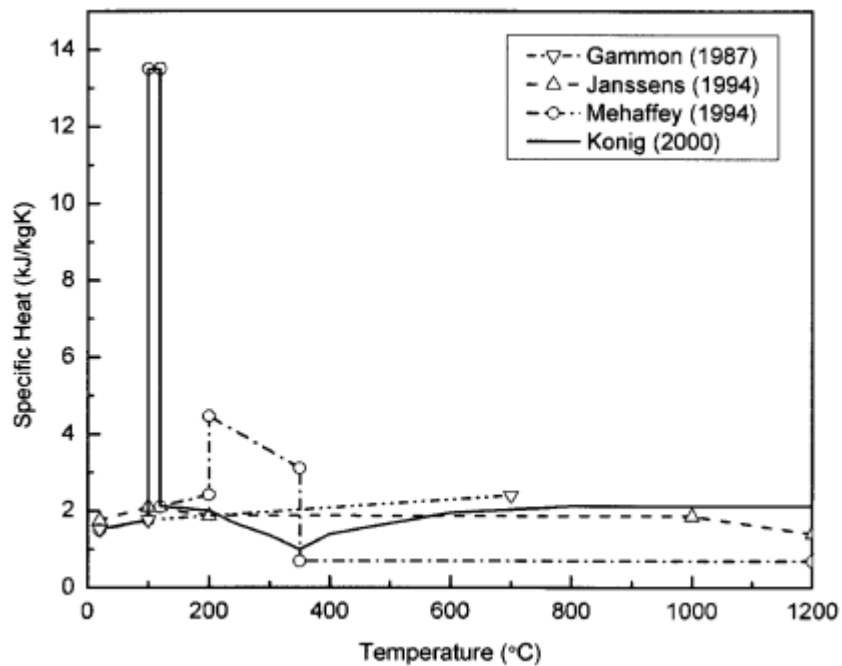


Figure 2.33 Temperature vs. specific heat of wood (Adapted from Peng et al., 2011).

Density

Figure 2.34 shows the relationship between the density ratio (density/dry density) of wood products with respect to temperature, as obtained by the different studies. Research studies conducted by

Lie (1992), Mehaffey and Takeda (1998), and Janssens (1994), presented similar results. As shown in Figure 2.34, the density decreases as the temperature increases. This is due to water evaporation within the wood as the temperature increases. Beyond 300°C, there is a sharp drop in the density ratio from 0.8 to 0.4, which is due to the thermal decomposition of the wood. After 400°C, the density is gradually reduced.

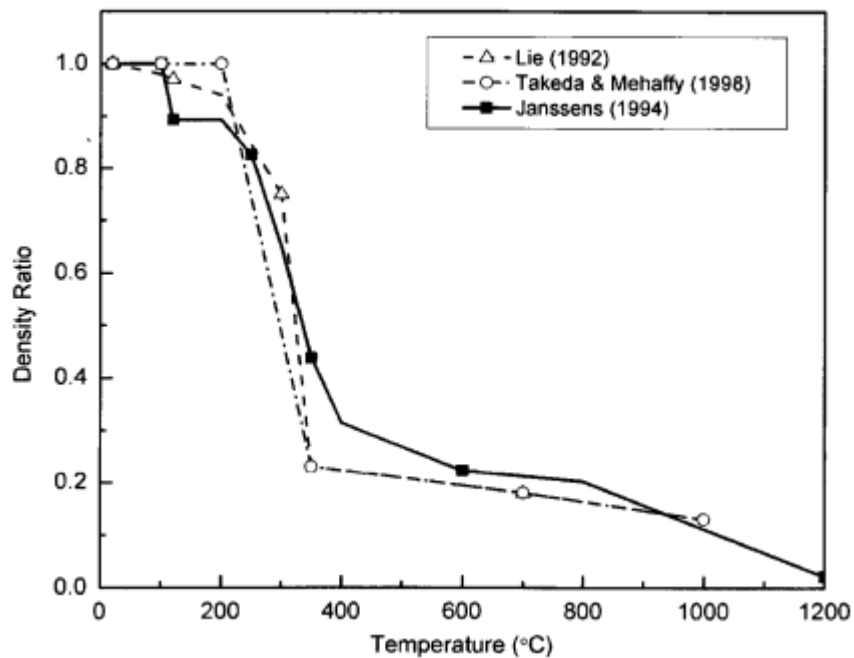


Figure 2.34 Temperature vs. density of wood (Adapted from Peng et al., 2011)

2.7.3 Effects of fire on the mechanical properties of wood

Mechanical properties of wood, including compressive, shear, and tensile strength are important in determining the fire resistance of wood members. Unlike steel, the mechanical properties of wood products are not constant, and it varies with different types of wood products and loading direction with respect to the grain (Peng et al., 2011). Figure 2.35 illustrates the reduction factors k_0 for compression, tension, and shear strengths of softwood as provided by Eurocode 5, 2004).

The same reduction factors can be used for parallel and perpendicular to grain compression, and shear. As evident from Figure 2.35, the compression, shear, and tensile strength decrease at a faster rate up until 100 °C. Beyond 100°C, the decreases become more gradual. At 300°C, when charring occurs, all three strengths become negligible. It is worth noting that compression strength diminishes faster compared to other strengths. Further, the reduction in modulus of elasticity factor in tension and compression of softwood members loaded parallel to grain with respect to temperature is shown in Figure 2.36. As can be seen, the modulus of elasticity reduction factor experienced the same pattern as the strength reduction factor (Eurocode 5, 2004).

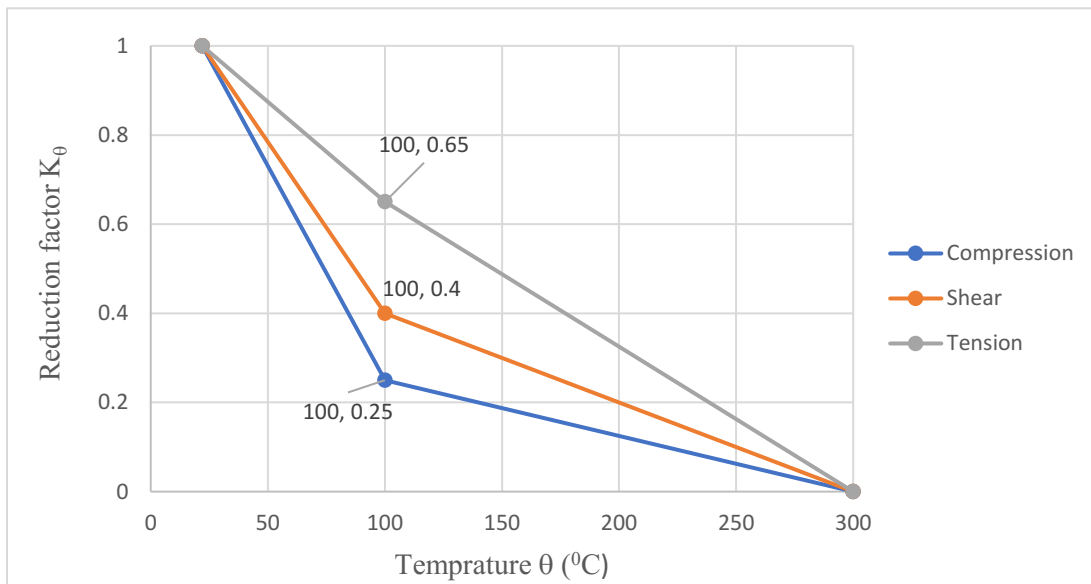


Figure 2.35 Effect of temperature on the strength of softwood (Adapted from Eurocode 5, 2004)

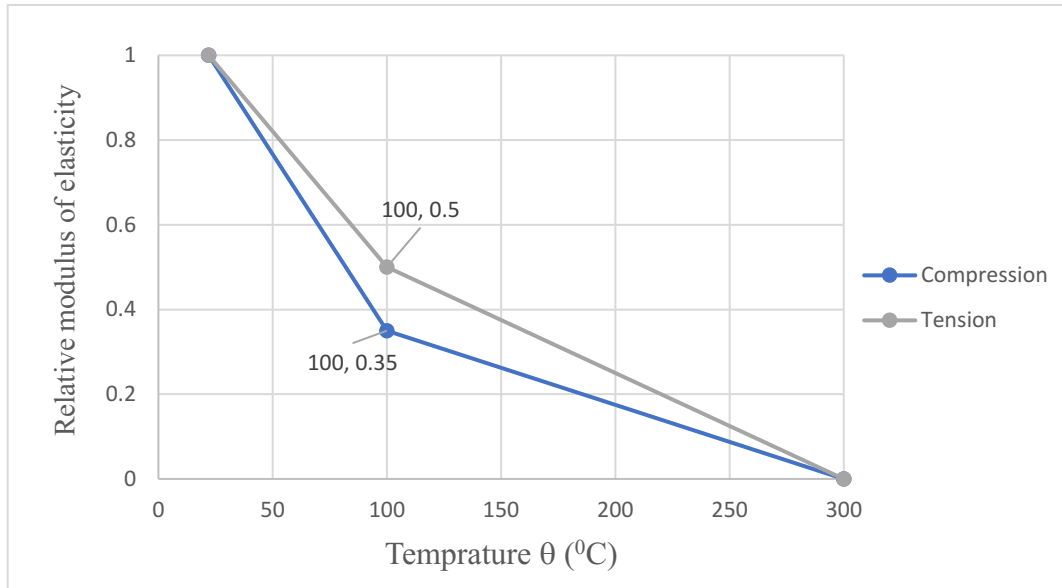


Figure 2.36 Effect of temperature on the modulus of elasticity of softwood (Adapted from Eurocode 5, 2004)

2.8 Behavior of Wood-Steel-Wood-Connections in Fire

2.8.1 Heat transfer in hybrid wood-steel-wood connections in fire

In structural wood assemblies with WSW connections subjected to fire, the connection is the weakest part of the assembly (Peng, 2010). This is attributed to the fact that steel fasteners conduct heat much faster than wood and it affects the wood section by expediting the charring of the section. The strength of the section is dependent on the residual section after charring has occurred. During a fire, the connection strength also depends on the strength of the fastener. As the fire progresses, the increase in the temperature of metal fasteners reduces their strength. Peng et al. (2011) conducted a 3D finite element analysis on the heat transfer in a WSW connection subjected to ISO 834 standard fire on four sides. The software used to conduct this analysis was Abaqus/Standard V6.6. The connection model consisted of 3 dowels and 1 bolt, and a slotted-in steel plate which

had a gap of 6 to 8 mm. The connection used for this study is shown in Figure 2.37. No load was applied in this model.

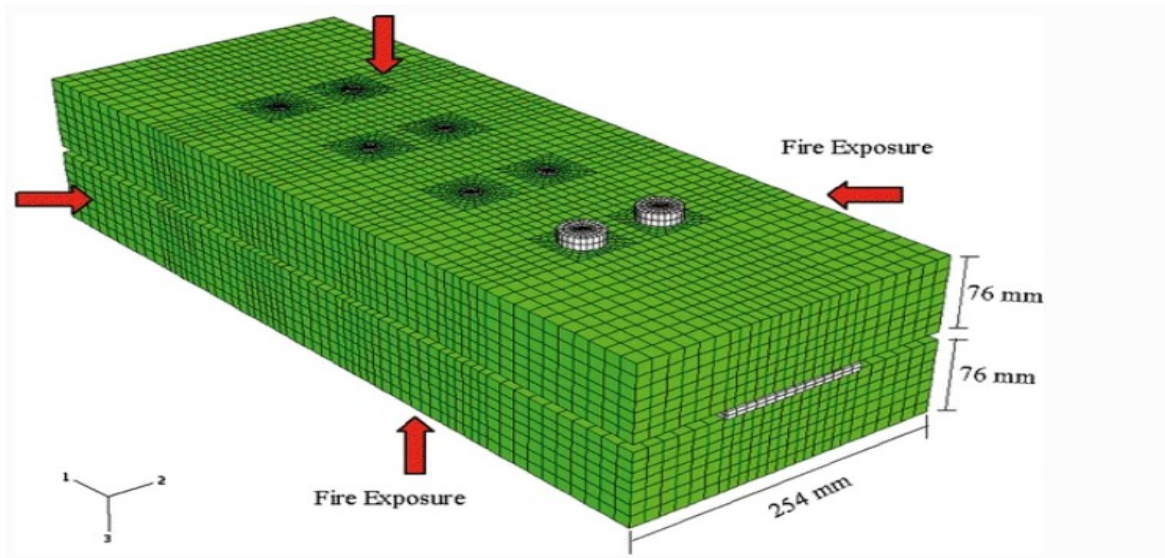


Figure 2.37 Thermal analysis finite element model (Adapted from Peng et al., 2011).

To validate the model results, the outcomes of this finite model were compared to an experimental study conducted by Ayme (2003). In this study, the wood section had dimensions of 254 x 152 mm with a density of 445 Kg/m³ and moisture content of 10%. A mixture of bolts and dowels was used for this connection. For every three dowels used, one bolt was used to keep the section intact. The bolts were 20 mm in diameter and the dowels varied from 12, or 16 mm in diameter. The specimen was loaded to 10% of its ultimate capacity and thermocouples (T) were installed to measure the temperatures of the bolts, dowels, and wood section throughout the test. T1 and T2 measured the temperature of bolts, T3 and T4 of the dowels, and T5 and T6 of the wood sections. This section failed after 56 minutes. The schematic for the Ayme (2003) test set up is shown below in Figure 2.38.

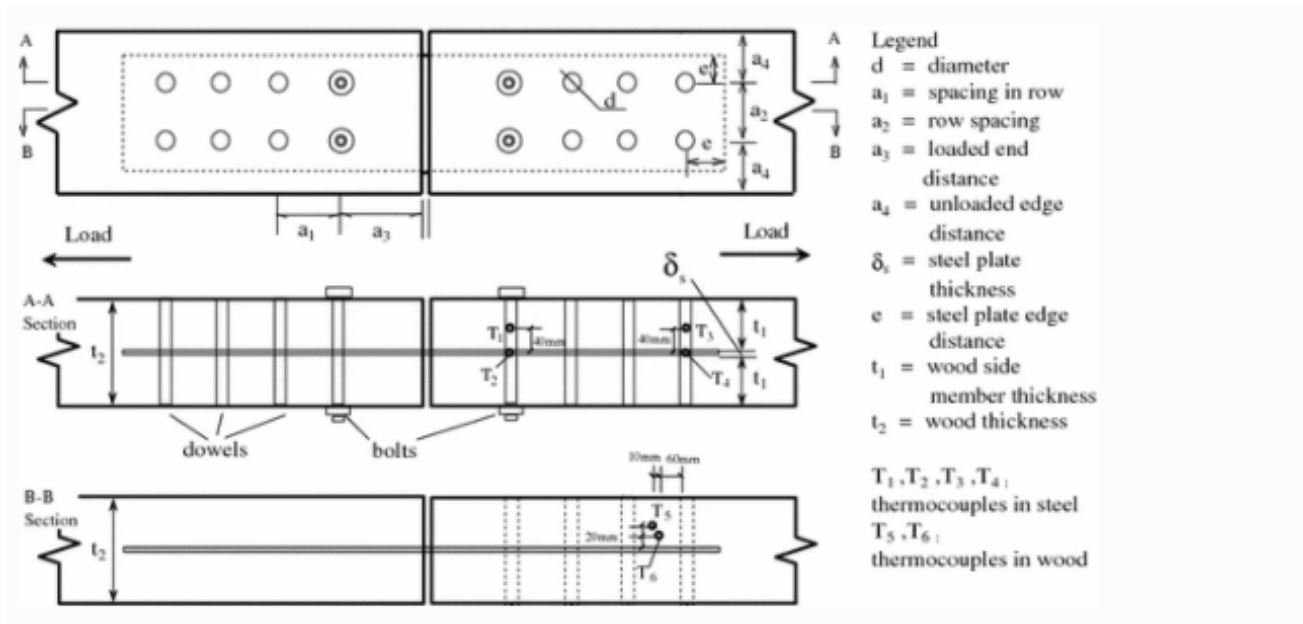


Figure 2.38 Schematic for test specimens (Adapted from Peng et al., 2011).

The temperature-time curves for the thermocouples for both the model and the Ayme (2003) experiment are depicted in Figure 2.39. As shown in Figure 2.39, the temperature of the bolts is higher compared to the dowels. This can be explained by the presence of the head and nuts on the bolts which resulted in a larger fire area compared to the dowels. Furthermore, for both the model and experimental study, the temperature of the steel members (T_1 to T_4) increased almost linearly with time. On the other hand, the temperature of the wood section (T_5 and T_6) was not consistent between the model and the experimental study. This could be attributed to uncertainty in the properties of the wood section, the fire effect on bolt arrangement, and the fact that moisture content was not considered in the model. Therefore, it can be concluded that the increases in temperature within metal fasteners are linear with respect to time, whereas the heat transfer of wood can not be accurately predicted as it depends on the arrangement of bolts, moisture content, and thermal properties which vary for different wood specimens.

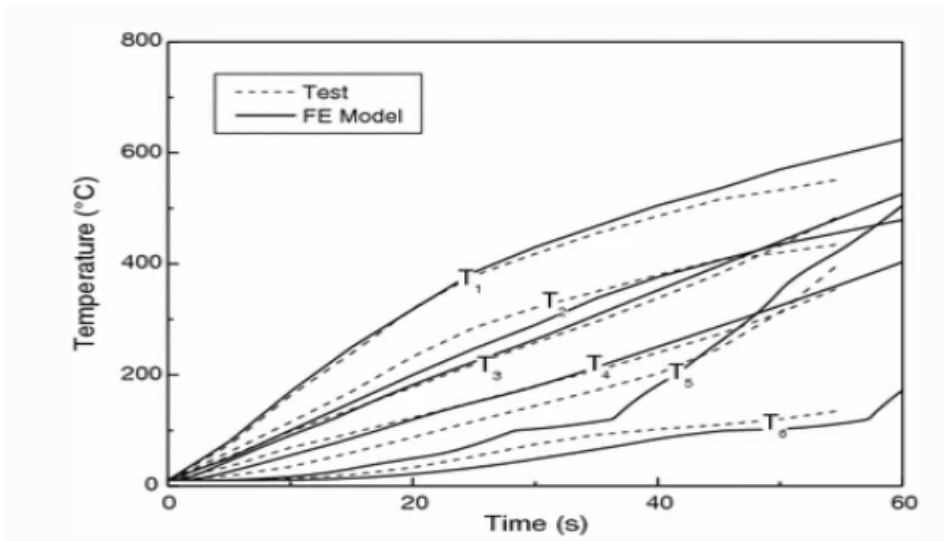


Figure 2.39 Temperature vs. time for FE model and experiments (Adapted from Peng et al, 2011)

In another test conducted by Ayme (2003), where the specimen was loaded to 30% of the ultimate capacity, the connection failed after 36 minutes. The heat transfer through the wood section where bolts and dowels are located was also studied. Similar to the first test, it was shown that regions of wood sections where bolts were present had higher temperatures compared to wood sections where dowels were located. Figure 2.40 and Figure 2.41 shows the temperature distribution at the bolts cross-section and the dowels cross-section, respectively, after 36-minute fire exposure. The temperature of the wood at the surface was higher compared to the metal fastener due to the higher thermal conductivity at the surface.

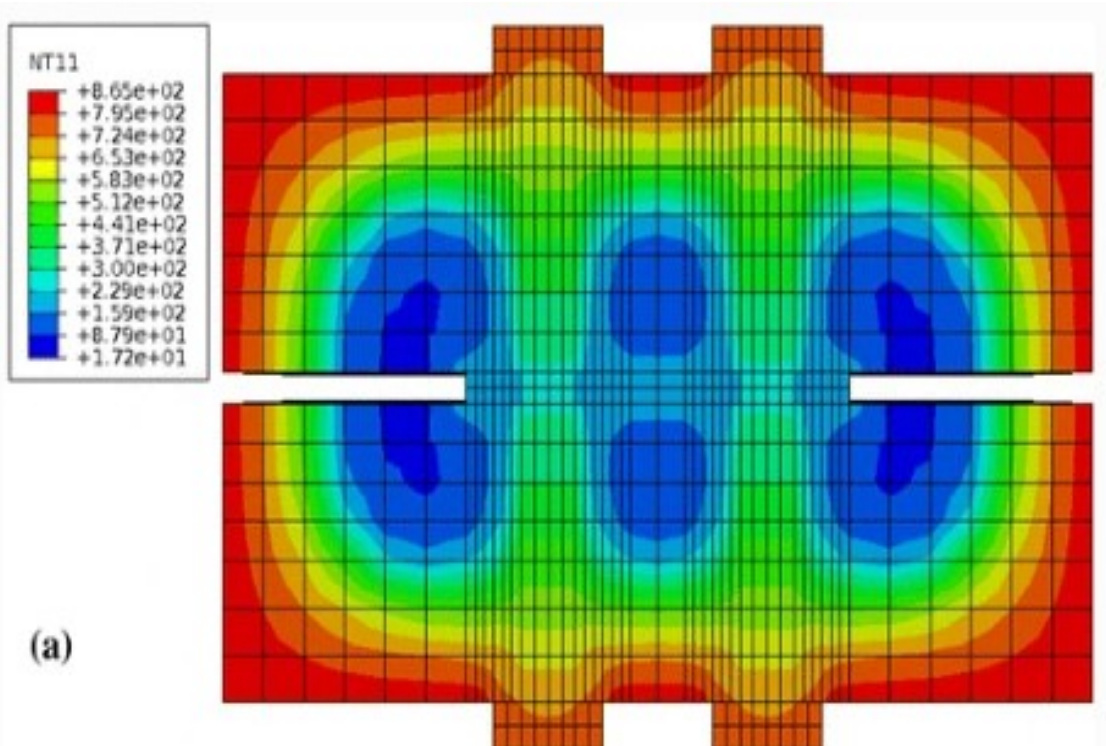


Figure 2.40 Bolt cross-section temperatures (Adapted from Peng et al., 2011).

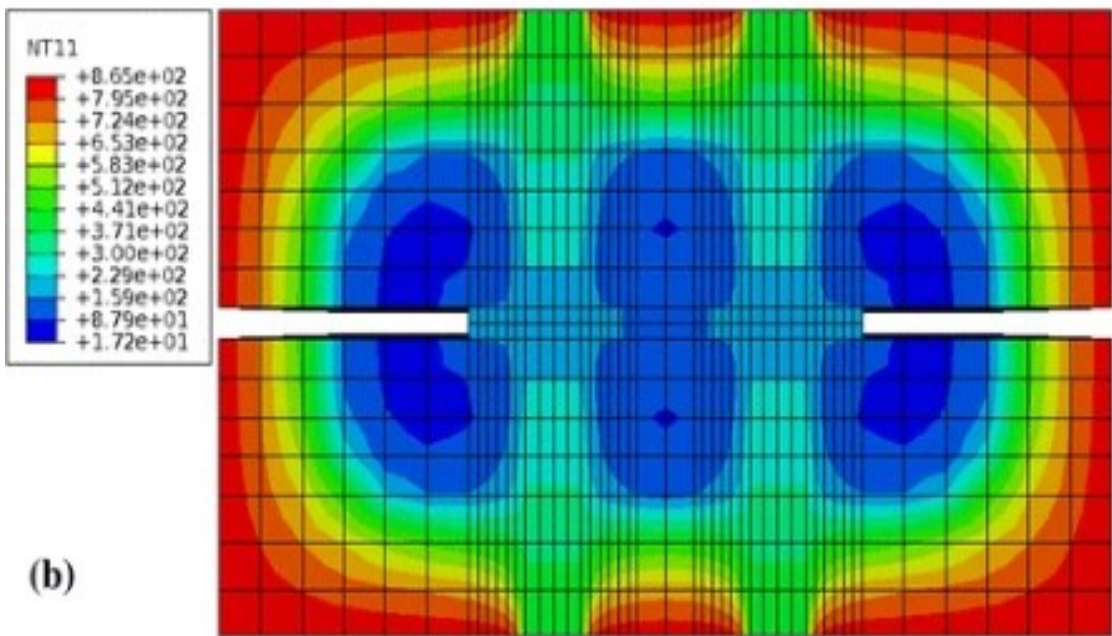


Figure 2.41 Dowel cross-section temperatures (Adapted from Peng et al., 2011).

2.8.2 Fire resistance of hybrid wood-steel-wood connections at elevated temperatures

Owusu (2019) conducted an experimental study to investigate the behaviour of unreinforced bolted connections when exposed to elevated temperatures. In this study, the effect of bolt arrangements, the number of bolts, and the use of wood plugs to conceal the bolts and nuts on the fire resistance of a glulam beam was studied. In total, ten fire tests were conducted, and eight different connection configurations were tested. All tests were subjected to CAN/ULC-S101 (2019) standard fire and were loaded to 100% of the ultimate design load of the weakest connection. The time-temperature curves for CAN/ULC-S101 (2019) standard fire and ISO 834 standard fire are shown in Figure 2.42.

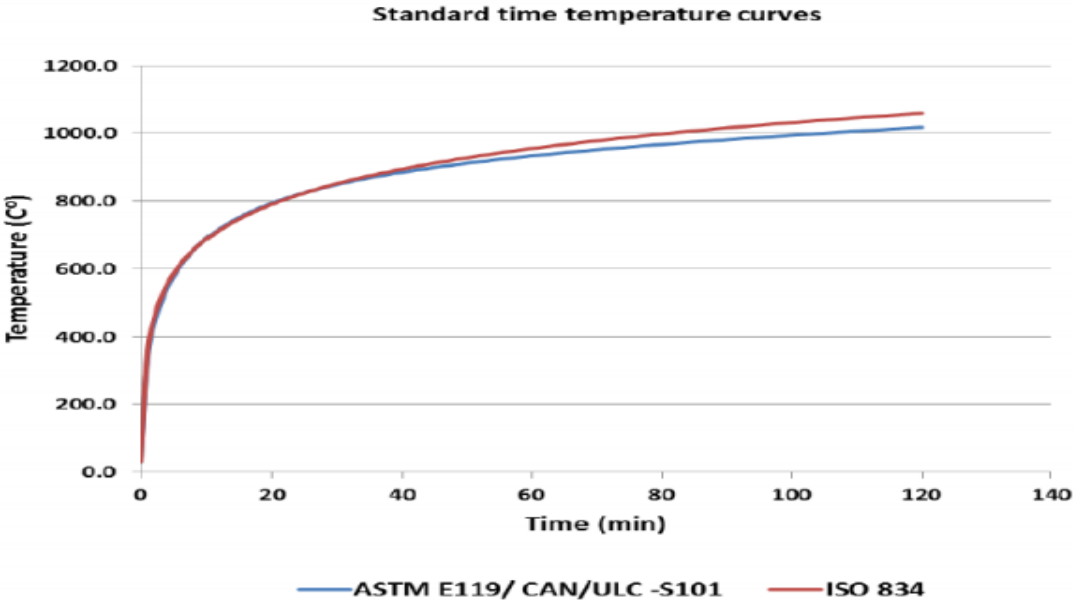


Figure 2.42 CAN/ULC-S101 and ISO 834 standard fire curves (Adapted from CAN/ULC-S101-19, 2019).

In the first fire test where four bolts were placed symmetrically near the top and bottom of the beam, with no wood plugs used to conceal steel bolts and nuts (4BP1NF₁), the connection failed due to splitting and row shear out along the top bolts row after 33 minutes. In the second

configuration (4BP2NF₁), the bottom bolts were raised to mid-height of the beam to further resist the tensile stresses at the top of the beam and no wood plugs were used to conceal the steel within the connection. The connection failed after 32 minutes due to splitting and row shear at the top bolt row.

When wood plugs were used to conceal the bolts in the four bolts arranged in pattern one (4BP1PF₁), the connection achieved a 56-minute fire resistance time and failed due to excessive charring. However, when the test was repeated for the same connection (4BP1PF₂), the connection failed after only 42 minutes due to a sudden glue line split along the top bolt row. Similarly, for the 4-bolt connection arranged in the second bolt pattern (4BP2PF₁), used with wood plugs, the connection failed due to as sudden glue line failure along the top bolt row after 48 minutes.

When six bolts were used in the first bolt pattern with no wood plugs (6BP1NF₁), the connection failed after 22 minutes due to a sudden glue line failure along the top bolt row. Similarly, in the connection configuration with six bolts arranged in the second bolt pattern with no wood plugs (6BP2NF₁), the connection failed after 27 minutes due to as sudden glue line failure.

When wood plugs were used to conceal the bolts in the six bolts arranged in pattern one (6BP1PF₁), the connection achieved a 48-minute fire resistance time and failed due to a sudden glue line split along the top bolt row. However, when the test was repeated for the same connection (6BP1PF₂), the connection achieved a 62-minute fire resistance and failed due to excessive charring. When wood plugs were used in the six-bolt connection arranged in the second bolt pattern (6BP2PF₁), the connection failed due to a sudden split at the glued plane at the second row of bolts after 41 minutes.

As evident from the above results, the predominate mode of failure in Owusu (2019) experimental program was an unexpected glue line splitting, which resulted in a premature and brittle failure for the majority of the specimens. A summary of Owusu (2019) test results, which include the time to failure, charring rate, and failure mode of each configuration, is shown in Table 2.10.

Table 2.10 Fire testing results (Adapted from Owusu, 2019).

Connection Bolt Pattern	Applied Moment (kN.m)	Time of Failure (min)	Charring Rate (mm/min)	Failure Mode
4BP1NF ₁	14.8	33.0	0.73	Splitting/row shear
4BP2NF ₁	14.8	32.0	0.82	Splitting/row shear
4BP1PF ₁	14.8	56.0	0.9	Splitting
4BP1PF ₂	14.8	42.0	0.96	Splitting
4BP2PF ₁	14.8	48.0	1.0	Splitting
6BP1NF ₁	14.8	22.0	0.81	Splitting
6BP2NF ₁	14.8	27.0	0.8	Splitting
6BP1PF ₁	14.8	48.0	1.03	Splitting
6BP1PF ₂	14.8	62.0	0.85	Splitting/row shear
6BP2PF ₁	14.8	41.0	0.77	Complete Splitting

2.9 Wood Reinforcement Behaviour When Exposed to Fire

FRP, like all other materials, lose strength as their temperature increases under fire loading (Italian National Research Council, 2007). When FRP reinforcement is exposed to fire, its stiffness and strength are reduced as the polymer matrix loses its mechanical properties. The epoxy adhesive begins to lose strength and softness at temperatures between 90-120°C, thereby affecting the bond between the wood and the reinforcement. The fire effect on externally bonded FRP is more pronounced than on internally placed FRP, as there is no insulation provided for the external beams. Martin and Tingley (2000) studied the performance of glulam reinforced with external and internal FRP while subjected to standard fire. The results showed that internally reinforced beams

had 44% higher fire resistance as compared to externally reinforced beams. One way to mitigate the strength loss for externally bonded FRP is to insulate it with wood materials. Another way is to increase the cross-section size to account for the charred section. In an experimental study conducted by Williamson and Yeh (2006) on a Douglas-Fir glulam beam reinforced with an external FRP layer placed on the bottom tensile side of the beam, it was proposed that increasing the beam height by 10% and adding one layer of lamination (38 mm) will result in a 1-hour fire rating. The beam section had a dimension of 170 x 343 mm, and the proposed beam height was 415 mm ($343 \times 1.1 + 38$). Due to manufacturing availability, a 170 x 420 beam was used. Two beams with this dimension were subjected to the standard ASTM E119 (2005) fire test. One beam achieved a 60-minute resistance while still supporting the design load, and the other one achieved a 56-minute fire resistance. After the fire testing was complete, it was noticed that the beam that achieved a 1-hour fire rating had an extra 15% fire capacity. Considering variabilities in fire testing and beam fabrication, it was deemed that a 1-hour fire rating was attainable with the proposed approach. It is worth noting that two different types of FRP reinforcement layers were tested, and their fire performance was similar.

Chapter 3: Methodology and Test Assemblies Details

3.1 Introduction

The main objective of this research is to investigate the effect of using self-tapping Screws (STS) to retrofit damaged glulam beam connections loaded in standard fire conditions. Initially, the beam-end connections were deliberately tested at ambient temperature until failure which caused damages mainly in the connection area (e.g., wood splitting). The beam-end connections were then reinforced with STS and tested again under standard fire exposure. Most of the ambient temperature tests were conducted in a related prior study conducted by Owusu (2019), which took place at Lakehead University Civil Engineering's Structures Laboratory, Whereas the fire resistance tests took place at Lakehead University Fire Testing and Research Laboratory (LUFTRL). The fire resistance test results of the specimens reinforced with STS were compared to those of the unreinforced, undamaged connections that were conducted by Owusu (2019) to investigate the strengthening effects of the STS. In this chapter, a description of the ambient and fire testing procedures, the materials used, loading, and test set up is provided.

3.2 Ambient Temperatures Testing

In total, eight (8) full-size glulam beam-end connections were tested at ambient temperatures until failure. The ambient temperature testing was mainly conducted in a prior related study conducted by Owusu (2019). In this research, only three (3) specimens were tested as a continuation of the ambient temperature experimental program initiated by Owusu (2019). The three (3) ambient tests that have been conducted as part of this research were of the connections with the four bolts arranged in pattern 2 (P2) and provided with protection (4BP2P), the six bolts arranged in pattern

1 (P1) without protection (6BP1NP), and the six bolts arranged in pattern 2 (P2) and provided with protection (6BP2P).

Figure 3.1 illustrates the ambient temperature test setup for the connection with the four bolts arranged in pattern 2 (P2) and fabricated to allow protection (4BP2P). Figure 3.2 shows a schematic that illustrates the details of the connection configuration with four bolts arranged in pattern 1 (P1) without protection (4BP1NP). Figure 3.3 illustrates the details of the connection configuration with four bolts arranged in pattern 2 (P2) without protection (4BP2NP). Figure 3.4 illustrates the details of the connection configuration with six bolts arranged in pattern 1 (P1) without protection (6BP1NP). Figure 3.5 illustrates the details of the connection configuration with six bolts arranged in pattern 2 (P2) without protection (6BP2NP). In the protected connection configurations, the steel bolt's heads and nuts and steel plate edges were concealed using wood plugs and strips, whereas, in the unprotected connection configurations, the steel bolt's heads and nuts and steel plate top and bottom edges were exposed.

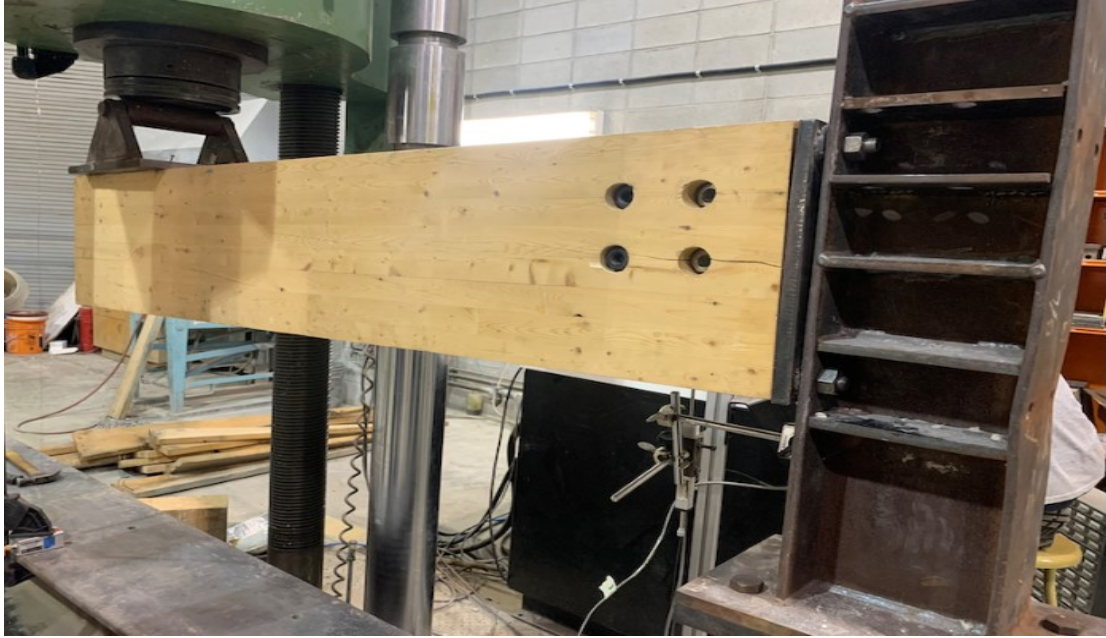


Figure 3.1 Ambient temperature test setup for the connection configuration with four bolts in pattern 2 without fire protection (4BP2NP).

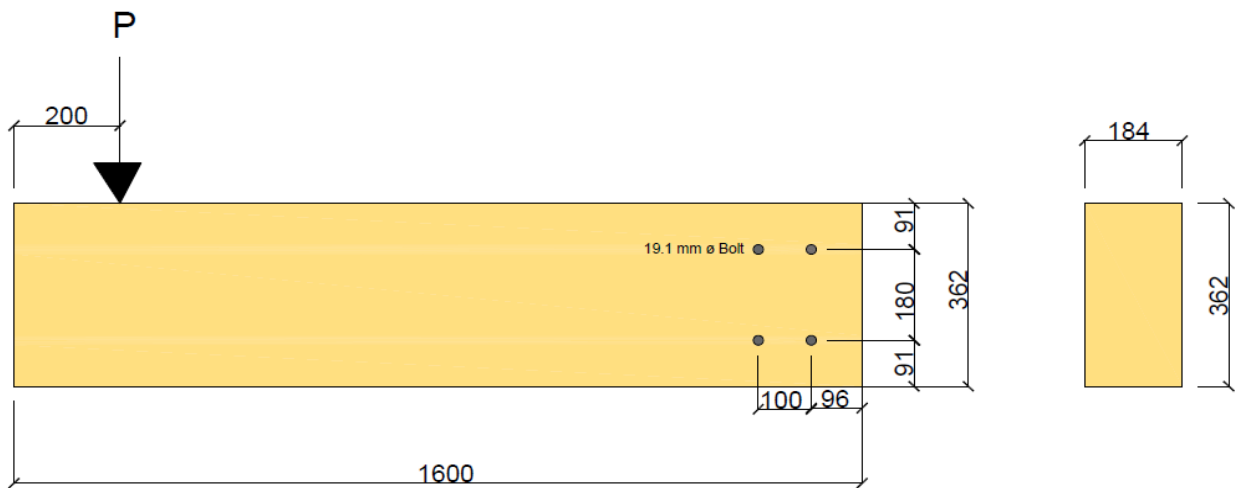


Figure 3.2 Details of the connection configuration with four bolts in pattern 1 without fire protection (4BP1NP).

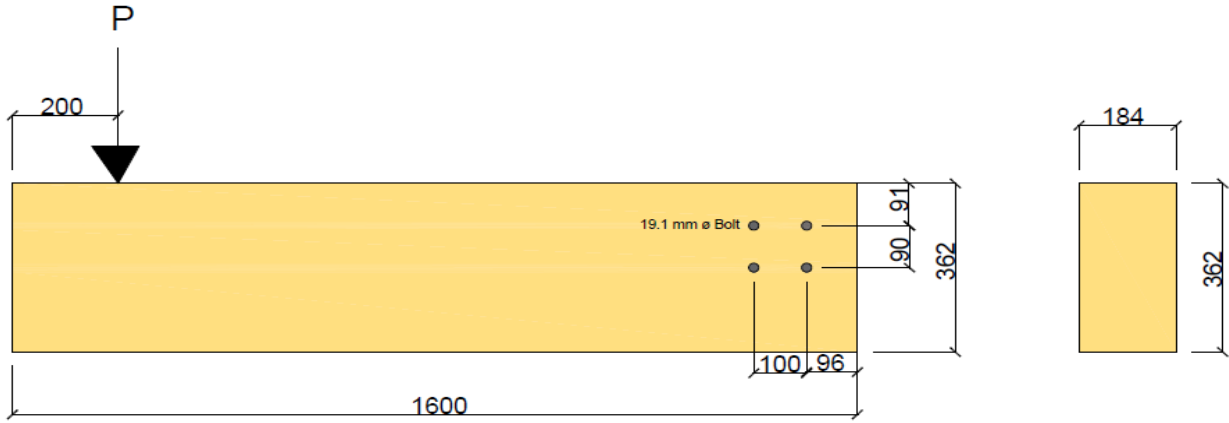


Figure 3.3 Details of the connection configuration with four bolts in pattern 2 without fire protection (4BP2NP).

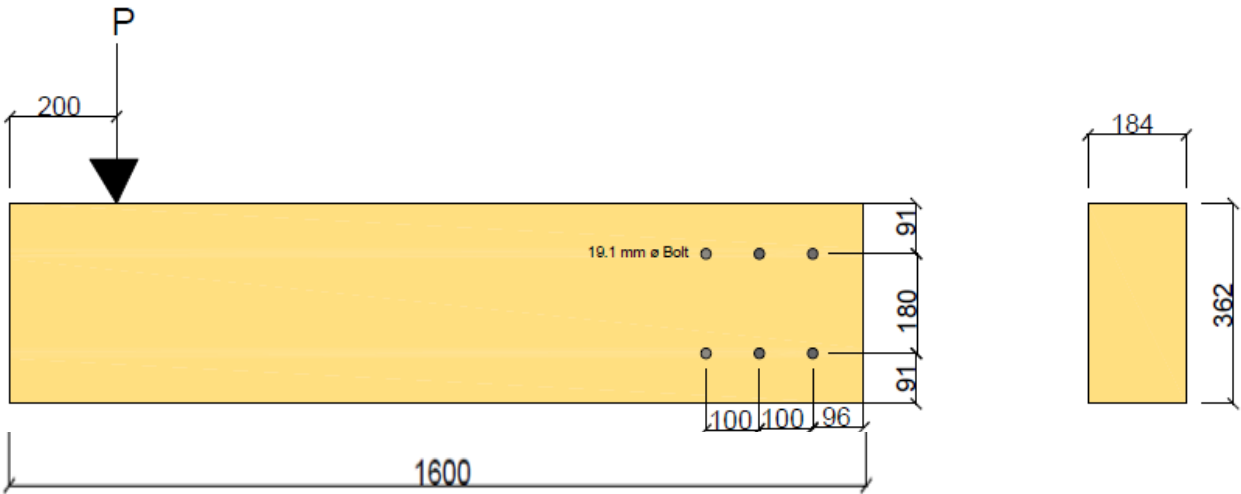


Figure 3.4 Details of the connection configuration with six bolts in pattern 1 without fire protection (6BP1NP).

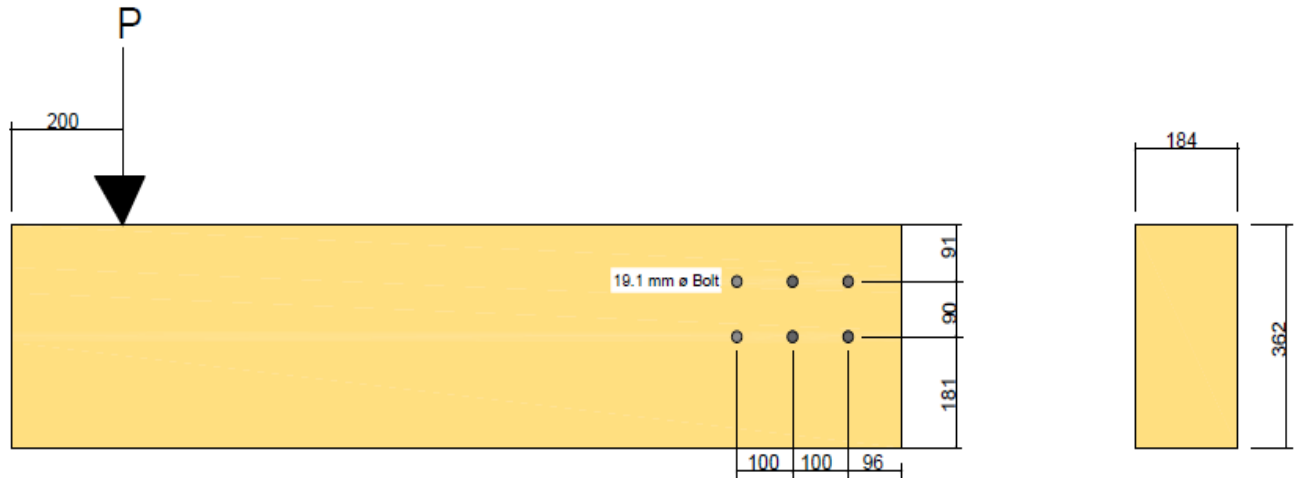


Figure 3.5 Details of the connection configuration with six bolts in pattern 2 without fire protection (6BP2NP).

As can be seen from Figure 3.1, the glulam beams were fixed at one end and free at the other. The beams were supported to a strong steel column using four 19.1-mm diameter short threaded steel rods that were welded to the steel T-stub connector embedded inside the glulam beam section.

During ambient temperature testing, the beams were deliberately loaded until failure where wood splitting occurred along the top and bottom rows of bolts, at which time the test was terminated. Figure 3.6 illustrates the typical failure mode of the 4-bolt protected connection utilizing the second bolt pattern (P2) when the test was terminated. Figure 3.7 illustrates the failure mode of the 4-bolt unprotected connections utilizing the first and second bolt patterns (P1 and P2) when the ambient tests were terminated, which were conducted by Owusu (2019).

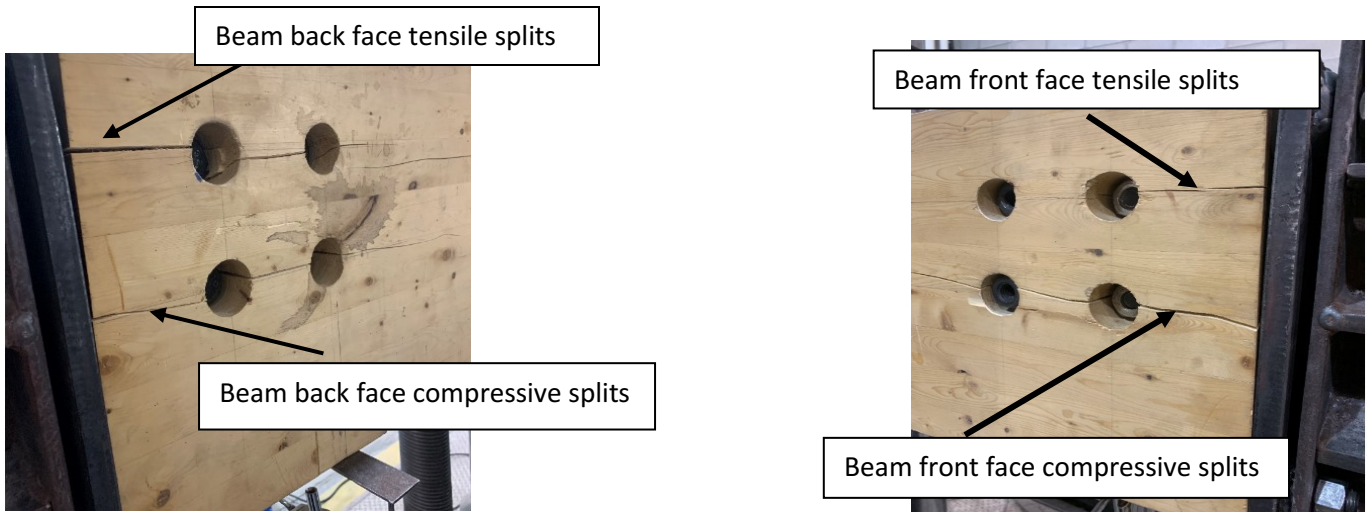


Figure 3.6 Depiction of the damage to the 4-bolt protected connections utilizing the second bolt pattern (P2) when the ambient test was terminated.

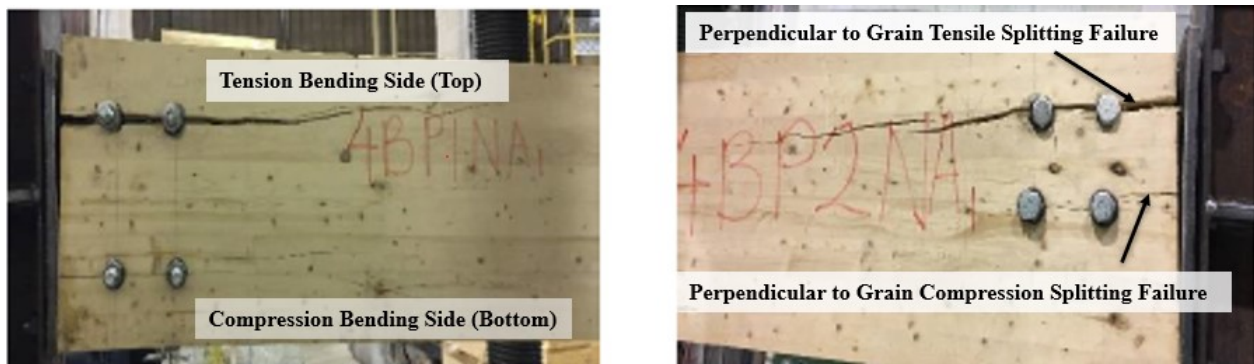


Figure 3.7 Failure modes exhibited by the 4-bolt unprotected connections utilizing the first and second bolt patterns (P1 and P2) when the tests were terminated (Adapted from Owusu, 2019).

3.3 Fire Resistance Testing

The fire resistance testing of the previously damaged eight (8) glulam beam-end connections that were subsequently retrofitted using STS took place at the state-of-the-art Lakehead University Fire Testing and Research Laboratory (LUFTRL). The Fire Lab building is shown in Figure 3.8.

The main apparatus of the Fire Lab is a large-size custom-designed fire testing furnace (Figure 3.9). The frame of the testing furnace is made of strengthened steel plated walls that are insulated from the inside with several layers of Fiberfrax® Ceramic Fiber blankets. The furnace has a movable front door and a movable top lid. The front door of the furnace has two observation ports which are utilized to observe the specimens during testing, as well as to take images throughout the fire tests. The door and top lid of the furnace can be removed using a 1.0-ton jib crane that is installed within the Fire Lab. The crane is also used to manoeuvre test specimens into and out of the furnace.

The furnace is equipped with two natural gas burners that allow the furnace to reach temperatures of up to 1300°C. The fire testing furnace is also equipped with a large exhaust duct and an afterburner unit to treat combustion gasses formed during fire testing in accordance with the Ministry of Environment requirements. The testing furnace operations, including its inside temperatures, are controlled via an advanced control panel that is equipped with a Human-Machine Interface (HMI) touchscreen.



Figure 3.8 Lakehead University Fire Testing and Research Laboratory (LUFTRL) (Courtesy of Dr. Salem, 2019).



Figure 3.9 Fire testing furnace (Courtesy of Dr. Salem, 2019).

As noted, after the beams were tested until failure at ambient temperature, they were reinforced with STS and tested again in standard fire conditions. The setup of the fire tests was similar to that of the ambient tests, except that Fiberfrax ceramic fibers blankets were used to insulate the steel supporting and loading elements. Also, the steel connecting components of the protected connections (i.e., steel bolts heads and nuts, and plate edges) were insulated using wood plugs and strips. In addition, the top side of the glulam beam was insulated with Fiberfrax ceramic fibers blankets in order to ensure the beam was exposed to standard fire on three sides only. Hence, the insulation depicted the existence of a slab on top of the beam as it would be in a realistic construction configuration. Figure 3.10 illustrates the typical setup for fire tests.

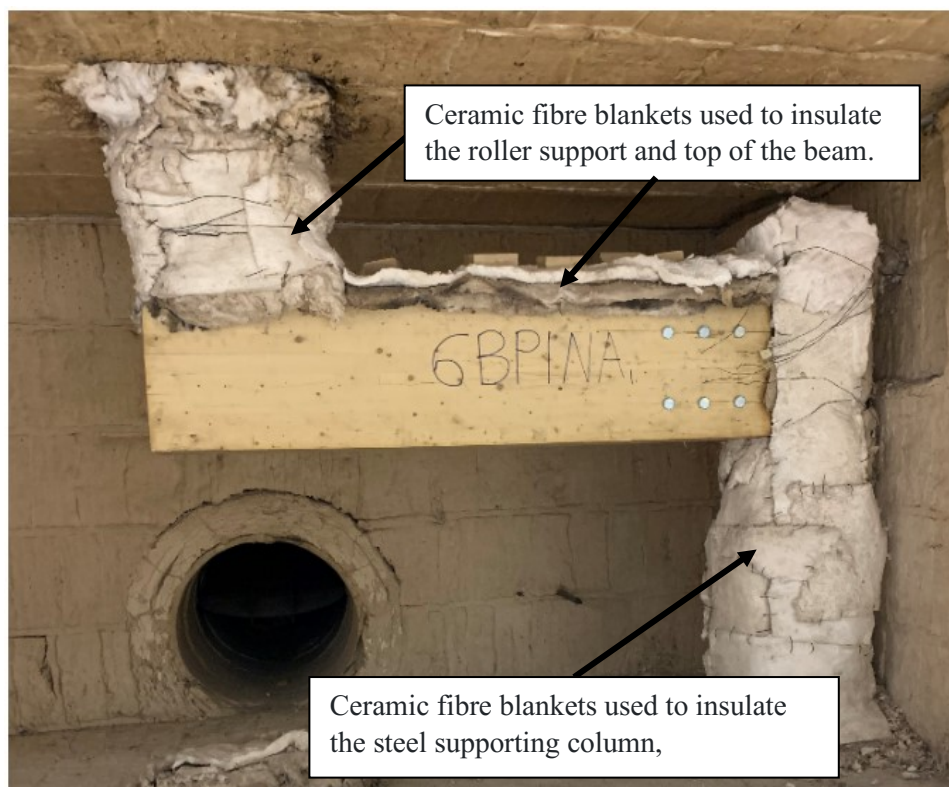


Figure 3.10 Typical fire test setup.

3.4 Materials

3.4.1 Glulam beam sections

The glulam beams used in this study are similar to those used in the Owusu (2019) study. The beams had cross-sectional dimensions of 184 mm x 364 mm x 1600 mm and were made of spruce/pine glulam stress grade 24f-EX. Laminas dimensions were 25 mm x 50 mm. The mechanical properties of the glulam used are shown in Table 3.1.

Table 3.1 24f-EX glulam beam mechanical properties (Adapted from Nordic Lam™ Structures, 2018).

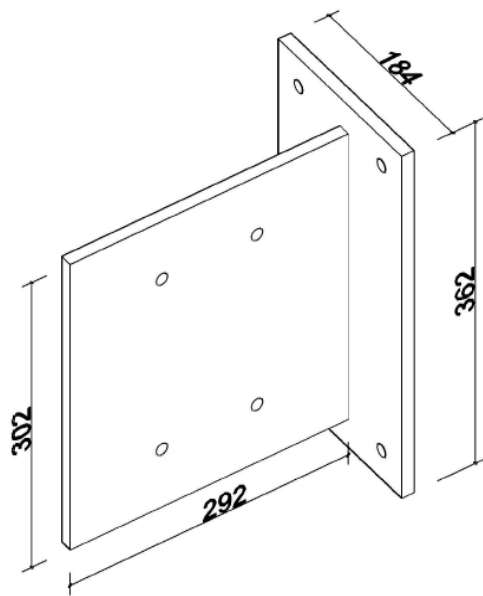
Property	Strength (MPa)
Compression parallel-to-grain	33.0
Compression perpendicular-to-grain	7.5
Tension-parallel-to-grain	20.4
Longitudinal shear	2.2
Flexural bending	30.7
Modulus of elasticity	13,100

The glulam beam was connected to a 300W grade 200 mm x 200 mm HSS steel supporting column using a 12.7-mm thick concealed steel T-stub connector. The steel plate was secured to the column using four fully threaded 19.1-mm diameter steel rods. As noted, in the fire tests, the HSS column was protected by Fiberfrax® Ceramic Fiber insulation.

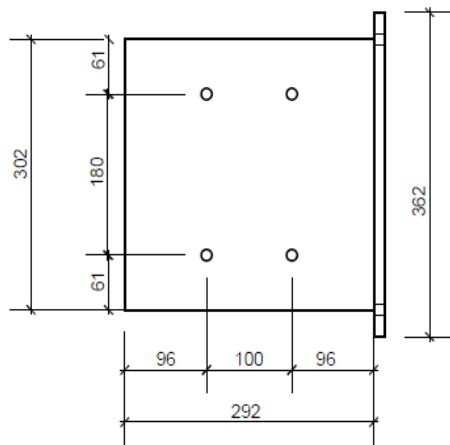
3.4.2 T-stub steel connectors

In order to connect the glulam beam to the steel supporting column, a 12.7-mm thick steel plate grade 300W T-stub connector was used. The fabrication of the steel connector depended on the

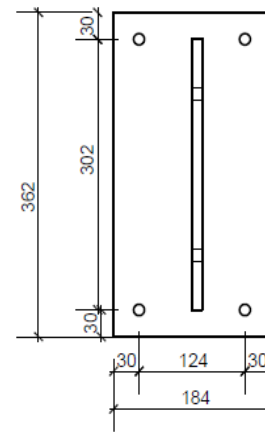
connection configuration tested. In this study, four different T-stub connector configurations were used. In the first connection configuration, the bolts were placed symmetrically near the top and bottom of the beam. Figure 3.11 shows the fabrication details of the 4-bolt connection configuration arranged in the first bolt pattern (P1). In the second connection configuration, the bottom row of bolts was installed at the mid-height of the section. These T-stub connectors were used for the connection configuration with four and six bolts arranged in the second bolt pattern (P2). Figure 3.12 shows the fabrication details of the 4-bolt connection configuration arranged in the second bolt pattern (P2). For each bolt pattern used (P1 or P2), either 4 or 6 bolts were utilized, hence the T-stub connector was fabricated to include either 4 bolts or 6 bolts. Figure 3.13 and Figure 3.14 illustrate the details of the T-stub connectors for the 6-bolt connection configurations arranged in bolt patterns P1 and P2, respectively.



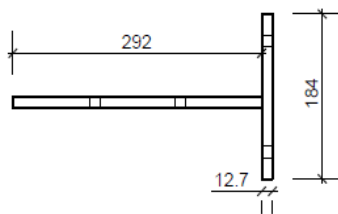
(a)



(b)

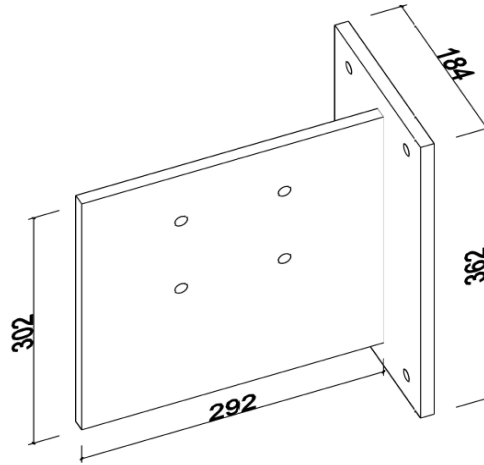


(c)

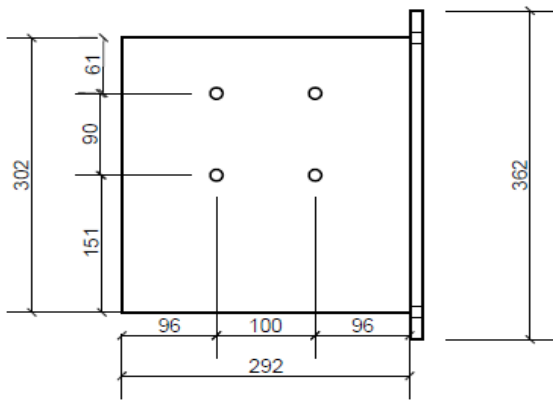


(d)

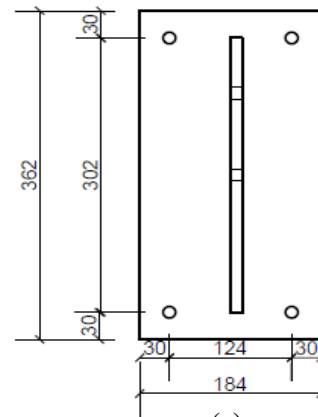
Figure 3.11 Steel T-stub connector details for the 4-bolt connection configuration with bolt pattern one (P1): (a) isometric view; (b) front view; (c) back view; (d) top view.



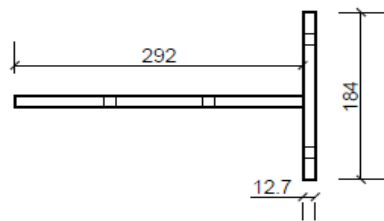
(a)



(b)



(c)



(d)

Figure 3.12 Steel T-stub connector details for the 4-bolt connection configuration with bolt pattern two (P2): (a) isometric view; (b) front view; (c) back view; (d) top view.

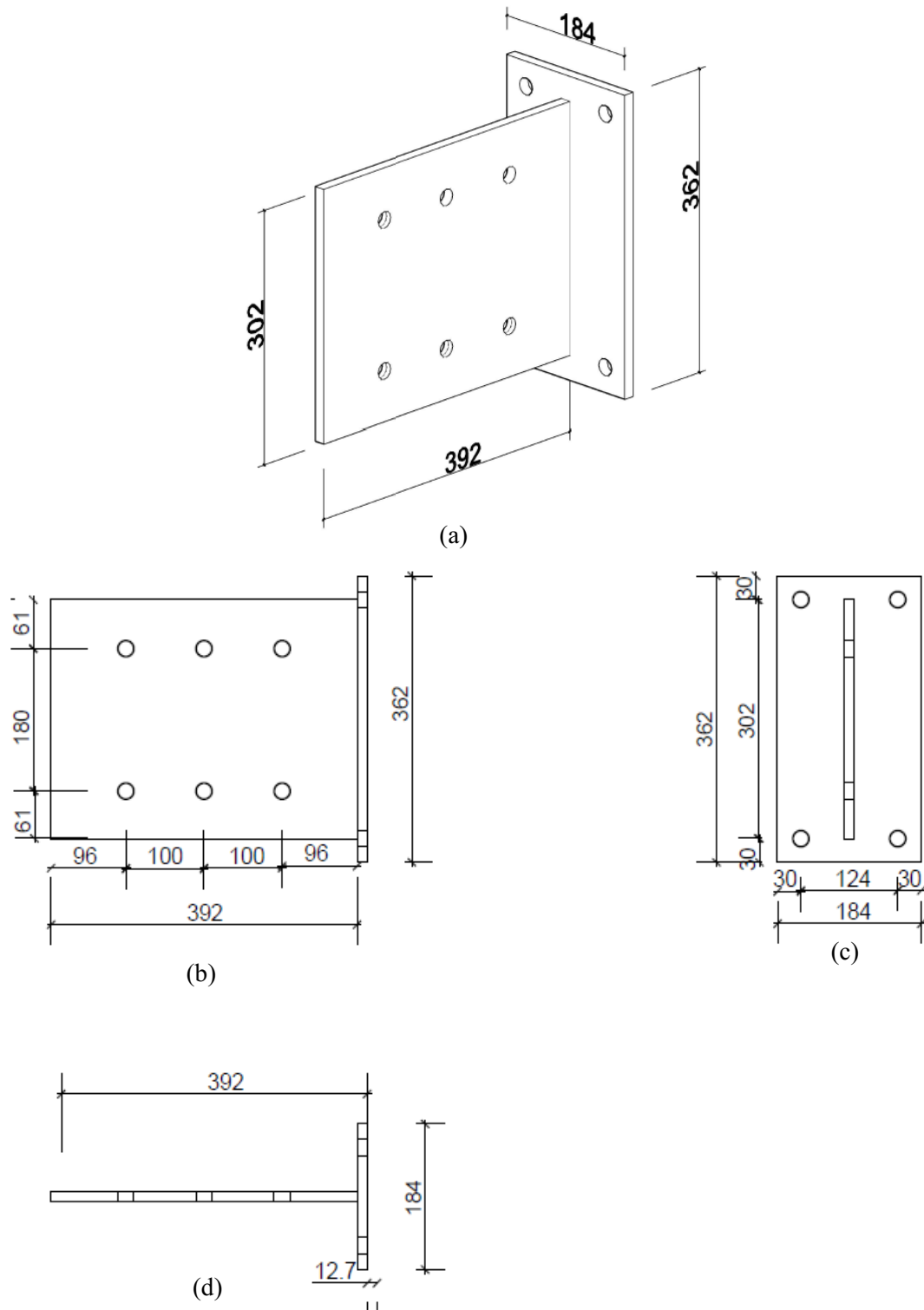


Figure 3.13 Steel T-stub connector details for the 6-bolt connection configuration with bolt pattern one (P1): (a) isometric view; (b) front view; (c) back view; (d) top view.

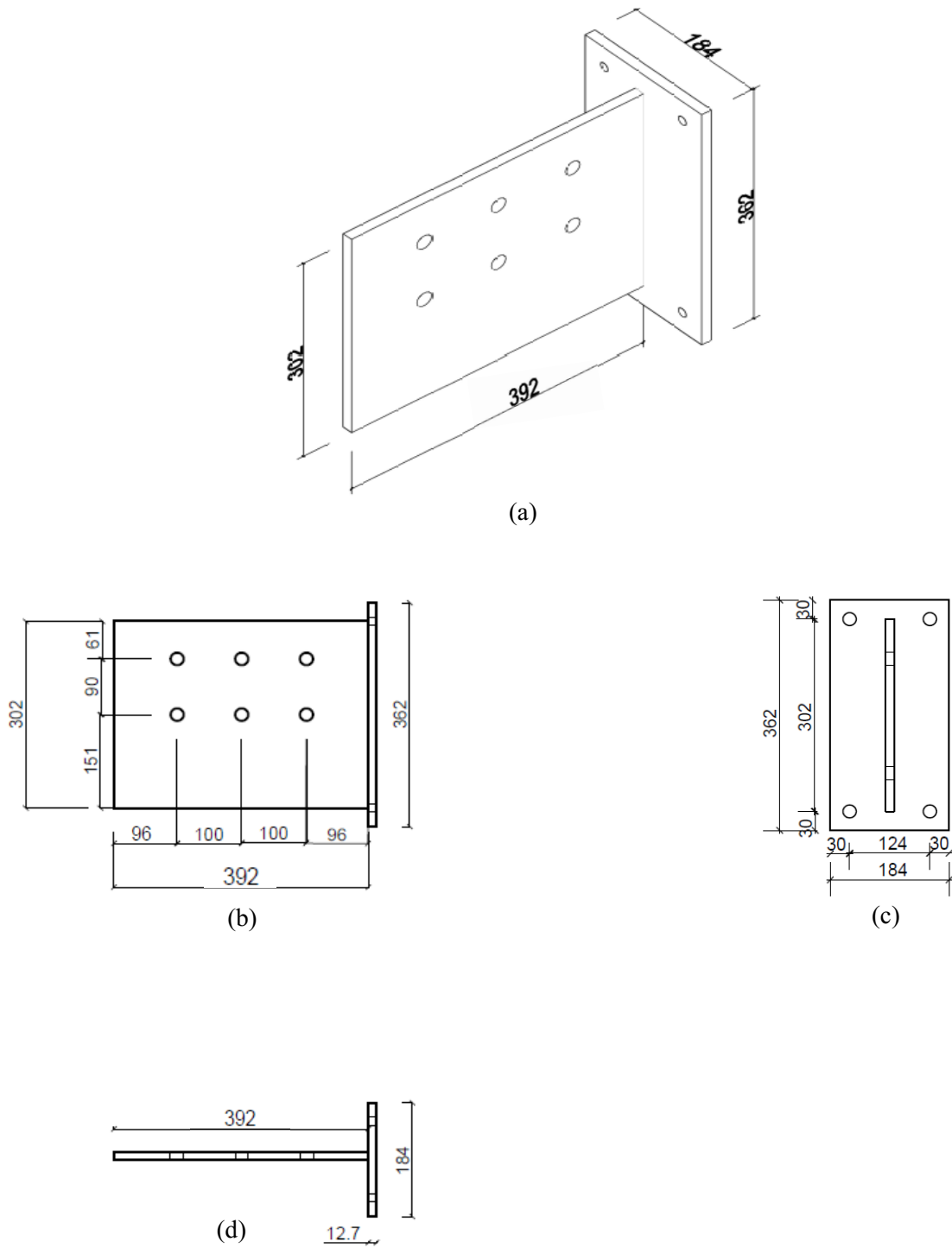


Figure 3.14 Steel T-stub connector details for the 6-bolt connection configuration with bolt pattern two (P2): (a) isometric view; (b) front view; (c) back view; (d) top view.

3.4.3 Self-tapping screws

The STS used to reinforce the glulam beam-end connections were SWG ASSY VG plus CSK (MTC Solutions). The self-tapping screws had a length of 300 mm and a head diameter of 10 mm (8 mm outer thread diameter). Before driving in the STS, a pilot hole was drilled using a 3 mm diameter drill bit to a depth of 280 mm. The predrilling was done to prevent splitting of the glulam section. After the pilot hole was drilled, the STS was driven into the glulam section perpendicular to the wood grain from the top side of the beam section using an electrical impact wrench. Figure 3.15 shows the STS that was used, and Figure 3.16 shows the top view of the beam where the STS were already installed.

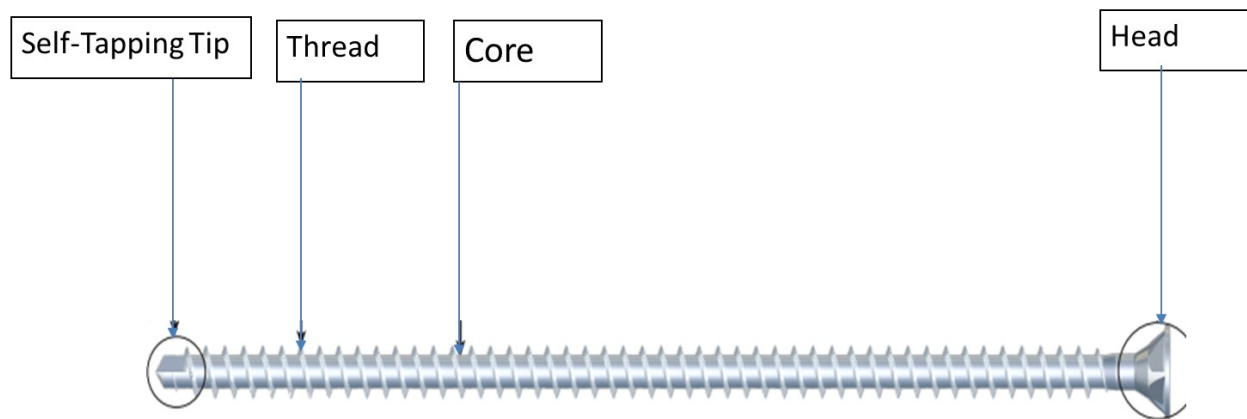


Figure 3.15 SWG ASSY VG plus CSK self-tapping screw (STS) (Adapted from MTC Solutions).



Figure 3.16 Top view of the glulam beam showing 6 STS installed.

3.5 STS and Bolts Spacing

The STS were spaced such that they are located midway between the bolt columns. This spacing was 100 mm. The edge spacing of the STS was 48 mm. Figure 3.17 illustrates the typical spacing of the STS. It should be noted that there are no codes that specify the required spacing of the STS. However, as was explained in the experimental study conducted by Gehloff et al., (2010), when STS were used to reinforce WSW connections there was an increase in the moment-resisting capacity of the connection due to increased embedment length of the installed STS. However, that increase was slight, suggesting that the location where the STS are placed has little effect on the strength capacity of the connection.

With respect to the spacing of the bolts, considering the specimens used are the same from the previous study conducted by Owusu (2019), the bolts were spaced as per the arrangement followed in Owusu (2019) study.

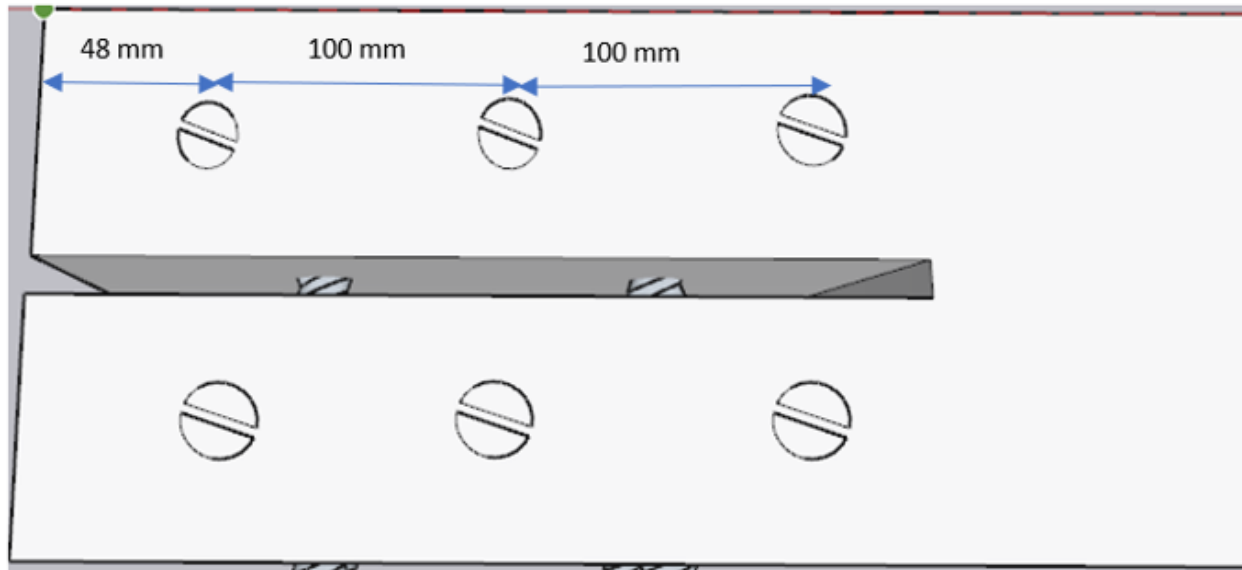


Figure 3.17 Spacing of installed STS.

3.6 Loading

During the ambient testing, the beams were loaded until the beam-end connections failed when splits were exhibited along the top and then the bottom row of bolts. The loading was applied at 1400 mm from the interface between the beam connected end and the internal face of the supporting column at a rate of 2kN/minute.

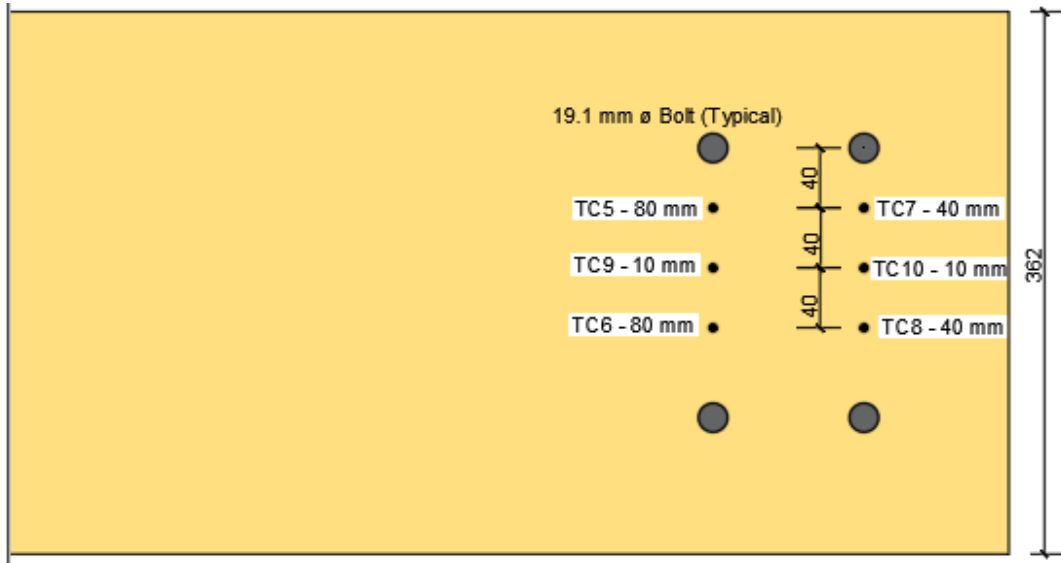
During fire testing, the applied load was continuously maintained at 10.5 kN which generated a moment of 14.8 kN.m. To be able to compare the results of the STS-reinforced connections of the present study to those of the unreinforced connections tested by Owusu (2019), the same loading level was applied. This loading level represents the ultimate design carrying capacity of the

weakest unreinforced connection configuration (4BP1) as per Cl. 12.4.4.7 of the WDM (2020). The load was applied using a loading cylinder connected to a manual hydraulic pump. A load cell was placed between the loading post and the piston of the loading cylinder and was used to accurately monitor the magnitude of the applied loads.

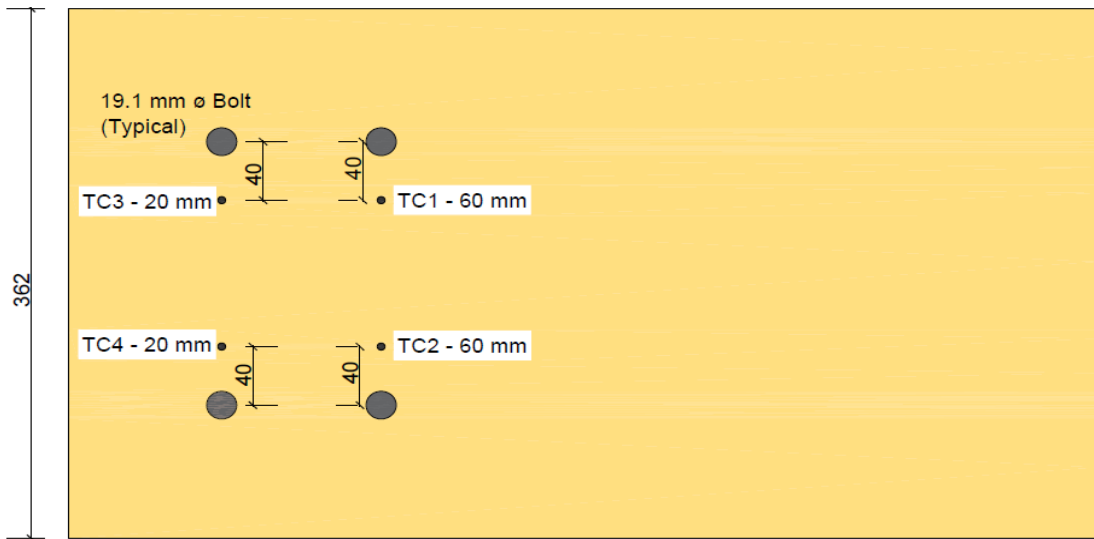
3.7 Thermocouples

In total, 12 Type-K high-temperature resistant metal-sheathed thermocouples (TC) were inserted at specific depths from the beam front, back, top, and bottom sides to measure the temperatures inside the glulam beam section during the fire tests. In addition to measuring the temperatures inside the glulam beam sections, thermal measurements were used to determine the actual charring rates of the glulam sections by generating the respective time-temperature curves.

Six (6) thermocouples were inserted from the front face, four (4) thermocouples from the back face, one (1) thermocouple from the top side, and one (1) from the bottom side of the beam. TC1 and TC2 were installed at the back face at a depth of 60 mm. TC3 and TC4 were inserted at 20 mm depth from the beam's back face. TC5 and TC6 were inserted at 80 mm depth to measure the temperature of the T-stub steel connector. TC7 and TC8 were inserted at 40 mm depth, and TC9 and TC10 were inserted at 10 mm depth. TC11 and TC12 were inserted to measure the temperature of one of the top bolts and one of the bottom bolts, respectively. Figures 3.18 and 3.19 illustrate the arrangement of the thermocouples on the beam front and back faces for the connection configurations with bolt patterns (P1 and P2), respectively.

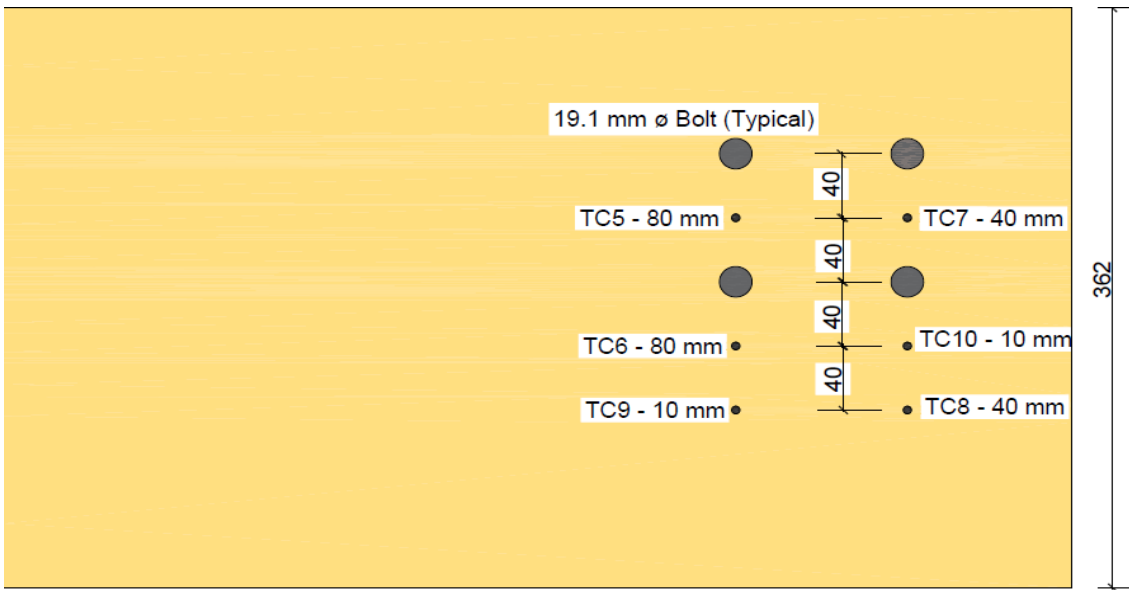


(a) Beam front face

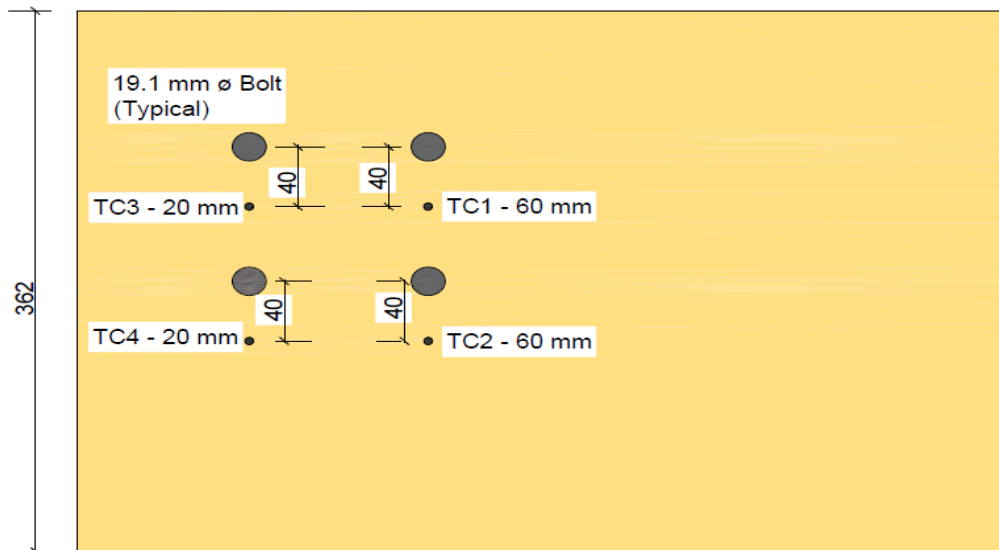


(b) Beam back face

Figure 3.18 Thermocouples arrangement in the connection configurations with bolt pattern (P1)



(a) Beam front face



(b) Beam back face

Figure 3.19 Thermocouples arrangement in the connection configurations with bolt pattern (P2)

3.8 Test Matrix

In total, eight (8) full-size previously damaged glulam beam-end WSW connections that were retrofitted using STS were subsequently tested in standard fire conditions. The parameters that were investigated in this study are the influence of the STS and the effects of the number of bolts, bolt pattern, and the applied protection of the connection steel connecting components (i.e., bolts heads and nuts, and steel plate edges) on the fire resistance time of the retrofitted connections.

Table 3.2 outlines the test matrix of the present study.

Table 3.2 Test matrix

Connection Configuration ID.	Load Applied (kN)	Moment Applied (kN.m)	No. of Bolts Used	No. of STS Used
4BP1NP	10.5	14.8	4	6
4BP2NP	10.5	14.8	4	6
6BP1NP	10.5	14.8	6	8
6BP2NP	10.5	14.8	6	8
4BP1P	10.5	14.8	4	6
4BP2P	10.5	14.8	4	6
6BP1P	10.5	14.8	6	8
6BP2P	10.5	14.8	6	8

Notes: 4B = 4 bolts; 6B = 6 bolts; P1 = Pattern 1; P2 = Pattern 2; NP = Not protected; P = Protected.

Chapter 4: Experimental Tests Results and Discussion

4.1 Introduction

This chapter outlines the experimental results and discussion of the ambient and fire tests conducted as part of the experimental program of this research. It should be noted that the ambient tests conducted as part of the present study are a continuation from those tests conducted by Owusu (2019) in order to deliberately damage a few additional glulam beams that were not damaged or were not tested during the said prior related study. The main objective of this research is to investigate the strengthening effect of STS reinforcement on damaged glulam beam connections under standard fire exposure. The experimental results of the eight (8) tested glulam beam connection configurations are presented herein. Additionally, the effects of the STS reinforcement on the fire resistance of each connection configuration were compared to that of the unreinforced connections which were examined by Owusu (2019) in order to investigate the strengthening effect of the STS. The failure modes of the reinforced connections were compared to those exhibited by the unreinforced connections and the effects of the initial damage (wood splits) on the fire resistance of each connection configuration were evaluated and discussed. Other factors including the effects of the number of bolts, and bolt patterns on the connection rotational behaviour and fire resistance time were also investigated. Finally, the actual charring rates and the time-temperature curves of each connection configuration were determined and presented in this chapter.

4.2 Ambient Temperature Tests Results

The ambient testing was a continuation of the tests conducted by Owusu (2019). In total, eight (8) specimens were tested at ambient temperatures. In the current study, three specimens were tested. Testing of the other five specimens was completed as part of the Owusu (2019) study. The results

of the ambient testing, including failure loads, maximum moments, and maximum rotations are summarized in Table 4.1.

At ambient temperature, the beams were deliberately loaded until splits were present along the top and then the bottom row of bolts. The glulam beams were then reinforced with STS and retested under standard fire exposure to investigate the effects of the STS as a reinforcing technique on the damaged beams.

Table 4.1 Ambient temperature results.

Connection Configuration ID.	Failure Load (kN)	Maximum Moment (kN.m)	Maximum Rotation (rad)	Failure Mode
4BP1NP	18.9	26.5	0.013	Splitting
4BP2NP	36.3	50.9	0.047	Splitting/Eventual row shear out
6BP1NP	31.4	44.0	0.015	Splitting
6BP2NP*	56.0	78.0	0.041	Splitting
4BP1P	17.7	24.8	0.017	Splitting
4BP2P*	24.8	34.7	0.037	Splitting
6BP1P	21.6	30.2	0.016	Splitting
6BP2P*	32.9	46.1	0.034	Splitting

Notes: 4B = 4 bolts; 6B = 6 bolts; P1 = Pattern 1; P2 = Pattern 2; NP = Not protected; P = Protected.

* Specimens that were tested as part of the current study. The other tests were conducted by Owusu (2019).

4.3 Fire Resistance Test Results

After the glulam beams were experimentally tested until their end connections failed at ambient temperature, they were reinforced with STS and then tested under standard fire exposure. As noted, eight (8) full-size retrofitted glulam beams were experimentally examined at elevated

temperatures. Table 4.2 summarizes the results of the fire resistance tests, as well as the results of the fire resistance tests conducted by Owusu (2019) on identical but unreinforced connection configurations for comparison purposes.

Table 4.2 Summary of all fire resistance tests.

Connection configuration ID.	Unreinforced connection fire resistance time – Owusu (2019) (Minutes)	Unreinforced connection failure mode	Reinforced connection fire resistance time (Minutes)	Reinforced connection failure mode
4BP1NP	33	Wood splitting and row shear at the top bolt row	22	Excessive cracking and slight row-shear out due to high initial cracks width in the top bolt row
6BP1NP	22	Glue line Plane Failure	31	Excessive cracking along the top rows of the bolts. Glue line failure was prevented
4BP2NP	32	Wood splitting and row shear at the top bolt row	27	Localized failure at a natural defect (knot), which is a weak spot.
6BP2NP	27	Glue line Plane Failure	38	Excessive splitting along the top bolt row. Glue line failure was prevented
4BP1P	56	Wood split at the top bolt row	43	Excessive charring along the top bolt row and slight row-shear out. When compared to the 4BP1PF ₁ , 77% of the beam's original strength was restored. Glue line splitting was prevented
4BP1P(R)	42	Sudden glue line failure along the top bolt row		
6BP1P	48	Glue line failure along the top and bottom bolt row	60	Excessive charring along the top and bottom bolt rows. The

6BP1P(R)	62	Excessive charring and wood split at the top bolt row		section was severely charred at all locations at failure. When compared to the 6BP1PF ₂ , 97% of the beam's original strength was restored. Glue line failure was prevented.
4BP2P	48	Glue line split at the top bolt row	58	Excessive charring along the entire section.
6BP2P	41	Glued plane split at the second row of bolts along the.	57	Excessive charring in the entire section; Slight row-shear out. Glue line failure was prevented.

Notes: 4B = 4 bolts; 6B = 6 bolts; P1 = Pattern 1; P2 = Pattern 2; NP = Not protected; P = Protected; R = Repeated.

It should be noted that for the undamaged, unreinforced, and unprotected connections tests by Owusu (2019), two connection configurations were tested twice (4BP1P and 6BP1P), as those two configurations achieved the greatest fire resistance time in at least one of the two tests. In the current study, all connection configurations were tested once. It should be also noted that glue line failure was very common in the unreinforced connections Owusu (2019). Once glue line failure splits occurred in the unreinforced connection, the specimen failed almost immediately Owusu (2019). As explained in this section, this mode of failure was prevented in the STS-reinforced connections, which resulted in greater fire resistance times.

In the following sections, a comparison of the fire resistance test results of the STS-reinforced connections with those of the undamaged, unreinforced connections is provided to illustrate the strengthening effect of the STS on each of the eight beam-end connection configurations tested. The time-rotation and time-temperature curves for each connection configuration are also presented. Lastly, the average charring rate for each of the eight configurations is addressed.

4.3.1 Effects of using self-tapping screws in the unprotected connections

For the STS-retrofitted connection configuration that utilized four bolts in the first bolt pattern (P1), the fire resistance time was 22 minutes. The fire resistance time of the identical undamaged, unreinforced connection tested by Owusu (2019) was 33 minutes. The retrofitted connection failed due to excessive splitting and slight row-shear out along the top row of bolts. The width of the initial main split of the connection due to ambient testing was approximately 5 mm. Figure 4.1 illustrates the initial state and splits that existed in the beam at the connection location.

During the initial 15 minutes of the fire test, it was observed that the splitting of the specimen did not propagate. However, as the fire progressed, and due to the initial extensive splitting of the specimen, the heat penetrated the wood core which eventually increased the width of the initial main split and led to the failure of the beam connection. Images of the beam during fire testing were taken at 15-minute intervals and are shown in Figure 4.2. As such, the initial splitting resulted in 11 minutes less fire resistance time as compared to the undamaged connection tested by Owusu (2019).



Figure 4.1 Initial state of the STS-retrofitted, unprotected connection configuration that utilized four bolts in the first bolt pattern (4BP1NP).



After 15 minutes



At failure (22 minutes)

Figure 4.2 Fire testing timeline for the STS-retrofitted, unprotected connection configuration that utilized four bolts in the first bolt pattern (4BP1NP).

For the STS-retrofitted, unprotected connection configuration that utilized six bolts in the first bolt pattern, the fire resistance time was 31 minutes. The beam failed due to excessive splitting along the top row of the bolts. The fire resistance time of the identical unreinforced, undamaged, and unprotected connection failed after 22 minutes only due to an unexpected glue line delamination. When using STS, the sudden glue line delamination that occurred in the unreinforced, undamaged connection did not take place. This kept the glulam beam section intact at the connection location and hence resulted in longer fire-resistant time. The initial splitting of the beam at the connection was approximately 1-2 mm. The small initial splitting width further contributed to the increased fire resistance time of this specimen as compared to the undamaged connection and the four-bolt, STS-retrofitted damaged configuration. The initial state of the STS-retrofitted, unprotected connection configuration that utilized six bolts in the first bolt pattern (P1) connection is shown in Figure 4.3.



Figure 4.3 Initial state of the STS-retrofitted, unprotected connection configuration that utilized six bolts in the first bolt pattern (6BP1NP).



After 15 minutes



At failure (31 minutes)

Figure 4.4 Fire testing timeline for the STS-retrofitted, unprotected connection configuration that utilized six bolts in the first bolt pattern (6BP1NP).

For the STS-retrofitted, unprotected connection configuration that utilized four bolts in the second bolt pattern (P2), the fire resistance time was 27 minutes. In this specimen, it can be observed from Figure 4.5 that there was a natural defect (knot) to the left of the bolt labeled No. 1. After 15 minutes into fire testing, it was observed that a glue line delamination almost at the mid-height of the beam section started to take place. As the fire progressed, it was observed that the flames propagated upwards towards the knot, which resulted in increased localized charring. Upon failure, it can be observed from Figure 4.6 that the location of the knot is charred much more significantly as compared to the top or bottom rows of bolts. Therefore, it is believed that the presence of this wood natural defect contributed to the failure, and the beam could have achieved a longer fire resistance time if this knot did not exist, as the top and bottom rows of bolts mostly remained intact till the end of the fire test. The undamaged beam connection had 32 minutes of fire resistance time and failed due to excessive splitting at the top row of bolts.

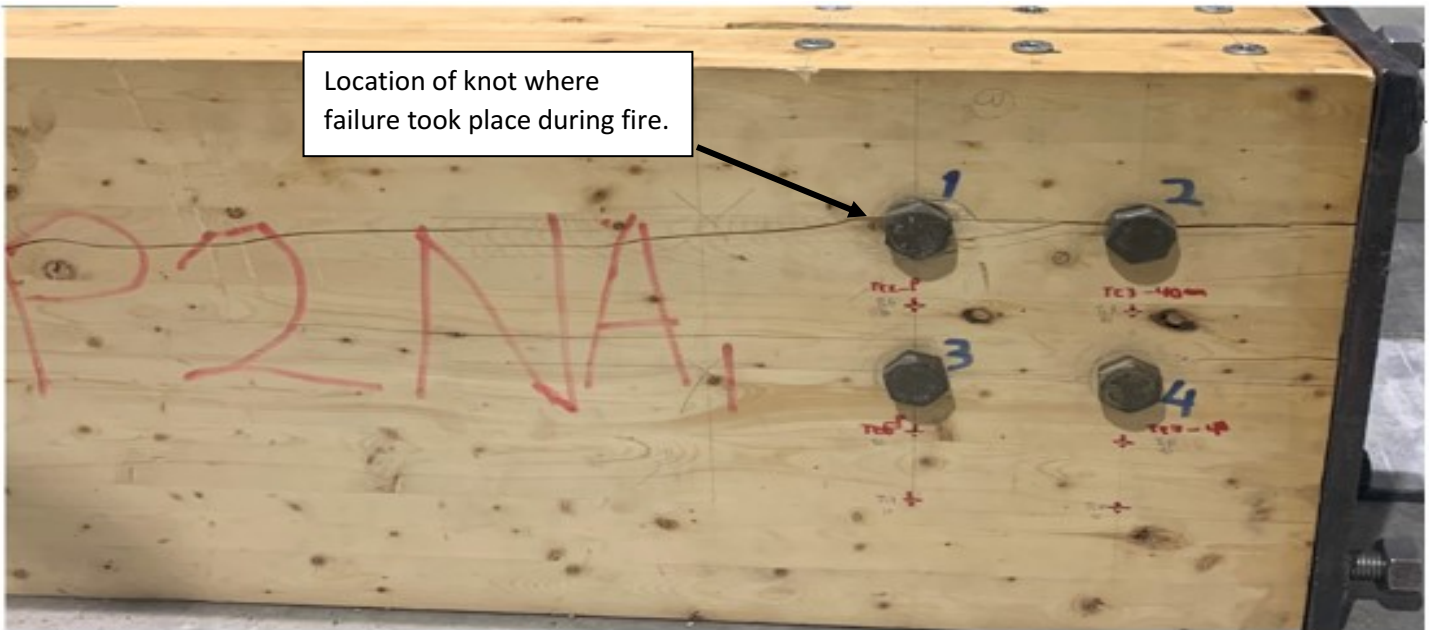
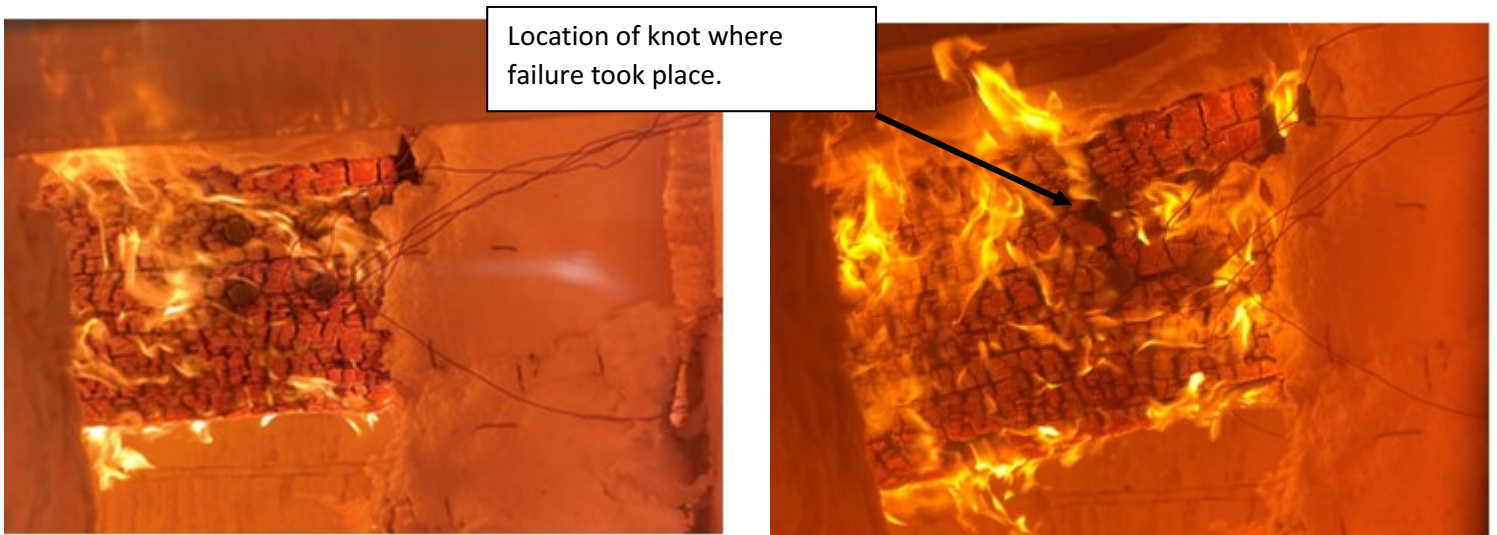


Figure 4.5 Initial state of the STS-retrofitted, unprotected connection configuration that utilized four bolts in the second bolt pattern (4BP2NP)



After 15 minutes

At failure (27 minutes)

Figure 4.6 Fire testing timeline for the STS-retrofitted, unprotected connection configuration that utilized four bolts in the second bolt pattern (4BP2NP).

For the STS-retrofitted, unprotected connection configuration that utilized six bolts in the second bolt pattern (P2), the fire resistance time was 38 minutes. The initial split in the beam had an approximate width of 1 mm (Figure 4.7). The reinforced beam failed due to excessive splitting along the top row of bolts. The identical undamaged connection tested by Owusu (2019) had a fire resistance time of 27 minutes and failed due to unexpected glue line delamination that resulted in a sudden splitting along the top row of bolts. After 15 minutes into the fire test of the retrofitted connection, it was noticed that a glue line delamination started to occur between the top and bottom rows of bolts (Figure 4.8). Although this glue line delamination was observed in both the undamaged and the retrofitted connections, in the STS-reinforced connection, it did not result in immediate failure of the beam-end connection as failure was governed mainly by a reduction in the connection strength due to charring. This can be attributed to the presence of the STS which kept the glulam beam section intact with the wood fibers confined in the perpendicular-to-wood grain direction and thus, prevented the propagation of the initial splits. Accordingly, this resulted in a noticeable reduction in the fire resistance time of the beam core.



Figure 4.7 Initial state of the STS-retrofitted, unprotected connection configuration that utilized six bolts in the second bolt pattern (6BP2NP).

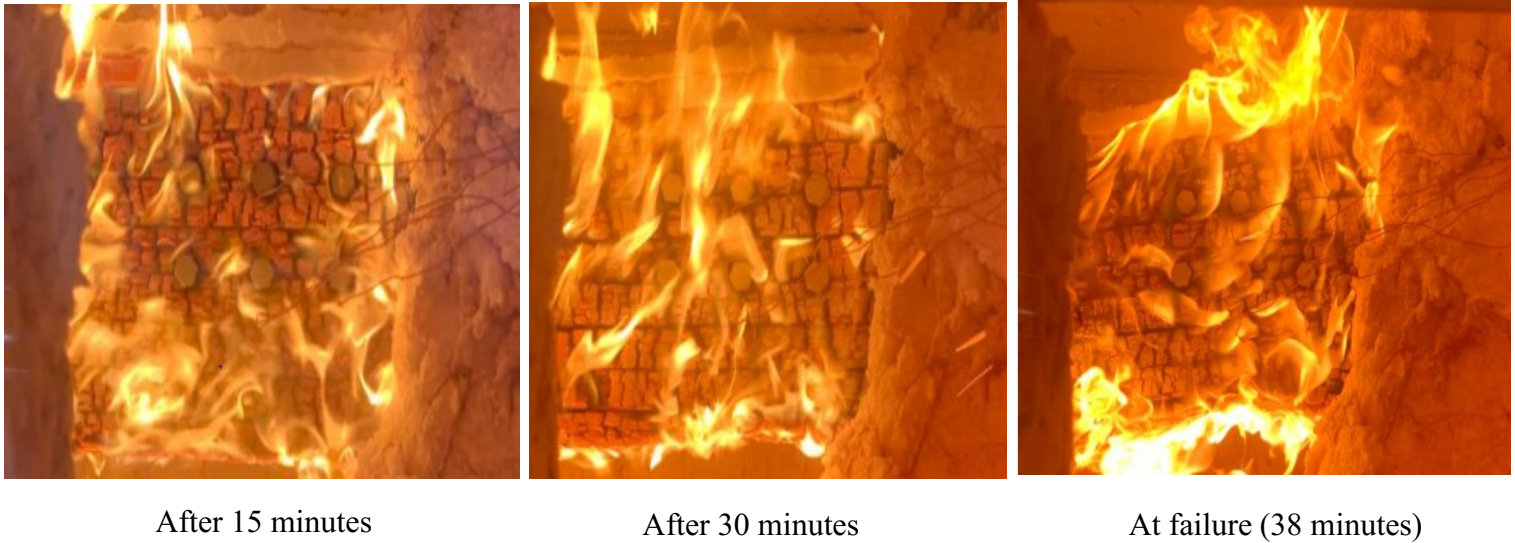


Figure 4.8 Fire testing timeline for the STS-retrofitted, unprotected connection configuration that utilized six bolts in the second bolt pattern (6BP2NP).

4.3.2 Effects of using self-tapping screws in the protected connections

For the STS-retrofitted, protected connection configuration that utilized four bolts in the first bolt pattern (P1), the fire resistance time was 43 minutes. The initial split of the beam formed along the top row of bolts had a width of approximately 3 mm (Figure 4.9). The STS-reinforced beam connection failed due to a reduction in the strength because of charring. The identical undamaged, unreinforced connection tested by Owusu (2019) was tested twice. The fire resistance times were 56 and 42 minutes (average of 49 minutes). The 14 minutes less fire resistance time of the connection examined in the second fire test compared to the same connection examined in the first test can be attributed to wood splitting that occurred at a glue line due to delamination. Therefore, the damaged, STS-retrofitted connection achieved a lower fire resistance time by 13 minutes compared to the undamaged, unreinforced connection which did not experience glue line delamination. It also had a 1-minute greater fire resistance time than that of the identical undamaged, unreinforced connection in which the glue line delamination caused the earlier failure.

Based on the above-mentioned results, it can be concluded that the STS restored 77% of the beam's original fire resistance time and the wood splitting failure due to the glue line delamination was prevented. According to the images taken during the fire test (Figure 4.10), excessive charring localized along the top row of bolts with small wood chunks falling off was observed. It is believed that the relatively wide initial split that existed in the connection before being refitted (3 mm) may have resulted in this excessive localized charring, as it caused the heat of the fire to penetrate through and accelerated the wood burning.



Figure 4.9 Initial state of the STS-retrofitted, protected connection configuration that utilized four bolts in the first bolt pattern (4BP1P).



After 15 minutes

After 30 minutes

At failure (43 minutes)

Figure 4.10 Fire testing timeline for the STS-retrofitted, protected connection configuration that utilized four bolts in the first bolt pattern (4BP1P).

For the STS-retrofitted, protected connection configuration that utilized six bolts in the first bolt pattern (P1), the fire resistance time was 60 minutes. The initial split had a width of approximately 3 mm and thus, the connection failed due to excessive charring localized mainly along the top row of bolts, where the main split existed. It was also observed after failure (Figure 4.12) that the beam section was severely charred at the bottom as well. Glue line delamination was observed to happen in the STS-reinforced connection between the top and bottom rows of bolts; however, this did not result in any accelerated failure of the connection. Conversely, in the identical undamaged, unreinforced connection tested by Owusu (2019), the fire resistance time was only 48 minutes and the connection failed suddenly mainly due to glue line delamination that occurred along the top row of bolts. When the test was repeated for this connection configuration by Owusu (2019), the connection was able to sustain the applied loads for 62 minutes, since no glue line delamination took place. Therefore, the fire test results of the STS-retrofitted connection show that the presence of the STS prevented the glue line delamination and enhanced the fire resistance time of the

connection where approximately 97% of the fire resistance time was restored. The difference in the fire resistance time of the STS-retrofitted connection and that of the second undamaged, unreinforced connection tested by Owusu (2019) can be attributed to the presence of the initial split in the STS-retrofitted connection, which led to 2 minutes less fire resistance.



Figure 4.11 Initial state of the STS-retrofitted, protected connection configuration that utilized six bolts in the first bolt pattern (6BP1P).



After 15 minutes



After 30 minutes



After 45 minutes



At failure (60 minutes)

Figure 4.12. Fire testing timeline for the STS-retrofitted, protected connection configuration that utilized six bolts in the first bolt pattern (6BP1P).

For the STS-retrofitted, protected connection configuration that utilized four bolts in the second bolt pattern (P2), the fire resistance time was 58 minutes. The initial split exhibited by the connection had a width of less than 1 mm (Figure 4.13). Thus, the beam connection failed due to excessive reduction in its strength as a result of charring, and not due to any glue line delamination (Figure 4.14).

It was noticed that the fire resistance time of the identical undamaged, unreinforced connection tested by Owusu (2019) was 48 minutes and it failed due to wood splitting as a result of a glue line delamination that occurred along the top row of bolts. The significant increase in the fire resistance time of the STS-retrofitted connection compared to that of the undamaged, unreinforced connection tested by Owusu (2019) is primarily due to the STS preventing wood splitting as a

result of the glue line delamination. In addition, the very minimal width of the initial split exhibited by the beam reduced fire heat penetrated through it into the beam section. This is unlike the six-bolt connection configuration where the initial split had greater width (almost three times wider).



Figure 4.13 Initial state of the STS-retrofitted, protected connection configuration that utilized four bolts in the second bolt pattern (4BP2P).



After 15 minutes



After 30 minutes



After 45 minutes



At failure (58 minutes)

Figure 4.14 Fire testing timeline for the STS-retrofitted, protected connection configuration that utilized four bolts in the second bolt pattern (4BP2P).

For the STS-retrofitted, protected connection configuration that utilized six bolts in the second bolt pattern (P2), the fire resistance time was 57 minutes. The initial split had a width of approximately 1 mm. Also, the beam connection failed due to a reduction in its strength as a result of excessive charring when subjected to fire. The undamaged, unreinforced connection tested by Owusu (2019) had a fire resistance time of only 41 minutes and failed prematurely due to a wood splitting as a result of glue line delamination that occurred along the top row of bolts. Similar to other STS-retrofitted connection configurations, the glue line delamination mode of failure was prevented due to the presence of the STS. This combined with the small width of the initial split resulted in the STS-retrofitted connection achieving 16 minutes of additional fire resistance time as compared to the identical undamaged, unreinforced connection.



Figure 4.15 Initial state of the STS-retrofitted, protected connection configuration that utilized six bolts in the second bolt pattern (6BP2P).



After 15 minutes



After 30 minutes



After 45 minutes



At failure (57 minutes)

Figure 4.16 Fire testing timeline for the STS-retrofitted, protected connection configuration that utilized six bolts in the second bolt pattern (6BP2P).

4.3.3 Effects of the number of bolts on the fire resistance of the unprotected connections

For the STS-retrofitted, unprotected connection configurations that utilized six bolts in the first and second bolt patterns (P1 and P2), the fire resistance times achieved were 31 and 38 minutes, respectively. Whereas for the STS-retrofitted, unprotected connection configuration that utilized only four bolts in the first and second bolt patterns (P1 and P2), the fire resistance times achieved were 27 and 27 minutes, respectively. This shows that increasing the number of bolts from four to six increases the fire resistance times.

4.3.4 Effects of the number of bolts on the fire resistance of the protected connections

The STS-retrofitted, protected connection configuration that utilized six bolts in the first bolt pattern (P1) achieved a fire resistance time that is 17 minutes greater than that of the connection with four bolts arranged in the same bolt pattern (P1). Both STS-retrofitted connections had the width of their initial splits of approximately 3 mm. Therefore, it can be seen that increasing the number of bolts from four to six resulted in better load distribution amongst the group of six bolts, which reduced the stresses on each bolt, leading to greater fire resistance time. On the other hand, the effect of increasing the number of bolts from four to six bolts arranged in the second bolt pattern (P2) was negligible, since the fire resistance times achieved were 58 and 57 minutes, respectively. Whereas the undamaged, unreinforced connection with four bolts arranged in the second pattern (P2) tested by Owusu (2019), had a greater fire resistance time than that of the six bolts arranged in the same bolt pattern by approximately 8 minutes. This was mainly due to the brittle failure as a result of glue line delamination that was more pronounced in the six-bolt connection. However, when the connections were retested, the six-bolt connection achieved a 20-minute higher fire resistance time compared to the four-bolt connection utilizing the same bolt pattern (P2).

In general, failure in the STS-reinforced connections depended mainly on the extent of the initial splits in the glulam beam. The greater the width of splitting is, the earlier the beam-end connection failed under standard fire exposure. Also, when the width of the initial split was the same, it was found that increasing the number of bolts from four to six resulted in a greater fire resistance time.

4.3.5 Effects of the bolt pattern on the fire resistance of the unprotected connections

In the unprotected connection with four bolts arranged in the first bolt pattern (4BP1NP), it was observed that the connection rotation slightly increased linearly for the first 10 minutes of the fire test. At approximately 15 minutes, the rotation began to increase in more of an exponential trend until failure at only 22 minutes. On the other hand, in the unprotected connection with four bolts arranged in the second bolt pattern (4BP2NP), the rotations increased more linearly for the first 20 minutes. Afterward, the connection rotation began to increase exponentially until failure. As a result, the connection with four bolts arranged in the second bolt pattern (P2) had 5 minutes longer fire resistance time. Figure 4.17 depicts the time-rotation relationships for the 4BP1NP and 4BP2NP STS-reinforced connections.

For the undamaged, unreinforced, and unprotected connection tested by Owusu (2019), it was noticed that both four-bolt connection configurations experienced very slight rotations for the first 17 minutes or so. Afterward, the rotation began to increase exponentially until failure. Therefore, it can be seen that usage of the STS allowed the connection to experience more ductile behaviour and a more gradual increase in its rotation until failure. Figure 4.18 depicts the time-rotation relationships for the 4BP1NF1 and 4BP2NF1 undamaged, unreinforced, and unprotected connections tested by Owusu (2019).

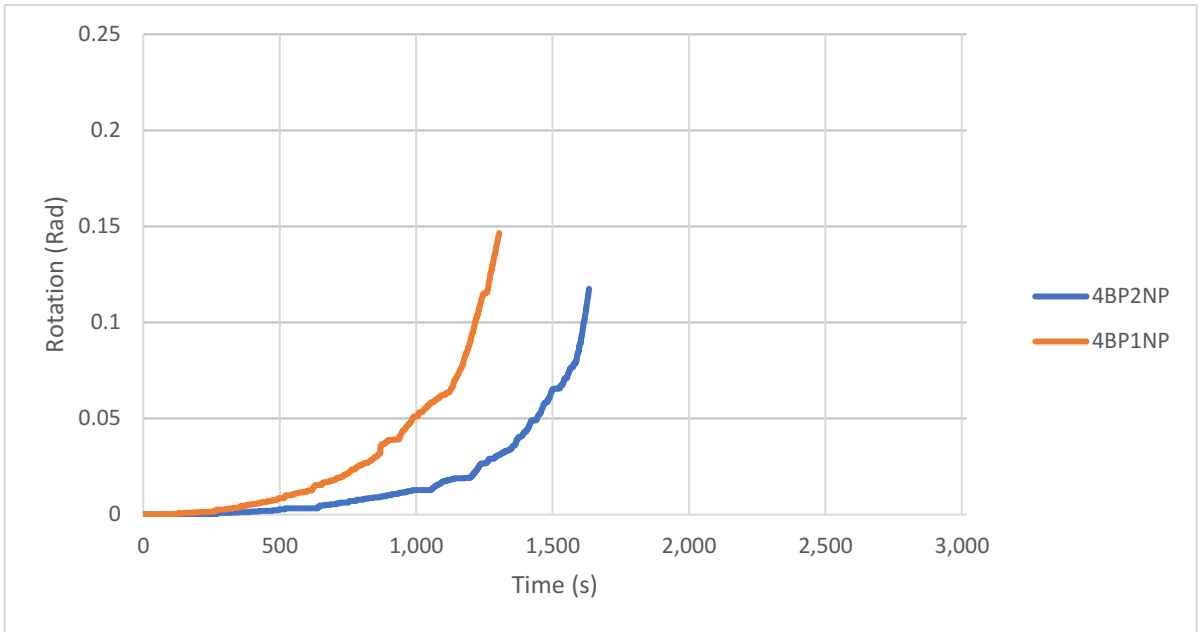


Figure 4.17 Time-rotation relationships of the STS-retrofitted, unprotected connection configurations that utilized four bolts in the first (4BP1NP) and second bolt patterns (4BP2NP).

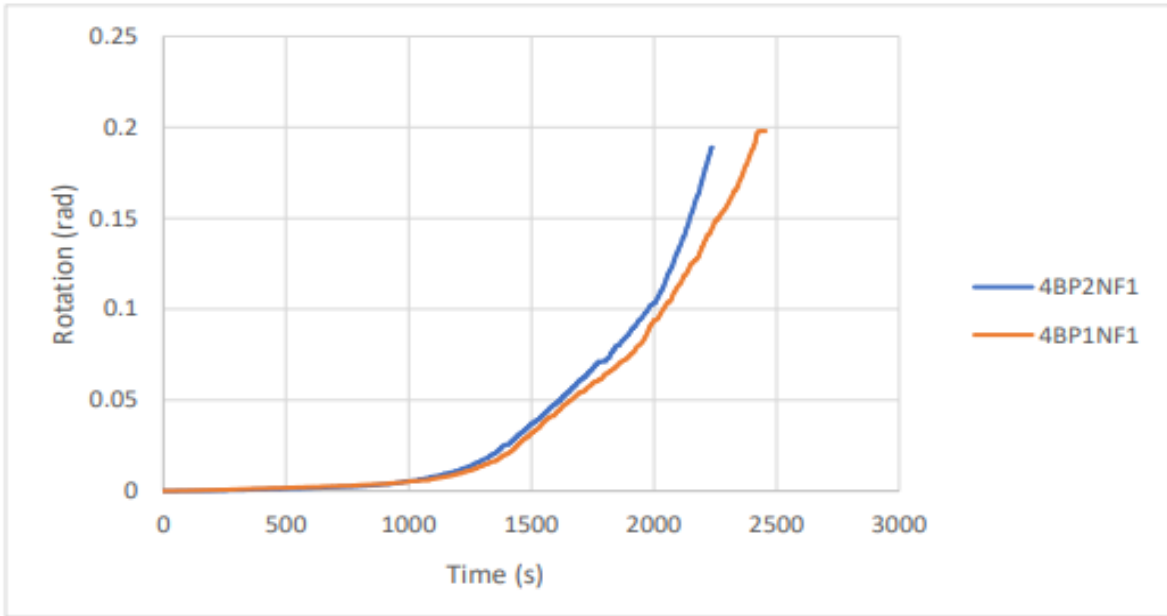


Figure 4.18. Time-rotation relationships of the undamaged, unreinforced and unprotected connection configurations that utilized four bolts in the first (4BP1NF1) and second bolt patterns (4BP2NF1) (Adapted from Owusu, 2019).

The STS-reinforced, unprotected connections with six bolts arranged in the first and second bolt patterns experienced similar rotations for the first 15 minutes of the fire test. Afterward, the rotation of the configuration that utilized the first bolt pattern (P1) began to increase exponentially until failure. Whereas the six-bolt connection configuration that utilized the second bolt pattern (P2) continued to increase linearly until 20 minutes and then, began to increase in a more exponential trend compared to that configuration that utilized the first bolt pattern (P1) until failure. The more exponential rotation increase trend in the connection configuration that utilized the second bolt pattern (P2) resulted in a 7-minute greater fire resistance time. Figure 4.19 depicts the time-rotation relationships for the 6BP1NP and 6BP2NP STS-reinforced connection configurations.

For the undamaged, unreinforced, and unprotected connection tested by Owusu (2019), it was observed that both six-bolt connection configurations experienced very limited rotations for the first 19 minutes of the fire test. Afterward, the connections underwent a steep increase in rotations, resulting in immediate failure. This was due to the brittle glue line delamination failure in both connection configurations. Figure 4.20 depicts the time-rotation relationships for the 6BP1NF1 and 6BP2NF1 undamaged, unreinforced, and unprotected connections tested by Owusu (2019).

As the STS prevented the brittle failure that was seen in the undamaged, unreinforced, and unprotected connections, the rotation of the connection reinforced with STS increased in a more linear trend and hence had longer fire resistance time compared to the unreinforced connections.

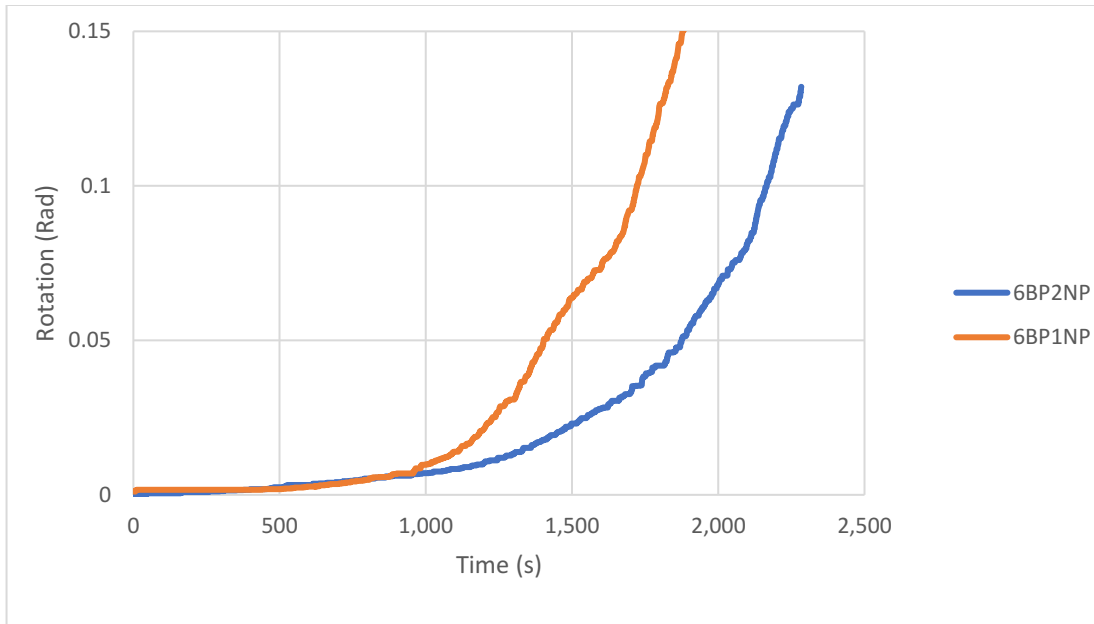


Figure 4.19 Time-rotation relationships of the STS-retrofitted, unprotected connection configurations that utilized six bolts in the first (6BP1NP) and second bolt patterns (6BP2NP).

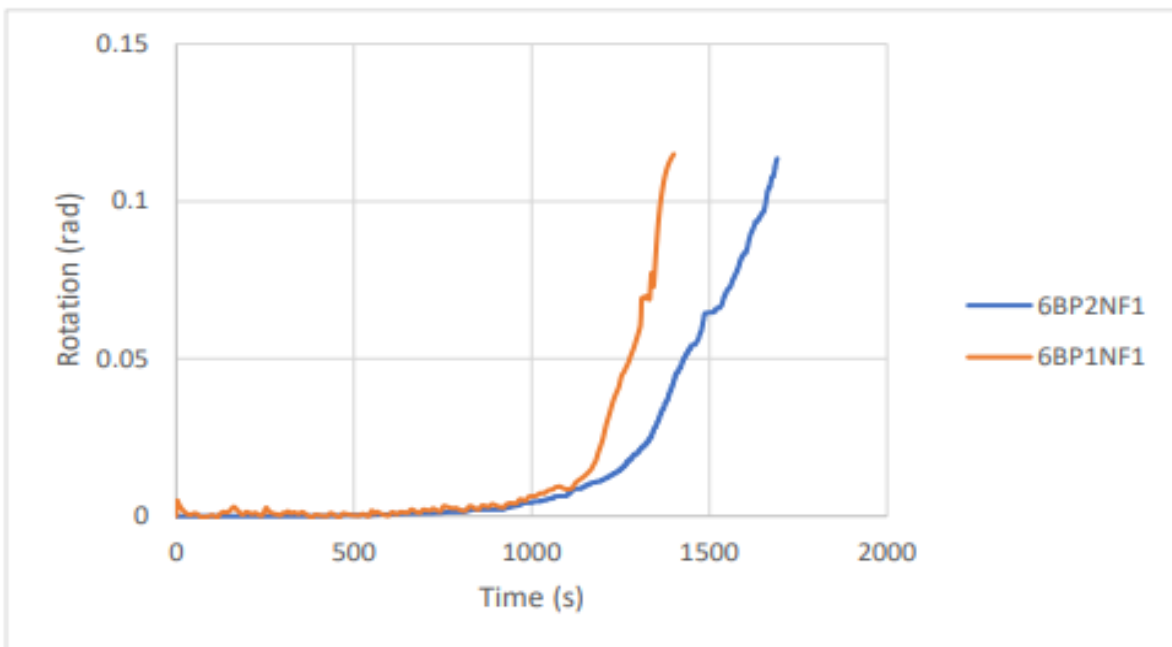


Figure 4.20 Time-rotation relationships of the undamaged, unreinforced, and unprotected connection configurations that utilized six bolts in the first (6BP1NF1) and second bolt patterns (6BP2NF1) (Adapted from Owusu, 2019).

4.3.6 Effects of the bolt pattern on the fire resistance of the protected connections

For the STS-reinforced and protected connection with four bolts arranged in the first bolt pattern (P1), the rotation increased linearly for the first 23 minutes. Afterward, the rotation began to increase more rapidly and in an exponential trend until failure at 43 minutes (Figure 4.21). Similarly, the connection configuration with four bolts but arranged in the second bolt pattern (P2) experienced linearly increased rotations for most of the fire test duration. The rotation increased linearly for the first 50 minutes and then, it began to increase more rapidly and in an exponential trend until failure at 58 minutes (Figure 4.21). Figure 4.21 depicts the time-rotation relationships for the 4BP1P and 4BP2P STS-reinforced connection configurations.

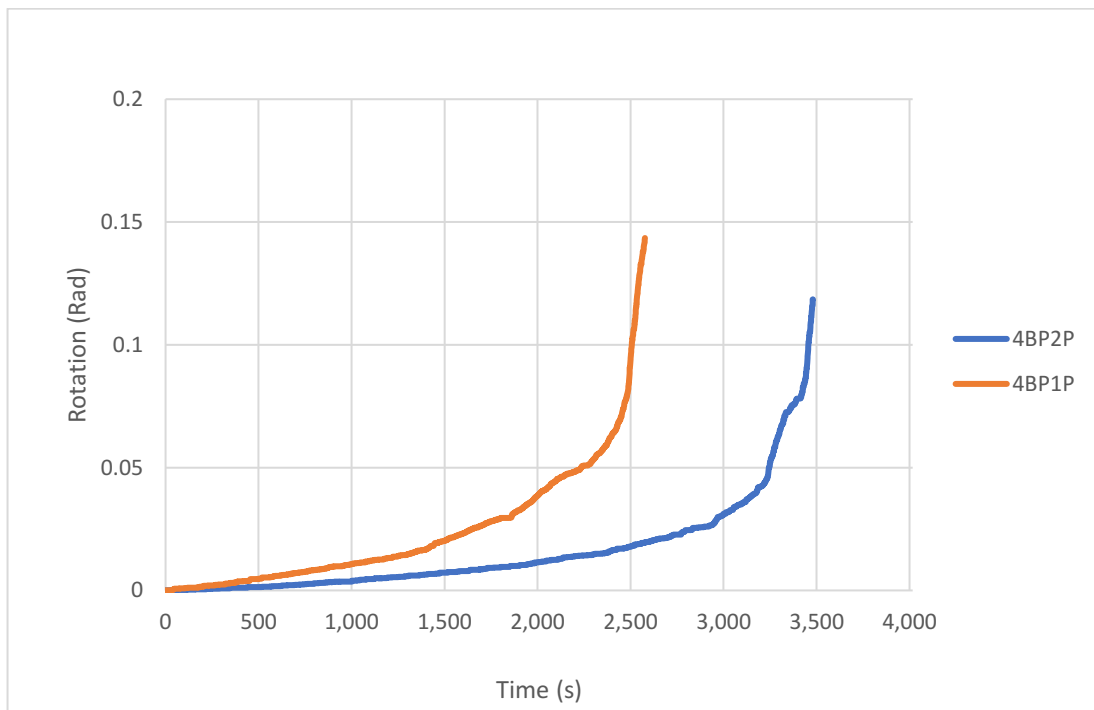


Figure 4.21 Time-rotation relationships of the STS-retrofitted, unprotected connection configurations that utilized six bolts in the first (6BP1NP) and second bolt patterns (6BP2NP).

Whereas for the undamaged, unreinforced, and protected connections tested by Owusu (2019), it was noticed that for the configuration with four bolts arranged in the second bolt pattern (P2) the connection experienced a sharp exponential increase in its rotation after 40 minutes into the fire test, which led to immediate failure shortly afterward. This was due to the splitting occurring at the glue line aligned with the top row of bolts in the connection. On the other hand, the similar connection configuration with four bolts but arranged in the first bolt pattern (P1) experienced similar linearly increased rotations but for a slightly longer time in the fire test, which resulted in greater fire resistance time than that of the connection with four bolts arranged in the second bolt pattern (P2).

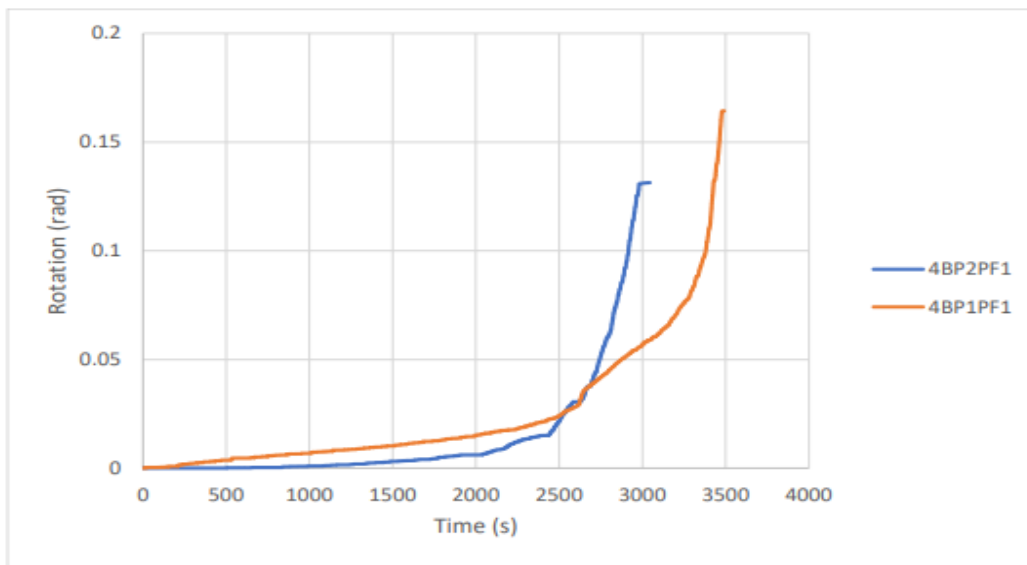


Figure 4.22 Time-rotation relationships of the undamaged, unreinforced, and protected connection configurations that utilized four bolts in the first (4BP1PF1) and second bolt patterns (4BP2PF1) (Adapted from Owusu, 2019).

It can be seen that the usage of the STS resulted in more ductile failure of the connection. Also, failure due to the glue line delamination was common in the undamaged, unreinforced connections tested by Owusu (2019) and resulted in a sharp increase in the connection rotations and shortly thereafter failure was prevented in the reinforced connection due to the presence of the STS.

The STS-reinforced, protected connections with six bolts experienced similar behaviour as the connections with four bolts. In the six-bolt connection configuration that utilized the first bolt pattern (P1), the rotation increased linearly for the first 38 minutes. The rotation then began to increase more rapidly between 38 and 49 minutes and then increased exponentially from 49 minutes until failure at 60 minutes (Figure 4.23). Similarly, the six-bolt connection configuration that utilized the second bolt pattern (P2) experienced linearly increased rotation for the first 47 minutes and then, the rotation began to increase more rapidly until failure at 58 minutes (Figure 4.23). Figure 4.23 depicts the time-rotation relationships for the 6BP1P and 6BP2P STS-reinforced connection configurations.

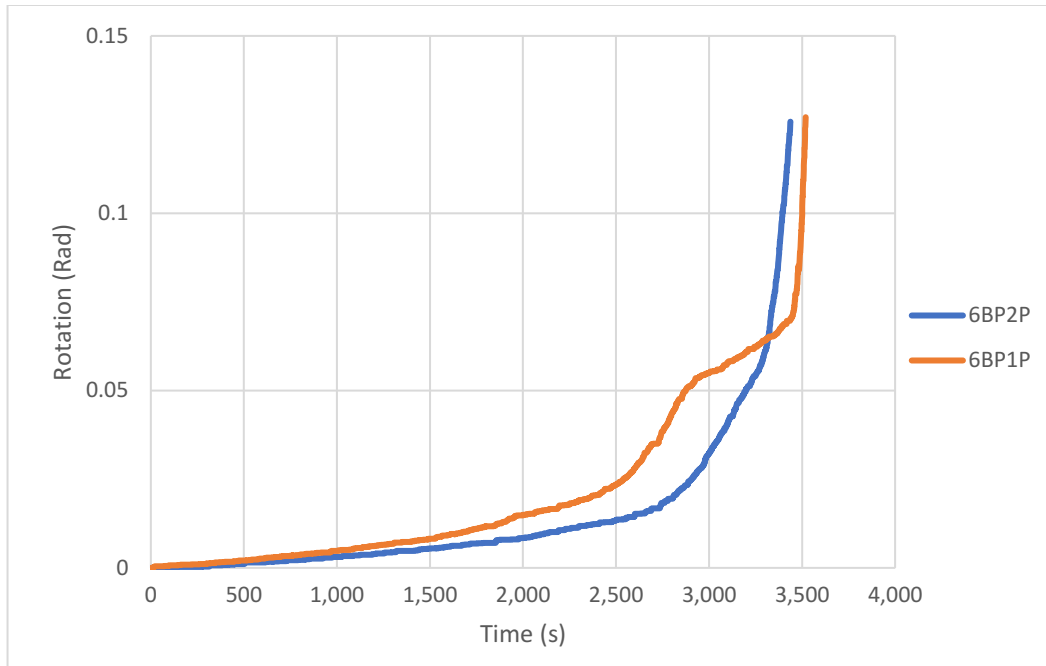


Figure 4.23 Time-rotation relationships of the STS-retrofitted, protected connection configurations that utilized six bolts in the first (6BP1P) and second bolt patterns (6BP2P).

In the undamaged, unreinforced, and protected connections tested by Owusu (2019), it was noticed that the connection underwent an initial linear behaviour, after which there was an extremely rapid increase in the connection. The sudden increase in the rotation was a result of the unexpected glue line failure within the connection. Figure 4.24 depicts the time-rotation relationships for the 6BP1PF1 and 6BP2PF1 undamaged, unreinforced, and protected connections tested by Owusu (2019).

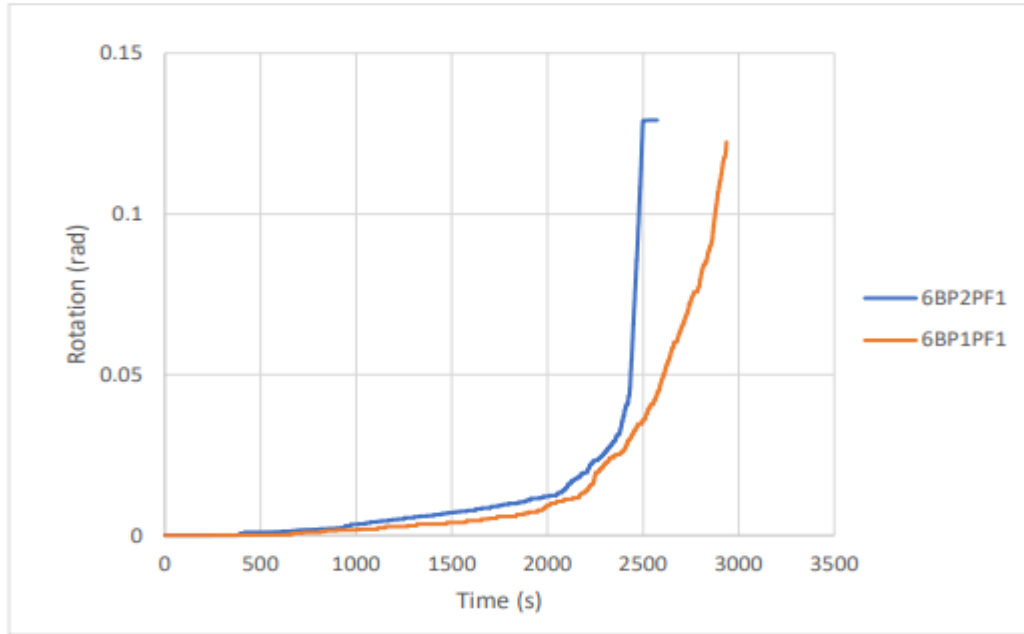


Figure 4.24 Time-rotation relationships of the undamaged, unreinforced, and protected connection configurations that utilized six bolts in the first (6BP1PF1) and second bolt patterns (6BP2PF1) (Adapted from Owusu, 2019).

4.4 Time-Temperature Curves

Data from the twelve thermocouples (TCs) were used to construct the time-temperature curves for each connection. Figures 4.25 through 4.32 show the time-temperature curves for the eight different connection configurations tested in the current study.

4.4.1 Time-temperature curves of the unprotected connections

Figures 4.25 through 4.28 illustrate the time-temperature curves for the four unprotected connection configurations. At 100°C, the moisture within the wood begins to evaporate and at this point, the wood begins to pyrolyze before starting to char. The charring stage begins at a temperature of 300°C.

For the unprotected connection configuration with four bolts arranged in the first bolt pattern (P1) (Figure 4.25), the charring began between 5 minutes (based on TC-09 and TC-10 readings at a temperature of 300 °C) and 18 minutes (based on TC-03 and TC-04 times at a temperature of 300 °C) after the start of the fire test. Since the readings of TC-01, TC-02, TC-05, TC-06, TC-07, and TC-08 did not reach the charring temperature of 300 °C, the charring did not reach the 40 mm, 60 mm, or 80 mm depth of the beam, indicating that this specimen experienced minimal charring. Hence, the shorter fire resistance time can be attributed to the initial splits in the beam section. As noted, this specimen had the greatest split width (5 mm) of all the specimens, which allowed the heat of the fire to penetrate the wood core and accelerate charring and thus causing failure.

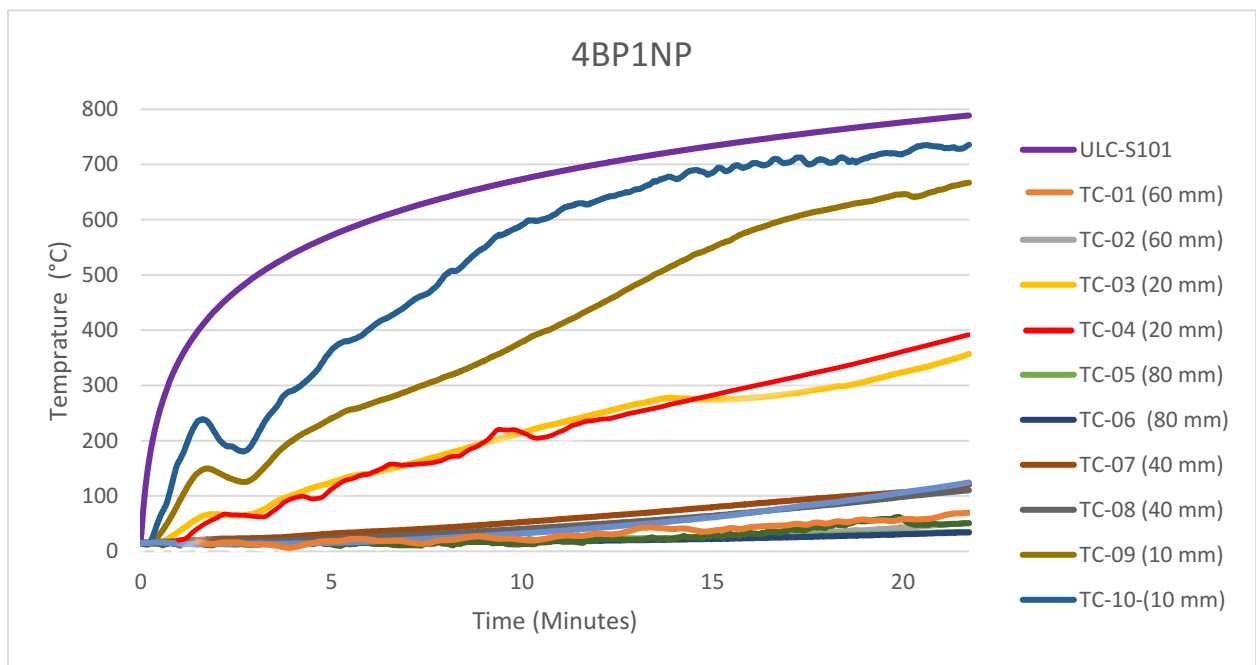


Figure 4.25. Time-temperature relationships of the STS-retrofitted, unprotected connection configurations that utilized four bolts in the first bolt pattern (4BP1NP)

For the STS-retrofitted, unprotected connection configuration with four bolts arranged in pattern two (P2), charring began between 3 and 22 minutes. This specimen experienced higher charring as compared to the connection configuration with four bolts arranged in pattern two (P1). As can be seen from Figure 4.26, charring was reached up to the depth of the T-stub plate which was installed at a depth of 80 mm into the beam. This resulted in slightly higher fire resistance times. Also, as can be seen from TC-09, the temperature at 10 mm depth into the beam reached the furnace temperature after approximately 10 minutes into the fire test. For the 20 mm depth (TC-04), the temperature reached the furnace temperature after roughly 15 minutes after the start of the test.

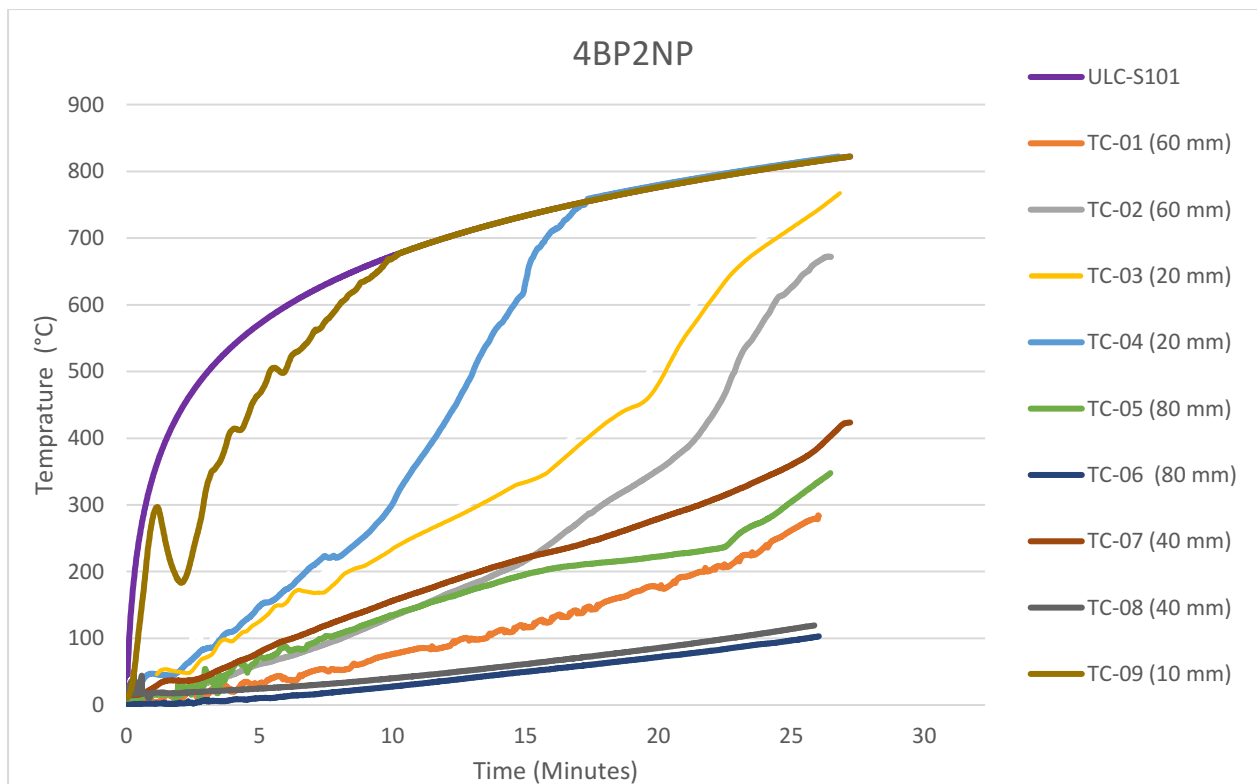


Figure 4.26 Time-temperatures relationships of the STS-retrofitted, unprotected connection configurations that utilized four bolts in the second bolt pattern (4BP2NP)

For the STS-retrofitted, unprotected connection configuration with six bolts arranged in pattern two (P1), charring began between 2 and 7 minutes. As evident from Figure 4.27, the beam lasted approximately 28 minutes after the charring point was first reached before failure occurred, indicating a prolonged charring stage. As evident from TC-11 readings, charring was reached until the top bolt. However, as evident from TC-05 and TC-06, the T-stub did not contribute to charring. The temperature at the face of the beam (10 mm depth) reached the furnace temperature after approximately 10 minutes into the fire test and after roughly 20 minutes for the 20 mm depth into the beam.

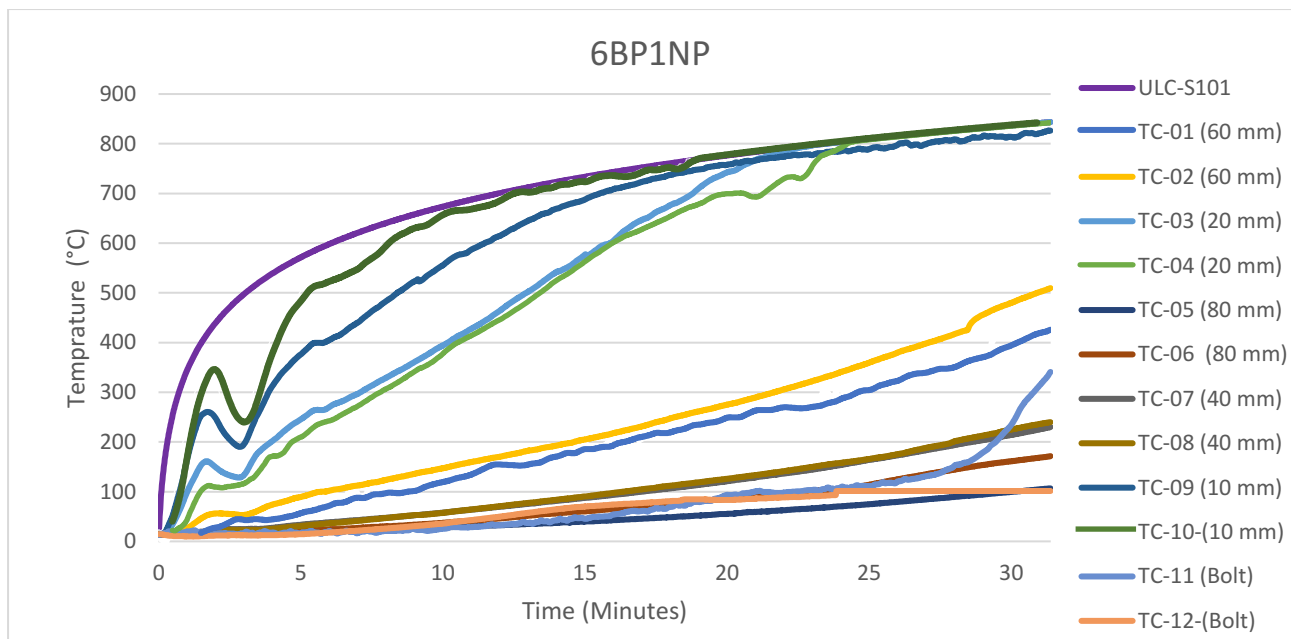


Figure 4.27 Time-temperatures relationships of the STS-retrofitted, unprotected connection configurations that utilized six bolts in the first bolt pattern (6BP1NP)

Similar to the connection that utilized six bolts arranged in the first bolt pattern (P1), for the connection that utilized six bolts but arranged in the second bolt pattern (P2), charring began between 2 and 11 minutes after the start of the test. As evident from the temperatures measured by TC-03, TC-04, TC-09, and TC-10 in Figure 4.28, the thickness of the char layer developed in the

beam section was limited to up to approximately 20 mm, resulting in less charring when compared to that of the connection that utilized six bolts arranged in the first bolt pattern (P1). Although this connection experienced less charring as compared to that of the connection that utilized six bolts but arranged in the first bolt pattern (P1), it had a 7-minute more fire resistance time. This can be attributed to the width of the initial split which was much smaller in the P2 configuration as compared to that developed in the P1 configuration.

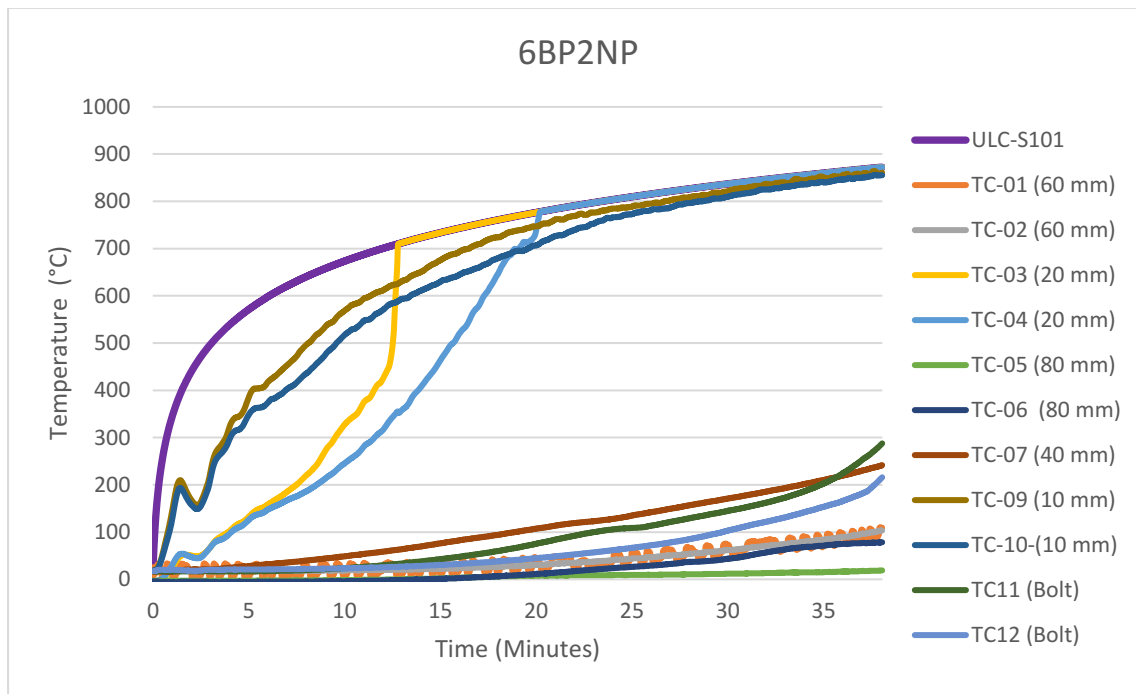


Figure 4.28 Time-temperatures relationships of the STS-retrofitted, unprotected connection configurations that utilized six bolts in the second bolt pattern (6BP2NP).

4.4.2 Time-temperature curves of the protected connections

Figures 4.29 through 4.32 depict the time-temperature curves for the STS-retrofitted, protected connection configurations. For the protected connection configuration that utilized four bolts arranged in the first bolt pattern (4BP1P), charring at the face of the beam (TC-9 and TC-10) began almost instantly after the start of the test. The temperature at the face of the beam reached the furnace temperature after roughly 5 minutes from the start of the test. As shown in Figure 4.29, charring for this connection was limited to a thickness of 40 mm from the exposed surface of the beam. It should be noticed that this connection had a relatively wide initial split (3 mm) as compared to the other protected connection configurations. Therefore, this could indicate the failure was mainly a result of the initial splitting.

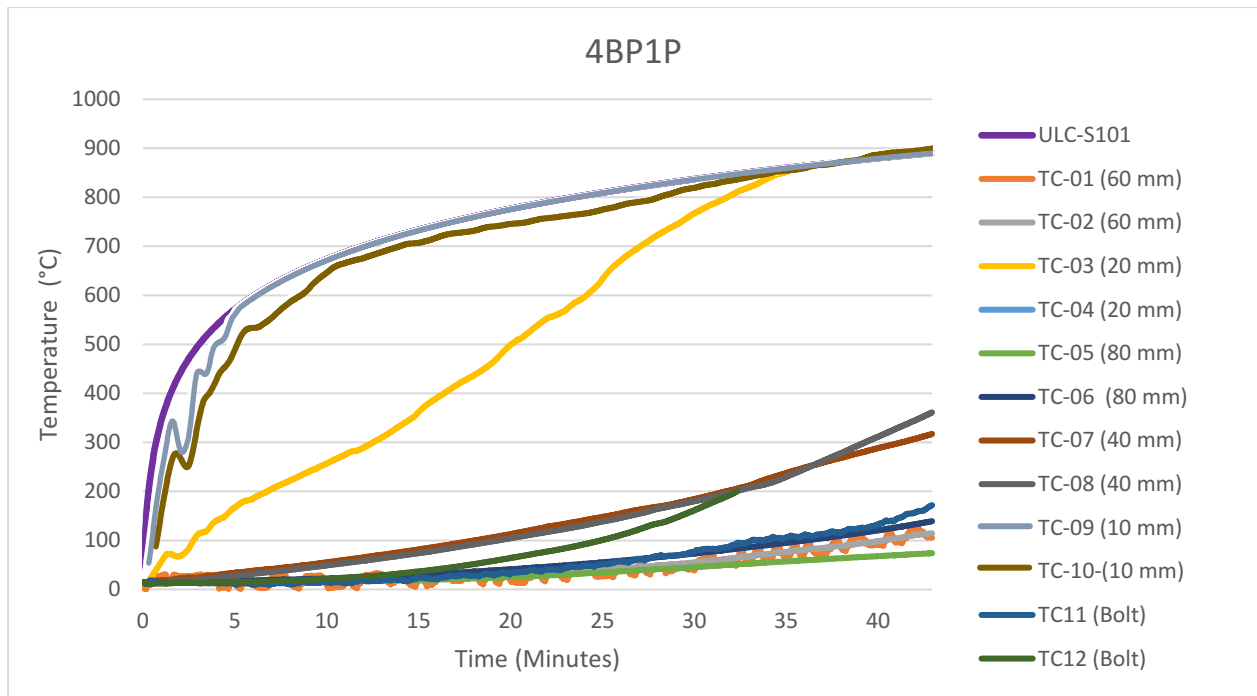


Figure 4.29 Time-temperatures relationships of the STS-retrofitted, protected connection configurations that utilized four bolts in the first bolt pattern (4BP1P)

On the other hand, for the connection configurations that utilized four bolts arranged in the second bolt pattern (4BP2P), charring took place within 20, 40, and 60 mm as well as up to the bolt's depths from the exposed surfaces. This significant char layer thickness resulted in a 15-minute more fire resistance time as compared to the 4BP1P configuration.

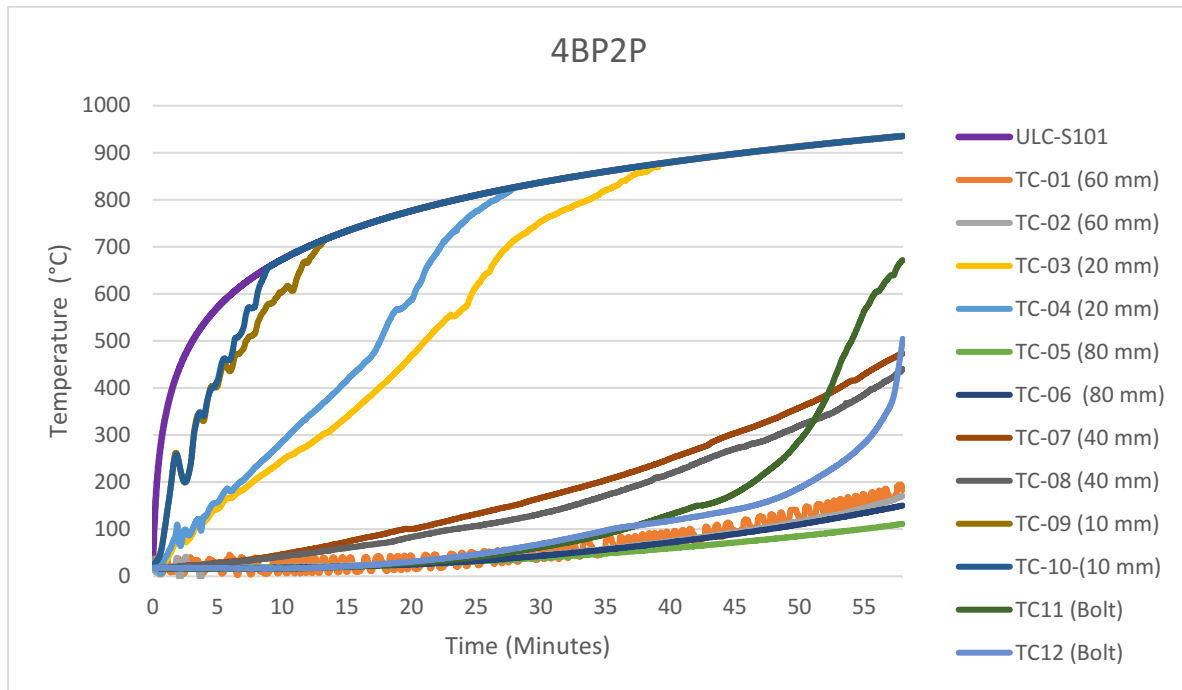


Figure 4.30 Time-temperatures relationships of the STS-retrofitted, protected connection configurations that utilized four bolts in the second bolt pattern (4BP2P)

Similar to the 4BP2P, for the connection configurations that utilized six bolts arranged in the first and second bolt patterns (6BP1P and 6BP2P), the charring took place within 20-, 40-, and 60-mm depths from the exposed surfaces. The T-stub steel connector (installed at 80 mm depth from the exposed surface) did not contribute to the charring of the wood core according to the temperature measured by TC-5 and TC-6 upon conclusion of the fire tests. This significant char layer thickness confirms the extended fire resistance times that those connection configurations lasted under standard fire exposure (60 and 57 minutes, respectively).

It should be noted that in the connection configuration with six bolts arranged in the second bolt pattern (6BP2P), TC-03 (installed at 20 mm depth from the exposed surface of the beam) was observed falling off from the specimen at approximately 5 minutes into the fire test and thus, the temperatures measured by TC-4, which was also installed at 20 mm depth from the exposed surface of the beam, were used instead to analyze the time-temperature curves of this connection configuration.

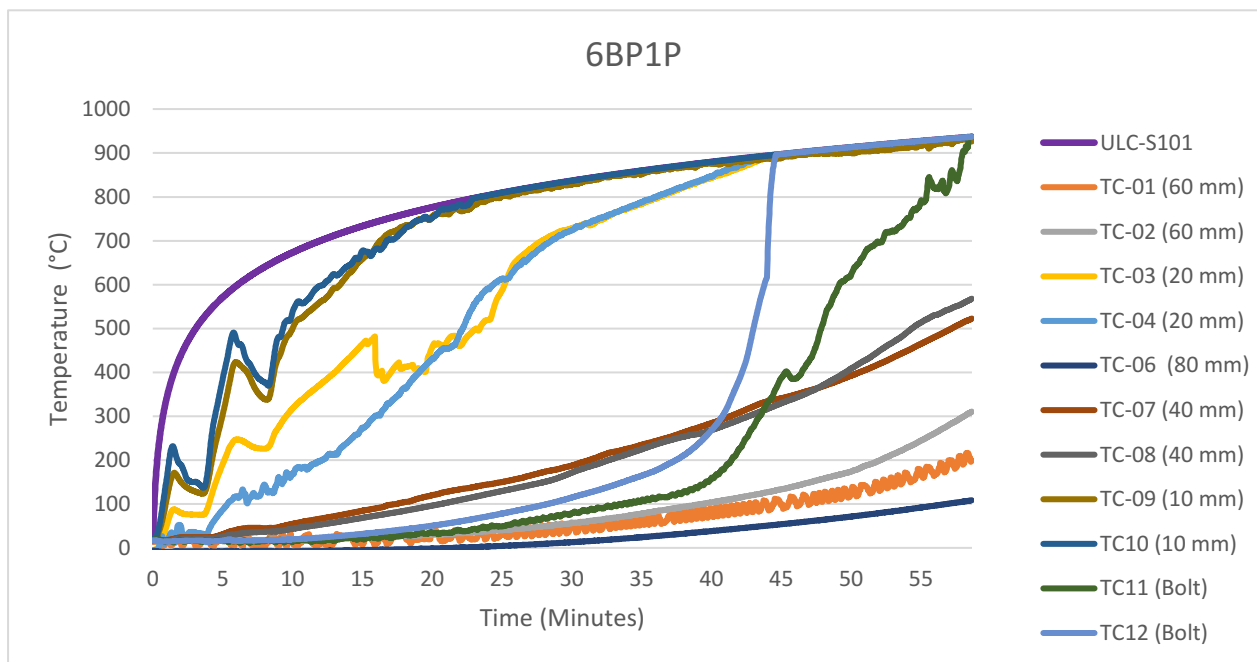


Figure 4.31 Time-temperatures relationships of the STS-retrofitted, protected connection configurations that utilized six bolts in the first bolt pattern (6BP1P)

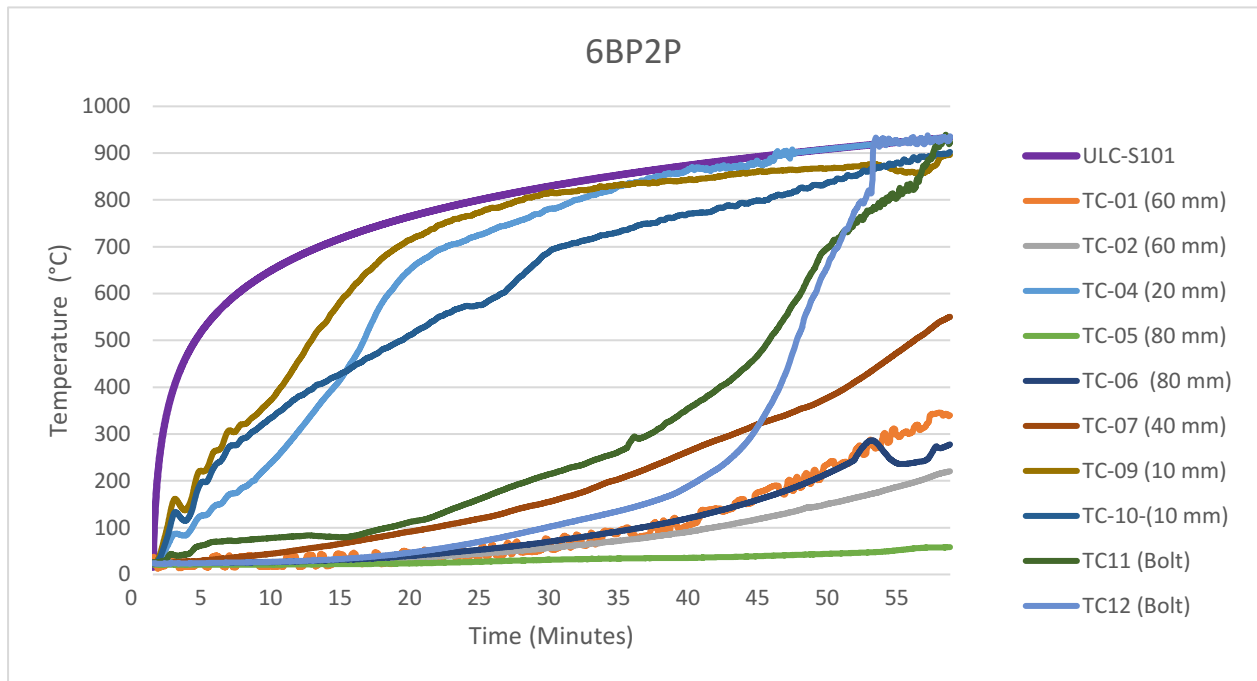


Figure 4.32 Time-temperatures relationships of the STS-retrofitted, protected connection configurations that utilized six bolts in the second bolt pattern (6BP2P)

4.4.3 Charring rates

As noted in section 2.7.2.1, charring rate (β) is defined as the ratio between the charring depth (mm) and duration of fire exposure (min) and thus, it is expressed in units of mm/min. The charring rate is calculated by determining the distance between the outer surface of the beam and the position of the char line after the fire test is completed. The char line is defined as the location where the wood temperature reaches 300 °C (also known as the char front). Considering that the specimens were completely burned when the furnace was opened after the cooling down phase ended, there was no possible way of determining the charring rate by measuring the actual distance to the char line. Hence, analyzing the developed time-temperature curves was the only way of estimating the charring rates of the different connection configurations experimentally tested in

this research study. The charring rates were calculated for depths between 10 and 20 mm from the exposed surface of the glulam beam, as per the following equation.

Equation 4.1 Charring rate

$$\beta = \frac{c}{t} \quad \text{Eqn. (4.1)}$$

Where c , in mm, is the char depth. Since the charring rate is calculated between the 10- and 20-mm depths, $c = 10$ mm. t (in minutes) is the difference in time when the thermocouples installed at 10 mm and 20 mm reached 300 °C (Char Front).

Below is a sample of the charring rate calculations for the unprotected connection configuration that utilized four bolts arranged in the first bolt pattern (4BP1NP).

- The time when TC 9 (inserted at 10 mm depth into the beam) reached 300 °C = 7.4 minutes
- The time when TC 3 (inserted at 20 mm depth into the beam) reached 300 °C = 18.6 minutes

Therefore, $t = 18.6 - 7.4 = 11.2$ minutes

Since $c = 10$ mm, the charring rate $\beta = 10/11.2 = 0.893$ mm/min

Table 4.3 summarizes the charring rates calculated for all eight STS-retrofitted connection configurations tested in this study.

Table 4.3. Calculated charring rates.

Connection ID.	Charring Rate (mm/min)
4BP1NP	0.89
4BP2NP	0.98
6BP1NP	1.33
6BP2NP	1.32
4BP1P	0.99
4BP2P	1.00
6BP1P	0.87
6BP2P	-

The average charring rate for the four unprotected connections is 1.13 mm/min, whereas it was calculated at 0.95 mm/min for the protected connections (excluding the 6BP2P connection which the charring was not able to be accurately calculated due to a significant discrepancy in the Thermocouple readings). Therefore, it can be concluded that the protected connections experienced a lower average charring rate compared to that calculated for the unprotected connections. Also, it was seen that the lower the charring rate is, the greater the fire resistance time was achieved. Figure 4.33 illustrates the relationship between the calculated charring rate and fire resistance time of the eight connection configurations tested in this study. As illustrated, the STS-retrofitted, protected connection configuration with six bolts arranged in the first bolt pattern (6BP1P) which had the greatest fire resistance time experienced the lowest charring rate (0.87 mm/min).

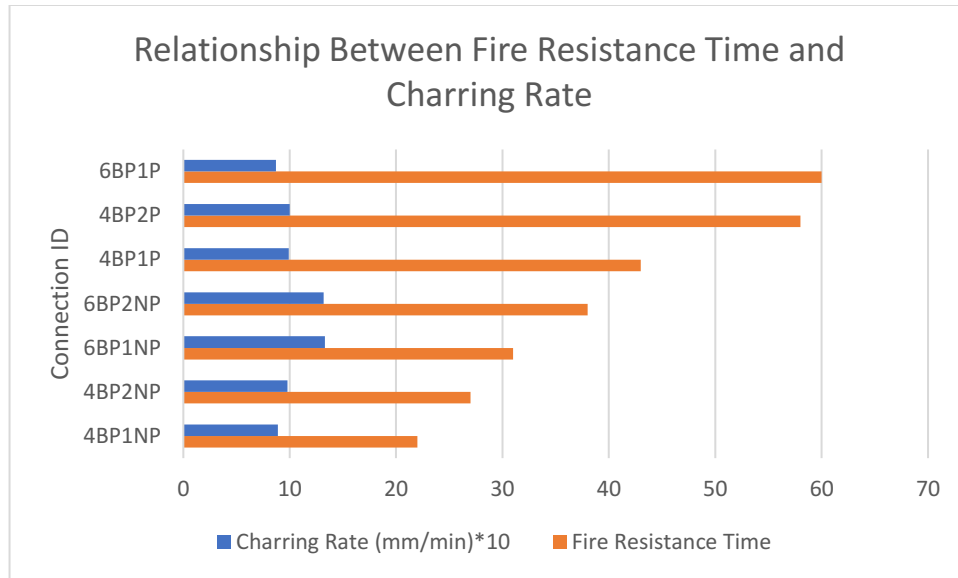


Figure 4.33 Relationship between the calculated charring rate and fire resistance time of the eight STS-retrofitted connection configurations tested.

Chapter 5: Conclusions and Recommendations

5.1 Conclusions

The following is a summary of the advantages of utilizing self-tapping screws (STS) as a perpendicular-to-wood grain reinforcement to retrofit damaged glulam beams in fire conditions.

- The usage of STS prevented the brittle failure mainly caused by glue line delamination, which was common in the undamaged, unreinforced connections. This resulted in increased fire resistance time.
- Although the usage of STS resulted in the recovery of substantial fire resistance time, the full original strength and fire resistance time of the different connection configurations were never recovered. For example, the STS-retrofitted, protected connection configuration (6BP1P) had a fire resistance time of 60 minutes compared to 62 minutes achieved by the undamaged, unreinforced, and protected connection configuration with the same number of bolts arranged in the same bolt pattern. Also, the STS-retrofitted, protected connection configuration (4BP1P) had a fire resistance time of 43 minutes compared to 56 minutes achieved by the undamaged, unreinforced, and protected connection configuration with the same number of bolts arranged in the same bolt pattern.
- The average percentage of the recovered fire resistance time for the STS-retrofitted connection configurations tested in this study is approximately 85%. It should be noted that this average percentage is based on the results of the connections that did not experience glue line delamination failures. When glue line delamination failure occurred, the undamaged, unreinforced connection configurations had shorter fire resistance time compared to that of the STS-retrofitted connection configurations.

- When analyzing the time-rotation curves for both undamaged and STS-retrofitted connections, it was observed the usage of STS allowed the glulam beam-end connections to behave in a more ductile manner and failed in a more gradual manner when compared to the undamaged connections.
- The width of the initial splits exhibited by the glulam beam section significantly influenced the fire resistance of the beam-end connections. Accordingly, the beams with wider initial splits had less fire resistance time. Even with the usage of STS, damaged glulam beam sections with wide initial splits achieved considerably less fire resistance time.
- It was observed that glulam beam-end connections with higher charring rates experienced less fire resistance time. Also, unprotected connections had a higher charring rate compared to those of the protected connections.

5.2 Recommendations for Future Work

- As was shown in the results of this research, considerable wide splits (2-3 mm or more) significantly reduced the fire resistance times of the damaged connections. Hence, wide splits in timber members must be repaired to avoid any fire resistance deficiencies that can take place in case of a fire. Investigating split repair techniques and the impact that they will have on fire resistance times will be very useful in future studies.
- Instead of using wood plugs to conceal steel components within the connection, it would be advantageous to use alternative materials with higher insulating properties, such as Type-X gypsum board, to shield the steel bolts, nuts, and plates. Using more fire-resistive materials will result in lower heat conductivity from the steel to the wood and hence will lead to higher fire resistance times.

- In order to expand the scope of this study to investigate more parameters such as the effect of STS placement geometry, the presence of more cracks, usage of different connection types (i.e., WWW or SWS), moisture content, etc., on the fire resistance of damaged glulam beam connections, numerical modelling using computer software should be used in future research. As currently there are very limited guidelines on the calculation of the fire resistance of damaged glulam connections, using computer software to model damaged connections in fire can result in the development of equations or numerical methods to calculate the fire resistance of such connections.

References

- Ali, S. (2016). Fire performance of hybrid timber connections. Doctoral dissertation. Dept. of Civil And Environmental Engineering, Carleton University, Ottawa, Canada.
- Ayme, N. (2003). Assemblages bois-metal en double cisaillement. Rapport Du Comportement Au Feu D'Assemblages Bois, CTICM Ref. SR21-03/121-NA/PB. CTICM, Paris, France
- Angelajimenezhuamanlazo. (2014). Wood. biomimesisARQ. Retrieved from <https://biomimesisarch.wordpress.com/2014/10/07/wood/>
- Broughton, J. G., and Hutchinson, A. R. (2003). Review of relevant materials and their requirements for timber repair and restoration. LICONS (low intrusion conservation systems for timber structures, CRAF-1999-71216, Task 2.2.
- Cachim, P. B., and Franssen, J. M. (2010). Assessment of Eurocode 5 charring rate calculation methods. *Fire Technology*, 46(1), 169.
- Canadian Construction Materials Centre (CCMC) (2018). Evaluation report: Nordic Lam™. Report Number CCMC 13216-R.
- Canadian Wood Council, Wood Design Manual, Ontario, Canada, 2020.
- Coureau, J. L., Cuvillier, E., and Lavergne, C. (2001). Strength of locally PGF reinforced end-notched beams. *Joints in Timber Structures*.
- CAN/CSA O86-19, Engineering design in wood, Canadian Standards Association, Rexdale, ON, Canada, 2019.
- CAN/ULC S101-19, Standard methods of fire endurance tests of building construction and materials. Underwriters Laboratories of Canada, Fifth edition, Ottawa, Canada, 2019.

- Dietsch, P., and Brandner, R. (2015). Self-tapping screws and threaded rods as reinforcement for structural timber elements—A state-of-the-art report. *Construction and Building Materials*, 97, 78-89.
- Echavarría, C. (2007). Bolted timber joints with self-tapping screws. *Revista EIA*, (8), 37-47.
- EN 1995-1-2: 2004. (2004). Eurocode 5: Design of Timber Structures—Part 1-2: General—Structural Fire Design.
- Frangi, A., and Fontana, M. (2003). Charring rates and temperature profiles of wood sections. *Fire and Materials*, 27(2), 91-102.
- Fredlund, B. (1993). Modelling of heat and mass transfer in wood structures during fire. *Fire safety journal*, 20(1), 39-69.
- Falk, R. H. (2009). Wood as a sustainable building material. *Forest products journal*. Vol. 59, no. 9 (Sept. 2009): pages 6-12., 59(9), 6-12.
- Gammon, B.W., Reliability Analysis of Wood-Frame Wall Assemblies Exposed to Fire, Doctor of Philosophy, Thesis, University of California, 1987
- Harte, A. M., and Dietsch, P. (Eds.). (2015). Reinforcement of timber structures: A state-of-the-art report. Shaker.
- Hollaway, L. C. (2008). Strengthening and rehabilitation of civil infrastructures using fiber-reinforced polymer (FRP) composites. Elsevier.
- Italian National Research Council (2017). Guidelines for the Design and Construction of Externally Bonded FRP Systems for Strengthening Existing Structures.

- Janssens, M. L., and White, R. H. (1994). Temperature profiles in wood members exposed to fire. *Fire and Materials*, 18(4), 263-265.
- Jockwer, R. (2015). Structural behaviour of glued laminated timber beams with unreinforced and reinforced notches. *IBK Bericht*, 365.
- Johns, K. C., and Lacroix, S. (2000). Composite reinforcement of timber in bending. *Canadian Journal of Civil Engineering*, 27(5), 899-906.
- Knudson, R. M., RM, K., and AP, S. (1975). Performance of structural wood members exposed to fire.
- König, J. (2000). Timber frame assemblies exposed to standard and parametric fires. Part 2 A design model for standard fire exposure.
- Lam, F., Gehloff, M., and Closen, M. (2010). Moment-resisting bolted timber connections. *Proceedings of the Institution of Civil Engineers-Structures and Buildings*, 163(4), 267-274.
- Li, J., Hunt, J. F., Gong, S., and Cai, Z. (2017). Orthogonal model and experimental data for analyzing wood-fiber-based tri-axial ribbed structural panels in bending. *European Journal of Wood and Wood Products*, 75(1), 5-15.
- Livingstone, A. Timber connections - Edinburgh Napier University. Retrieved December 5, 2021, from <https://www.napier.ac.uk/~media/worktribe/output-404038/timber-connections.pdf>.
- Maraveas, C., Miamis, K., and Matthaiou, C. E. (2015). Performance of timber connections exposed to fire: a review. *Fire Technology*, 51(6), 1401-1432.

- Martin, Z., and Tingley, D. A. (2000). Fire resistance of FRP strengthened glulam beams. In World Conference on Timber Engineering, Whistler Resort, British Columbia, Canada
- Mehaffey, J. R., Cuerrier, P., and Carisse, G. (1994). A model for predicting heat transfer through gypsum-board/wood-stud walls exposed to fire. *Fire and materials*, 18(5), 297-305.
- NBCC, National Building Code of Canada. Canadian Commission on Building and Fire Code, National Research Council of Canada, Ottawa, ON, Canada, 2005.
- NBCC, National Building Code of Canada. Canadian Commission on Building and Fire Code, National Research Council of Canada, Ottawa, ON, Canada, 2020.
- Nowak, T. P., Jasieńko, J., and Czepiżak, D. (2013). Experimental tests and numerical analysis of historic bent timber elements reinforced with CFRP strips. *Construction and Building Materials*, 40, 197-206.
- Okunroumu, O., Salem, O. S., and Hadjisophocleous, G. (2022). Fire performance of hybrid mass timber beam-end connections with perpendicular-to-wood grain reinforcement. *Journal of Structural Fire Engineering*.
- Owusu, A. (2019). Structural Performance of Hybrid Timber Connections with Varying Bolt Patterns at Ambient and Elevated Temperatures. Masters' dissertation, Dept. of Civil and Environmental Engineering, Carleton University, Ottawa, Canada.
- Peng, L. (2010). Performance of heavy timber connections in fire. Doctoral dissertation. Dept. of Civil and Environmental Engineering, Carleton University.
- Peng, L., Hadjisophocleous, G. V., Mehaffey, J. R., and Mohammad, M. (2011). On the fire performance of double-shear timber connections. *Fire Safety*, 10, 1207-1218.

- Peng, L., Hadjisophocleus, G., Mehaffey, J., and Mohammad, M. (2011). Predicting the fire resistance of wood–steel–wood timber connections. *Fire technology*, 47(4), 1101-1119.
- Petrycki, A., and Salem, O. S. (2020). Structural integrity of bolted glulam frame connections reinforced with self-tapping screws in a column removal scenario. *Journal of Structural Engineering*, 146(10), 04020213.
- Pizzo, B., and Smedley, D. (2015). Adhesives for on-site bonding: Characteristics, testing and prospects. *Construction and Building Materials*, 97, 67-77.
- Raftery, G. M., and Harte, A. M. (2011). Low-grade glued laminated timber reinforced with FRP plate. *Composites Part B: Engineering*, 42(4), 724-735.
- Ruan, G., Filz, G. H., and Fink, G. (2021). Shear capacity of timber-to-timber connections using wooden nails. *Wood Material Science & Engineering*, 1-10.
- Steiger, R., Gehri, E., and Widmann, R. (2004, August). Glued-in steel rods: a design approach for axially loaded single rods set parallel to the grain. In CIB-W18 meeting thirty-seven, Edinburgh, UK.
- Steiger, R., Serrano, E., Stepinac, M., Rajčić, V., O'Neill, C., McPolin, D., and Widmann, R. (2015). Strengthening of timber structures with glued-in rods. *Construction and building materials*, 97, 90-105.
- Takeda, H., and Mehaffey, J. R. (1998). WALL2D: A model for predicting heat transfer through wood-stud walls exposed to fire. *Fire and Materials*, 22(4), 133-140.
- Triantafillou, T. C. (1997). Shear reinforcement of wood using FRP materials. *Journal of materials in civil engineering*, 9(2), 65-69.

- White, R. H., and Woeste, F. E. (2013). Post-fire analysis of solid-sawn heavy timber beams. STRUCTURE magazine, November 2013; pp. 38-40., 38-40.
- Widmann, R., Jockwer, R., Frei, R., and Häni, R. (2012). Comparison of different techniques for the strengthening of glulam members. In Enhance mechanical properties of timber, engineered wood products and timber structures: COST Action FP1004 Early Stage Researchers Conference (pp. 57-62).
- Williamson, T. G., and Yeh, B. (2006). Fire Performance of FRP Reinforced Glulam.
- Winandy, J.E., Wood properties, USDA-Forest Service, Forest Products Laboratory, Encyclopedia of Agricultural Science, Volume 4, pp. 549-561, 1994.
- Zaman, A., Gutub, S. A., and Wafa, M. A. (2013). A review on FRP composites applications and durability concerns in the construction sector. Journal of Reinforced Plastics and Composites, 32(24), 1966-1988.